DELFT UNIVERSITY OF TECHNOLOGY

MASTER OF SCIENCE THESIS

December 24, 2015

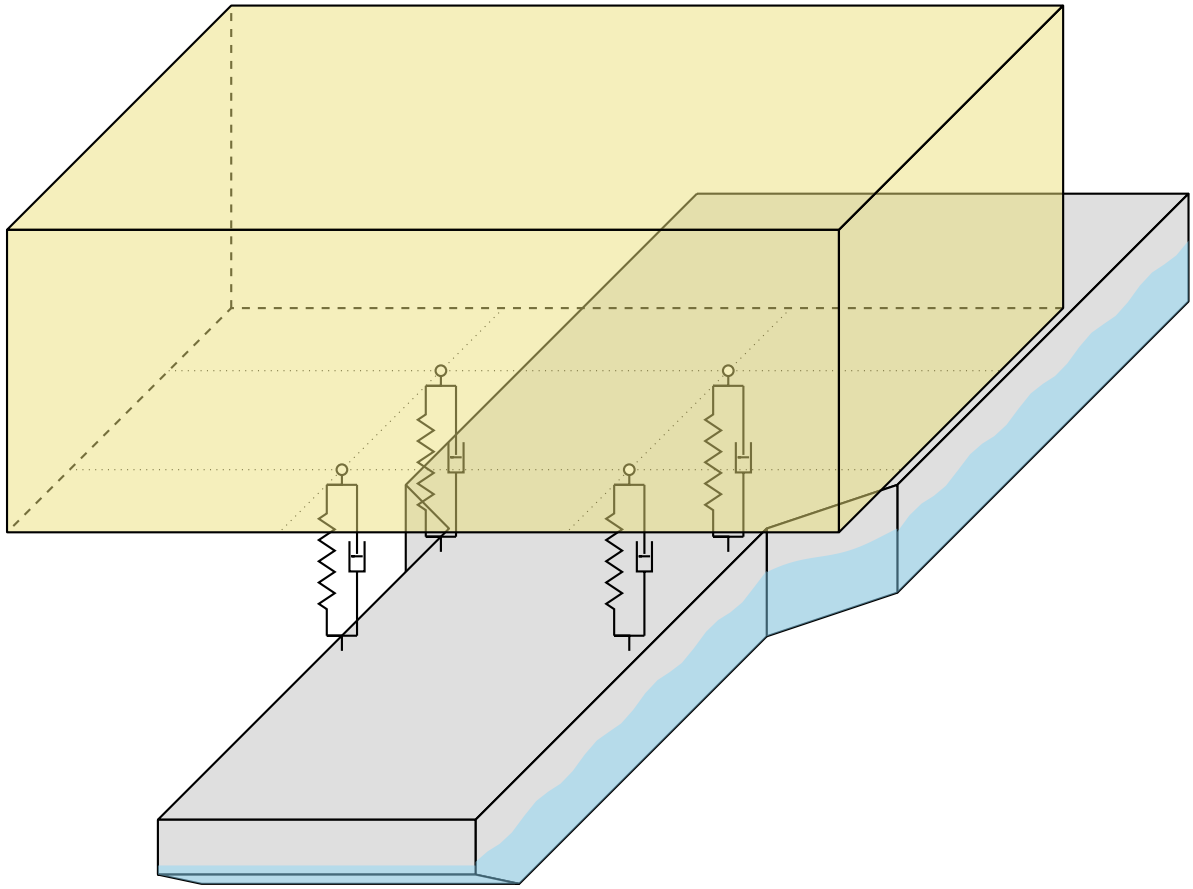

Heave compensated floatover operation

F.E. Wester

Graduation committee

DR. IR. S.A. MIEDEMA

PROF. DR. IR. R.H.M. HUIJSMANS

IR. X. CHEN

IR. M. DIJK

DR. IR. N.J. MALLON

PREFACE

Acknowledgements
This graduation has been a very instructive process. At the beginning there was one topic with an abundance of possible solutions. During the process I have learned to decide what is relevant, it turned out that there are not that many solutions as I previously imagined. It has been an interesting journey and I would like to take this opportunity to thank everybody who supported me throughout the journey.

First of all, I would like to thank my supervisors of Allseas. Graduating at Allseas has been a very good experience. I would like to thank Niels for his daily support and valuable insights, the feedback on my work was spot-on and effectively guided me through the process. Also, I would like to thank Marijn for offering me the opportunity to graduate in the naval architecture department. His out-of-the-box thinking kept me sharp in the beginning of the research and helped me the narrow down the scope efficiently.

Secondly, Sape and Rene have played a important role in progress of my work, therefore I would like to express my gratitude. During the progress meetings the feedback was very helpful, it made me realise what the bottlenecks of my research were. I would also like to thank Xiuhan Chen for being a part of my graduation committee.

Thirdly, Allseas in general has been a great setting to perform this graduation. The lunch breaks were always relaxing and the coffee machines have been of vital support. Therefore, I also want to thank everyone that has been a part of this experience, especially, Julius, Robbert, Paul, Sil, Roel and Ellen for helping me with problems and providing feedback of my thesis.

Graduation committee:
The graduation committee is represented by:

Dr. Ir. S.A. Miedema	Offshore & Dredging Engineering	TU Delft, 3ME
Prof. Dr. Ir. R.H.M. Huijsmans	Ship Hydromechanics & Structures	TU Delft, 3ME
Ir. X. Chen	Offshore & Dredging Engineering	TU Delft, 3ME
Ir. M. Dijk	Naval architecture department	Allseas Engineering
Dr. Ir. N. J. Mallon	Naval architecture department	Allseas Engineering

Reading guide
Chapter 1 start with the introduction, in which the cause of the research is presented. Chapter 2 follows with the problem definition, elaborating on the scope and constraints. Chapter 3 focusses on the method of deriving the installation limit. In chapter 4 the considered heave compensation concept is detailed, where special attention is given to the implementation of this concept in the model. The model is then explained in chapter 5, here the used methods and formulae are specified. This leads to the results, which are presented in chapter 6. An additional step is made in chapter 7, where the results are used to estimate the concepts dimensions. Chapter 8 discusses the research. The conclusions are drawn in chapter 9. Finally, the recommendations are listed in chapter 10.

For a short read the summary is advised. A more detailed view of the research is obtained by reading chapters 1, 2 and 9. To understand the steps taken in this research it is recommend to read all chapters. In this particular case the reader can also be interested in the possibilities of the heave compensation system, than chapter 2, 4, 8 and 9 are suggested.

ABSTRACT

The *Pioneering Spirit* is a newly built multi-purpose vessel owned by Allseas. Besides pipelaying activities the *Pioneering Spirit* is capable of the installation/removal of topsides and substructures. With this vessel Allseas wants to perform a leading role in the offshore installation and decommissioning market. For the installation/removal of topsides the *Pioneering Spirit* is equipped with the Topsides Lift System (TLS), installed on the two bows of the twin-hulled catamaran vessel. By enclosing the substructure with the two bows, the TLS is able to lift the topsides onto or from the substructure. For this method, the topsides and substructure have to comply with the restrictions due to the shape of the vessel. These restrictions follow from the width, length, water depth and air gap of the platform. The latter indicates the height of the topsides above mean seawater level. Platforms installed in West-Africa often have a small air gap, because the sea state is dominated by long swell waves and thus small amplitudes. The large height of the TLS makes the *Pioneering Spirit* unsuitable for the installation/decommissioning of these platforms. Hence, an alternative method is required if these topsides are to be installed/decommissioned by Allseas.

A common method to install the platforms in West-Africa is a floatover operation. In this method the topsides is placed onto a barge (or vessel), then the barge in positioned in the slot of the substructure. This slot is purposely built to align the topsides for the installation. When the barge is aligned the installation is executed, by ballasting the barge until the topsides is fully supported by the substructure. This procedure is governed by the motions of the barge and topsides, since these motions cause impact loads between the topsides and substructure legs. The long swell waves have a large influence on the vessel's motions. Therefore, floatover operation can have a long waiting period, which leads to high costs. Therefore, preventing this waiting is valuable. This is achieved by improving the workability of the operation.

The aim of this research is to investigate the possible gain in workability by implementing a heave compensation system in the floatover operation. In this preliminary study, the mating phase of the floatover operation is examined. The mating phase commences when the barge is moored inside the substructure slot and ends when the topsides is installed. The heave compensation system is the most valuable in this phase, because it includes the set down and load transfer of the topsides. To find the gain in workability with a the heave compensation system an already performed, and well documented, floatover operation is compared to the heave compensated floatover. To perform this comparison, the `Liwan 3-1` topsides (26,300 tons) installation in the Nigerian swell sea is considered. This topsides cannot by operated by the *Pioneering Spirit* and is installed with the floatover method.

The heave compensation concept assessment shows that passive heave compensation is the most promising concept. To avoid the large power demands of an active system. The concept consists of three main components: hydraulic cylinders to lift the topsides, pneumatic pressure vessels to provide passive actuation and accumulators to connect the cylinders with the pressure vessels. The topsides is supported by four of these systems that are placed in a rectangular configuration on the barge. The stroke of the hydraulic cylinder acts vertically and is assumed rigid in transverse direction. Therefore, the concept is able to compensate the vertical motions of the topsides. Because the cylinders are rigid in transverse directions, the horizontal motions of the topsides are related to the roll and pitch of the barge.

A model is developed to find the influence of the heave compensator on the hydrodynamic behaviour of the barge and topsides. The model consists of a frequency domain analysis which is performed with a linear hydrodynamic model. The heave compensation system is modelled as a linear spring-damper system. The stiffness of the system is related to the pressure and pneumatic volume in the pressure vessels. Linearisation of the adiabatic compression process leads to the stiffness value. The linearisation is valid because a large volume of pneumatic pressure is used, thus the non-linear behaviour is minimal. A large volume of air and high pressure relate to a low stiffness value, that increases the performance of the compensator. The damping is considered as a variable percentage of the critical damping of the system. A more realistic approach of the damping forces is not feasible in this concept study, because a high level of detail is required to realistically

estimate the non-linear damping forces. The performance of the heave compensation system is related to the pressure, pneumatic volume and damping percentage of the heave compensation system.

To compare the heave compensated installation and the `Liwan 3-1` installation a benchmark value for the installation limit is used. Based on the most critical loading condition, being the horizontal impact forces on the substructure. Since the substructure uses Leg Mating Units (LMU), the horizontal load depends on the stage in the mating operation. The most crucial point of the operation is found to be the initial impact of the topsides. This occurs when the topsides is almost in contact with the LMU's. The combined stiffness of the substructure and LMU's is used to obtain the energy balance between the topsides kinetic energy and the substructure spring energy. From this balance the maximum installation velocity of the topsides is acquired. The installation velocity is the maximum velocity at the topsides leg location. The installation limit is found as $0.4\,\frac{m}{s}$.

The results of the heave compensation system are promising. The heave compensated scenario almost doubles the workability in head waves, from 46% without heave compensation to 88% with heave compensation, based on the year-round sea statistics of Nigeria. Much higher gains are obtained in beam sea conditions, where the workability is 6% in the uncompensated scenario and 44% with the heave compensation. These workability gains are obtained with 200 bars of pressure, 2,600 m^3 of pneumatic storage and 20% of the critical damping. The results, in combination with an estimation of the size and weight of the system, lead to an indication of the feasibility of the concept. To estimate the size and weight, the dimensions of the three main elements are approximated. This leads to a system that contains 24 hydraulic cylinders, 8 accumulators and 96 pressure vessels. Combined with a deck support frame these elements weight 9,000 tons and cover 46.5% of the deck area. The original `Liwan 3-1` operation contains a deck support frame of 4,000 tons that covers 14.8% of the deck area.

The workability can be improved significantly in the mating stage of the operation by the use of the heave compensation system. This requires the implementation of a larger more complex system. However, the gain in workability might be worth this investment. It must be noted that the workability is assessed for the mating stage only and that the workability of the full operation is not solely dependent on this workability. Hence, the results are a good incentive for further investigation on the heave compensation concept, to check if comparable results are obtained with a non-linear model.

GLOSSARY

AG *Amazing Grace* is a new vessel currently in concept design. The vessel will have a larger lifting capacity than the *PS*

PS *Pioneering Spirit* the new vessel of Allseas

COG Center of Gravity

DOF Degree of freedom

DSF Deck Support Frame

DSU Deck Support Unit

FEM Finite Element Method

HCS Heave Compensation System

LMU Leg Mating Unit

PHC Passive Heave Compensation

RAO Response Amplitude Operator

LIST OF SYMBOLS

α	Angle of leg mating unit relative to the horizontal plane
γ	Peak enhancement factor
δ	Relative displacement
ζ	Damping
θ	Pitch
κ	Heat capacity ratio
λ	Slenderness ratio
μ	Friction coefficient
ρ	Density
σ_s	Spectral width parameter
σ	Design stress
ϕ	Roll
ω	Wave frequency
A	Area
A	Added mass matrix
B	Damping matrix
c_c	Corrosion allowance
c	Damping
D, d	Diameter
E	Energy
e	Welding factor
E_{st}	Youngs modulus of steel
F	Force
f_D	Darcy friction factor
H_s	Significant wave height
I	Moment of inertia
J	Inertia
k	Stiffness
K	Stiffness matrix
L, l	Length
m	Mass
M	Mass matrix
N	Number of substructure legs
n	Number or Amount
p	Pressure
Rm	Yield strength of steel
R	Response amplitude operator
r	Radius
S	Spectral density
T_p	Peak period
t	Wall thickness
u	Displacement
V	Volume
V_f	Safety factor
v	Velocity
x	Displacement
y	Displacement
z	Heave

CONTENTS

1

INTRODUCTION

The introduction consists of two parts. Firstly, the origin of the thesis is summarised, where the reason for this research is given. This section introduces multiple topics that are the foundation of this research. The second part explains the topics that are introduced in the origin. The topics are explained separately and the important aspects, for this research, are further detailed. Using the information of this section the aim for this research is determined.

1.1. ORIGIN

With the *Pioneering Spirit* (*PS*), Allseas enters the market of installation and decommissioning of topsides. Allseas wants to perform a leading role in this market. To achieve this Allseas wants to be able to operate all topsides installation and decommissioning projects. In theory this can be done with three vessels: the *PS*, the *Amazing Grace* (*AG*) and a vessel that handles the topsides that are not possible with the previous two vessels. The *AG* is currently being designed and focusses on the heaviest platforms, this vessel is planned to have the same catamaran hull shape as the *PS*.

The third vessel should focus on the platforms that the *PS* is not able to operate due to limitations other than weight since this is the main focus of the *AG*. This leaves three parameters: water depth, air gap and dimensions. There are several topsides that cannot be installed because of these parameters, therefore exploring a vessel dedicated to these topsides is worthwhile. These topsides are often installed with the floatover method; this method automatically results in large widths. A substantial amount of these floatover operations took place in the West-African region where long swell waves are dominant. These swell waves lead to a decrease in workability for floatover operations. This creates an opportunity for a high-tech solution that improves the workability in these circumstances.

To increase the workability a heave compensation system (HCS) can be used. These systems compensate vertical motions of a vessel. Therefore, the installation/decommissioning can occur in higher sea states. For the *PS* a HCS is designed and thus a lot of in-house knowledge about this subject is present at Allseas. When looking into the African swell, where ship motions are significant, a compensation system can be a very efficient way to increase the workability.

1.2. ELABORATION OF THE ORIGIN

In this section the origin is further elaborated. This is done by splitting the origin in different elements. Firstly the floatover operation and all its elements are explained, including a market analysis and growth expectations. Then the impossible platforms are studied, examining the quantity and locations of the platforms in the Allseas database. After this the African swell is introduced more thoroughly, including initial workability calculations. Finally, the HCS of the *PS* is explained and the possibilities for the new vessel are deducted.

1.2.1. FLOATOVER OPERATIONS

Firstly, the floatover installation process is detailed. This is done by explaining the sequence of events in a floatover operation. Secondly, the different techniques for floatovers are evaluated. After this a prediction of the expected floatover market in the future is presented. This section ends with the conclusion if and how the floatover technique should be improved.

THE FLOATOVER OPERATION

Floatover operations are used to install large topsides. In a floatover, the topsides is placed on a large floating structure, barge or vessel. The barge/vessel is smaller than the width between the topsides legs which causes the legs to float above the water surface, this is shown in Figure 1.1. The substructure is designed such that the barge/vessel fits in between the purposely built slot. From this position the barge/vessel will be ballasted until the topsides load is transferred on the jacket legs.

The main advantage of a floatover operation is that the topsides is installed as a single integrated module and therefore the installation is performed in a single procedure. Additionally little offshore commissioning is required. This significantly decreases the offshore working hours required for an installation procedure.

Figure 1.1: Example of a typical floatover operation. The topsides are skidded on a barge, which fits in the substructure slot. The lengthy side of the topsides hangs over the edge of the barge, such that the topsides legs can be lowered onto the previously installed jacket legs, from He et al. (2011).

According to Wang et al. (2010) a floatover operation can be divided in six major stages, these stages are listed with a small explanation:

- **Load out:** the integrated topsides is jacked on the Deck Support Frame (DSF) and subsequently skidded onto the barge/vessel.
- **Transportation:** the topsides is transported from the fabrication yard to the offshore location.
- **Pre-floatover preparations:** the final preparations are made on the offshore location, for example, connecting the mooring lines and checking the rigging procedures.
- **Docking operation:** The barge with topsides is navigated in the slot of the substructure until the correct position is reached. During this operation the position of the barge is controlled by the mooring winches and/or anchor handling tugs.
- **Mating operation:** In this stage the topsides load is transferred to the substructure by ballasting the barge/vessel. In most cases Leg Mating Units (LMU) are used to decrease the loads on the structures during installation.
- **Separation & undocking operation:** When the load transfer is done the ballasting continuous until a safe clearance between the structure and the barge/vessel is obtained to safely operate the barge/vessel away from the substructure.

The workability of a floatover operation is mainly determined by the performance of the vessel/barge in the docking, mating and undocking stage. In these phases contact with the substructure can lead to unacceptable loads in the structures. The load out stage is also critical for the structural integrity but this often done in sheltered waters and thus not related to the sea state.

CURRENT FLOATOVER TECHNIQUES

The first floatover installation was performed in 1977 for the Maureen project on a 18,600 tons platform (Wang et al., 2010) and the technique has developed ever since. Over the years several types of floatover installations were introduced; the most relevant types are listed in this section to show the used innovation in floatover techniques.

Hi-deck technique
This is the conventional floatover technique, as shown in figure 1.1, where the topsides is placed on a high DSF. The DSF creates enough clearance to safely enter the substructure slot. The installation is performed by ballasting the barge. In this method Leg Mating Units(LMU) are required to reduce the loads during installation (Wang et al., 2010).

Smart-leg technique
The first innovation for floatover technologies was the smart-leg technique used in 1997 by Mc Dermott. It consisted of passive heave compensation with hydraulic cylinders on top of the topsides legs (Labbe et al., 1998). These were used to install a 4,100 tons topsides. For the full transfer of the loads smart-shoes were used. These shoes were equipped with a collapse mechanism to create clearance between the topsides and barge. The effects of this technique on the topsides is visible in Figure 1.2.

(a) The Epke topsides, the extended legs are visible through the topsides. The hydraulic units are still installed, from Epke.

(b) Zoom of the Epke platform. The hydraulic jack assembly is visible, from (Wang et al., 2010).

Figure 1.2: The Epke gas compression platform installed with the smart-leg technique, Nigeria 1997.

UNIDECK technique
The UNIDECK concept is created by Technip and uses hydraulic jacks to reduce the installation time, which leads to a higher workability (Tribout et al., 2007). This method does not incorporate compensation of the movements. This is achieved by ballasting until a certain clearance is reached between the topsides and the leg mating units (LMU) installed on the legs. Then the jacks fully retract, transferring 50% of the topsides weight on the substructure. Due to the load transfer of the topsides from barge to substructure the draft of the barge decreases, this causes the barge and topsides to stay in contact. Ballasting continues whilst extending the jacks to keep the loads equal until enough stroke is gathered to ensure enough clearance after the retraction of the jacks.

Twin marine lift system
The twin marine lift system uses two vessels with lifting arms which perform a simultaneous lift of the topsides. Buoyancy tanks are used to provide the lift force. The principle is shown in figure 1.3. The lift is obtained by de-ballasting the inner tanks and ballasting the outer tanks (the latter are not visible in the figure) this creates a lever that lifts the topsides. The claimed lifting capacity is 34000 tons. The design shows a high level of detail. However, since 2013 no updates have been released regarding the progress of the vessels.

Figure 1.3: The twin marine heavy lift system, from (TMHL). The two vessels lift the topsides simultaneously using the buoyancy tanks, extra contra weight is created by ballasting the outer tanks (not visible in this illustration).

T-shape barge technique
In the last years the average weight of the platforms has increased. Therefore, the corresponding installation techniques need to be able to cope with larger loads. The solution is found with T-shaped barges. The T shape indicates that the barge has a broad stern width and a smaller bow width. This increases the maximum transport load whilst still being able to dock between the legs of the substructure. With these barges topsides of over 30,000 tons have been installed.

EXPECTED FLOATOVER MARKET

To motivate research for floatover innovation, confirmation of a growing demand for heavy floatover installation/decommissioning project is desired. In the period from 2005 to 2012, 264 installations are performed of which 73% lightweight installations, in this case lightweight implies less than 12.000 tons, and 27% heavy installations, from Martinez. 6% of the installation in the lightweight class were installed with floatover and more than 33% of the heavy weight classed installations. This shows that floatover is a common technique for heavy topsides installations. In the period 2014-2018 an estimated 480 lightweight and 93 heavy production platforms are expected to be installed. For the majority of the heavy category the installation method is known: 14 by floatover, 12 by crane, 1 by yard lift and 19 are unknown or undecided. The rest of the heavy installations are floating production storage and offloading facilities. From the heavy platforms within the scope 52% is expected to be installed with floatover, because the majority of the unknown/undecided category is expected to be floatover installations. It can be concluded that the floatover operation is becoming the preferred installation technique for heavy weight platforms.

In Hou et al. (2013) the crane lifting method is compared to the floatover operation. In this article the comparison is based on a heavy topsides installation in the South China Sea, where the floatover operation was chosen as preferred method. The arguments used in the paper are applicable in this setting. The major argument is the required offshore commissioning time and the unavailability of heavy lift derricks in the region. In addition to these arguments, the sea state of the South China Sea is milder than the West-African sea state, however this is a disadvantage for both installation methods. In the article they provided the deck weight trend over the years which is shown in figure 1.4. Adding this to the known information of multiple installations of 30.000 tons clearly shows that this trend is indeed present.

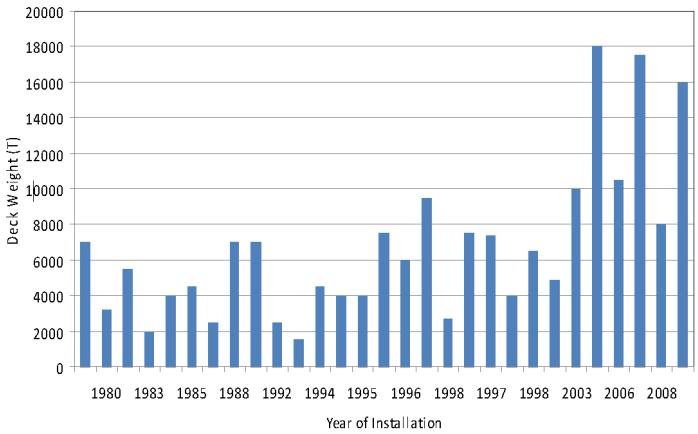

Figure 1.4: The average weight of the installed topsides from 1980 to 2008 (Hou et al., 2013). The heavy topsides trend of the past years is visible.

CONCLUSION

The floatover method has had some effective improvements over the past years. Significant reduction of the operation time is achieved and even light platform are installed with heave compensation. However, no attempt is made to use heave compensation on heavy topsides while the number of heavy topsides is increasing significantly. This creates an opportunity for a new floatover technique which is able to handle severe sea states during topsides installation.

1.2.2. PLATFORMS OUTSIDE OF PIONEERING SPIRIT SCOPE

In this section the platforms that are not possible to decommission or install with the *PS* are elaborated. This is done by analysing the limits first, from which the definition for the 'impossible' platforms is found. Afterwards the 'impossible' platforms are checked in the Allseas database and finally a conclusion is drawn.

DEFINITION OF IMPOSSIBLE PLATFORMS

The *PS* has a special designed hull shape. The shape is described as a catamaran hull bow with a rigid body attached to the twin hull front side. This creates the possibility to enclose a platform with the double bows, as can be seen in Figure 1.5. To perform this enclosing action the substructure has to fit in the slot of the *PS* and the topsides has to comply with the lifting installation dimensions and requirements of the vessel.

Figure 1.5: The Pioneering Spirit.

Table 1.1: Boundaries of the Pioneering Spirit topsides lift system. The impossible conditions are hard limits and the difficult conditions imply that it is possible if other parameters are favourable.

Condition		Impossible		Difficult
Length	>	95 m	>	85 m
Width	>	52 m	>	47 m
Weight	>	30.000 ton		
Air gap	<	15 m		
Water depth	<	30 m	<	40 m

The boundaries for a lifting operation of the *PS* consist of five categories: length, width, weight, air gap and water depth. The first two are related to the size of the slot and the configuration possibilities of the lift system. The third and fourth are related to the topsides lift system and loading conditions on the vessel. The latter is derived from the draft of the vessel. The boundary values are listed in table 1.1, these values are set by Allseas engineers that are working on the design of the *AG*. The weight boundary is also dependent on the width and mass distribution of the platform. When a platform is very small,the arms of the lifting system are operating outside their maximum range. Some boundaries are compiled from a combination of factors, for instance the water depth because this value is also related to the available air gap. To draw a conclusion limits had to be set and therefore the exceptions are not taken into account.

These values are set as the maxima. To be able to lift a platform there are a lot of considerations to take into account, for example: the shape of the substructure is not always rectangular. Some substructure are triangular, which results in an increase in lifting arm that decreases the lifting capacity. In this analysis only the maxima as defined in 1.1 are considered.

DATABASE ANALYSIS

The database used for this research is compiled by Allseas and contains gathered information of all topsides worldwide. The data is mainly focussed on the North Sea, in the rest of the world most values are estimated. For instance, when looking at the air gap criterion, more than half of the gaps are unknown. Therefore, the numbers extracted from this database are used as guidelines since there can be more/less platforms in the category after detailed studies. Additionally, only platforms over 10.000 tons are considered since light platforms are not lucrative to remove with high-tech solutions.

In the origin it is stated that a lot of the platforms that are impossible with the *PS* are installed using the floatover technique. The database contains 34 platforms installed with floatover and twelve are impossible with the *PS*. From this 34 platforms, 10 platforms contain detailed information and for the other 24 platforms essential data to link them to categories is missing.

When looking into the locations of the floatover platforms it is found that 7 platforms are installed in the West-African region, 20 in the Asian region, 4 in Australia and 3 in Russian waters. The majority of the installations is done in the Asian region; this makes sense since this region has milder sea states which significantly improves the workability of the floatover operations. The 7 operations in the African waters confirms the potential of the African market.

From this 7 African platforms 3 are impossible for the *PS* and the other 4 lack information. Using images of these platforms is concluded that it is highly likely that more of them are *PS* impossible. The Amenam AMP-1 platform, which is shown in figure 1.6, is impossible for the *PS* due to the air gap of the platform. The 4 remaining West-African platforms are assessed on their width to air gap ratio, 3 are concluded to be impossible for the *PS* and 1 platform is inconclusive. Therefore, 6 out of 7 of the West-African floatover installed platforms cannot be removed with the *PS*.

CONCLUSION

In the origin is stated that a significant amount of platforms installed with floatover cannot be removed by the *PS* and that several of these are situated in West-Africa, the Allseas platform database is used to assess this suspicion. The database showed at least 12 platform can not be removed by the *PS* and that six out of seven

Figure 1.6: The Amenam AMP-1 production platform installed in Nigeria, from (Amenam). The only available information about this project is the installation vessel, the Dockwise Mighty Servant 3. This vessels has a width of forty meters. Looking at the width/air gap ratio it can be estimated that the airgap is smaller than 15 meters.

West-African platforms are impossible with the *PS*. This is a viable basis for the investigation of an alternative decommissioning method. Especially when considering that the market for floatovers is growing and thus all future installations are added to this potential.

1.2.3. WEST-AFRICAN SWELL

In this section the West-African swell is investigated. The metocean database of Allseas is used to find the relevant data of this region. After this analysis, the maximum sea states of current floatover techniques are given and compared to the sea states of different countries. Added to these results are some possible improved scenarios and the correlating workability rates. Finally, a conclusion is drawn on the West-African swell.

METOCEAN DATABASE

To find representable characteristics for the West-African region, multiple locations are assessed to check for local statistics. The Metocean database of Allseas contains information of Angola, Congo, Equatorial Guinea, Nigeria and Ghana. These databases contain a variety of information and not every data file consists of the same type of information. For most of the locations data is available on the behaviour of wave heights in every month and wave heights versus peak periods, which is the data required for the swell analyses.

Most of the areas supply a chart of the significant wave height versus the wave peak period, which is the essential information for motion characteristics. These charts provide all year long omnidirectional numbers. From these charts the workability numbers can be extracted, this can be done for the all countries.
To identify the seasonal differences less sources are available. Specific wave heights per month data is available for Congo and Ghana. Wave direction data is available for Congo, Ghana and Nigeria. The year-round scatters for these locations are gathered in Appendix A.4.

WORKABILITY EXPECTATIONS

When considering a conventional floatover operation the limits of the sea state are low. In Yuan et al. (2013) the installation conditions for the SHWE topsides is given, the SHWE topsides of 26,000 tons is installed in the benign South China Sea. The maximum sea states for this operation are listed in table 1.2. When combining this information with the Metocean database, the workability of the conventional technique in West-Africa is found and displayed in 1.3. The numbers show that that the conventional floatover limits have a large downtime in most of the West-African sea states. It also shows great diversity of the workability rates for the different countries.

In Tribout et al. (2007) it is stated that the maximum sea state for the Technip floatover operation is characterised as shown in Table 1.2, unfortunately no details are given surrounding the exact definition of the period.

Table 1.2: The allowable sea states for the SHWE and Technip installation, installed with the conventional and UNIDECK technique respectively. Scenario 1 & 2 are indications of allowable sea states for a heave compensated installation, these are used to check the possible gain in workability.

SHWE		Technip		Scenario 1		Scenario 2	
H_s [m]	T_p [s]	H_s [m]	T_p [s]	H_s [m]	T_p [s]	H_s [m]	T_p [s]
1.0	8-18	1.50	3-10	1.75	3-10	1.75	3-10
0.5	18-22	1.25	10-14	1.5	10-14	1.5	10-16

Table 1.3: Workability rates of the SHWE and Technip installation for multiple location of West-Africa. Based on omnidirectional, all-year data. The workability values are derived using the allowable sea states of Table 1.2. Scenario 1 & 2 indicate the possible gain in workability when the heave compensation system is able to reach the allowable sea states indicated in the previously mentioned table.

Location	SHWE	Technip	Scenario 1	Scenario 2
Angola	56 %	68 %	72 %	88 %
Congo	4 %	34 %	54 %	60 %
Eq. Guinea	31 %	89 %	95 %	95 %
Nigeria	19 %	63 %	73 %	81 %
Ghana	9 %	59 %	78 %	85 %

Therefore, the period is assumed as the peak period because this is the most common notation. The results of these limits show significant improvement in relation to the SHWE characteristics. When analysing the limits with respect to the African Sea the workability rates are found. The rates show a significant improvement with respect to the conventional floatover scenario. Since these are year-round values the workability can still be low in the winter season. The Ghana database contains monthly sea state information, from this data the difference between summer and winter season is extracted. Looking at the workability for the Technip case the year round value for Ghana is 59%, in February (African Summer) this rate increases to 83%. However, in July the workability drops to 38%. This indicates the large fluctuations in workability in comparison to the all-year value.

To compare the workability of Technip, two scenarios are tested to check the difference with the Technip workability. The difference in allowable sea states of these scenario is shown in Table 1.2 and the corresponding new workability numbers are given in Table 1.3. The changes in the allowable sea states are small whilst the improvements in workability are significant. The two scenarios lead to an average increase of 10 and 20 percent respectively.

CONCLUSION

It is concluded that the workability rates in West-African swell are not that bad. However, significant profit can be made by increasing the workability such that a year round installation can be made realistic. The advantage is that small delays in other factors do not significantly impact the first oil date. Therefore, the conclusion is that the West-African swell is worth considering a better installation technique.

1.2.4. HEAVE COMPENSATION

In this section the current possibilities with heave compensation systems are analysed. Firstly, by looking into the available methods for heave compensation. Secondly, by analysing the heave compensation system of the *PS*. Finally a conclusion is made over the heave compensation possibilities.

HEAVE COMPENSATION SYSTEMS

In the current offshore market multiple applications for heave compensation systems are used, varying from human transport (Figure 1.7a) to the stabilisation of structures (Figure 1.7b). In these systems a distinction is made between passive and active compensation systems. The passive heave compensation (PHC) systems

use stored energy to perform the motion compensation, where active systems use a controlled actuation system. The two techniques can be combined to a semi-active system.

(a) The Ampelmann system is built to compensate the motion of the vessel to safely transfer employees and supplies. It consists of six hydraulic cylinders that compensate 6 degrees of freedom. The cylinders react on the motions of the barge and stroke in order to keep the platform stabilized. Therefore, this is an active heave compensation system.

(b) A cranemaster is placed between a crane and the load, the system is then tuned to compensate to motions of the crane. This enables a constant hoist speed and decreases the impact loads. With the tuning of the system the dynamic characteristics of the cranemaster are changed such that the motions are cancelled adequately. No power is added to the system, hence, this is a passive heave compensation system.

Figure 1.7: Two examples of heave compensation systems. Illustrating the different functions, human transport and stabilisation of loads, and the different types, passive and active, of heave compensation systems.

The most basic principle of passive heave compensation is shown in figure 1.8. The combined cylinder/gas system acts as a spring. When the vessel has a positive displacement, the force in the rope will increase, that leads to increased loads on the cylinder, which causes retraction of the piston. This retraction can be controlled with the working pressure and volume of the gas bottles. Since this system stores the energy, the piston will extent to the original position when the vessel moves back down to the water line.

The principle shown in figure 1.8 can be used to compensate lifting loads. Most of the available motion compensation techniques are used for lifting purposes. This is mostly done by either a compensator in the wire of the lifting application or a compensator in the crane used for the lifting operation. Currently, there are two companies that compensate the motion for an area: Ampelmann (1.7a) and Barge Master (1.7b). These techniques are interesting to investigate when considering potential systems for motion compensation. Ampelmann is typically used for the transport of people and Barge master is designed to compensate motions for cargo transfers. The systems are designed for maximum loads of 100 ton and 700 ton respectively. Even the largest available heave compensation system is thus designed for loads fifty times smaller than the *PS*.

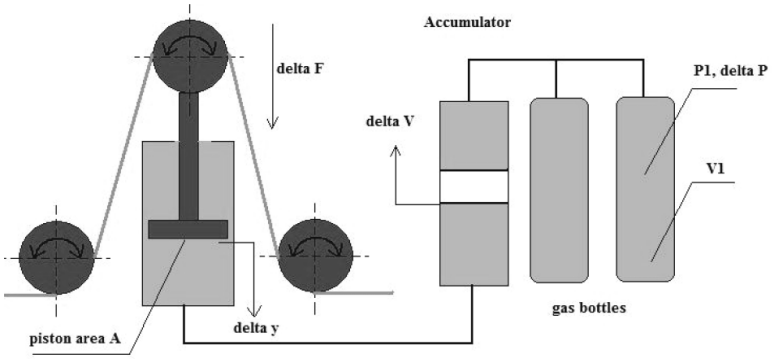

Figure 1.8: The basic principle of passive heave compensation for hoisting loads, from (Herdzik, 2014). The cable is placed over the piston pulley such that it exerts a static force due to the tension in the cable. The piston stroke is such that this static force is compensated. When the vessels move this static force gains a dynamic component. This dynamic component creates a stroke in the cylinder that compensated the motion of the barge. The actuation is done with the pressurized air, this also leads to the restoring characteristics of the compensation system.

The barge master system stabilizes a surface with the main purpose of transferring heavy loads offshore. The platform can stabilize the load such that it can be picked up from the other vessel/structure or such that a crane can be placed on the barge master that creates a stabilized crane tip.

PIONEERING SPIRIT HEAVE COMPENSATION

The *PS* contains a lifting system that is able to lift loads up to 48.000 tons. To cope with these loads the system consists of 16 lifting beams. In each beam an extensive system of hydraulic and pneumatic power is capable of performing multiple modes of operations. The two most important elements are the passive and active cylinders. The passive lift cylinder is capable of performing a fast-lift or quick lower of the topsides from/on the substructure. The active cylinder compensates the vessel motions to ensure correct placement of the yokes and minimal impact loads during the connection of the vessel to the topsides.

The vessel is not designed to actively compensate the topsides, the aim is to compensate the lifting lever motions before the topsides is attached to the beams. Therefore, the motion compensation system needs to be able to cope with the loads of the lifting levers and the dynamic contributions of the vessel. Since the *PS* is capable of creating sufficient clearance between the topsides and substructure with the fast lift system, no compensation of the topsides is required after lifting.

For this thesis the lay-out of the *PS* is very informative, because detailed information of heave compensation systems in not available in literature. A detailed study of the lifting system is performed, this creates useful insights in the advantages and disadvantages of heave compensation.

CONCLUDING

The current offshore market is familiar with heave compensating systems. However, no implementations are known in the same order of magnitude as required for topsides compensation, which is an incentive for this research. It might also imply that there are certain limitations to these operations that make the implementation unrealistic. There is no reason to believe the latter and therefore research is worthwhile.

2

PROBLEM DEFINITION

2.1. AIM

This research focusses on the relative improvement of a heave compensated floatover operation, no previous research on this topic is performed. Therefore, the amount of subjects that can/should be investigated is large, thus a framework is made to limit the scope. Firstly, this section elaborates on the goal and research questions, followed by an elaboration on the chosen aim.

2.1.1. MAIN GOAL AND RESEARCH QUESTIONS

The main research question identifies the goal of this thesis. To answer this question sub-questions are defined. To fit the questions in the time period of a graduation thesis, the scope is clearly delimited as is detailed in the next section.

The main goal is defined as:

> Investigate the added value of implementing heave compensation in a floatover operation considering swell dominated seas, using a system that is able to perform operations on platforms that are considered impossible with the *PS*.

This aim is supported by the following main research question:

> Does the implementation of heave compensation on a barge improve the workability of a floatover mating operation such that it increases significantly in swell conditions?

To process is guided by answering the following sub-questions:

- What are the installation limits during a floatover installation?
- What is the most suitable heave compensation concept?
- How does this concept influence the topsides and barge motions?
- What would be the ideal heave compensation parameters?
- How large would the heave compensation system become, in terms of weight and footprint?

2.1.2. CAUSE

The most effective floatover method in the current market is the UNIDECK technique from Technip. The UNIDECK technique creates an increase in workability mainly due to the significant decrease in ballast time, and thus operation time. Hence their concept is better applicable in swell conditions than conventional floatover method. Essential for the viability of heave compensation is whether the technique creates an improvement in workability such that it makes the more expensive operation a profitable option.

It is expected that the offshore floatover market will grow significantly, especially for heavy topsides. From 2005 to 2012 more than 33% of the heavy topsides (> 12.000 tons) were conducted with floatover and the expectations are that between 2014 and 2018 more than 52% of the heavy topsides will be installed with floatover operations, this is claimed by (Martinez). These expectations increase the commercial value of a high-tech solution. In the coast of West-Africa the floatover market is also growing, based on the increased number of platform installations last 20 years (this information is derived from the internal database of Allseas). Therefore, a heave compensated barge can be a lucrative solution for installation in swell dominated areas.

Combining the conclusions above with aspects as presented in the introduction chapter it is concluded that the heave compensated floatover concept is a promising concept that can become lucrative if the gain in workability is significant in relation to the competitors. Therefore, the aim of this thesis is set on determining the gain in workability.

2.2. SCOPE AND DEMARCATIONS

The focus of this thesis is determining the workability gain due to the Heave Compensation System (HCS). In order to find a substantiated result demarcations are made to frame the focus and to aid the aim of the thesis. In this part the demarcations, boundaries and assumptions are presented and elaborated on. A division is made between operational settings, heave compensation design and floatover approach.

2.2.1. OPERATIONAL SETTINGS

The operational settings determine the circumstances of the floatover operation. This implies that the operational settings describe the scenario where the operation takes place, including the type of sea and platform. To determine the effects of the heave compensation settings, a test scenario is created on a fixed platform, known location and a single barge. The settings are divided in two main components: the sea state and the topsides characteristics.

The **sea state** used in this thesis is based on African swell, this contains unidirectional long waves with a maximum significant height of 2 meters and a peak period up to 20 seconds. The exact location is set on the Nigerian sea, where the most heavy offshore platforms of Africa are present (according to the platform database of Allseas).

The considered **topsides** for the heave compensated floatover operation is the `Liwan 3-1` topsides, which is installed using a classic floatover operation in the South China Sea. The ensure that the test scenario contains the platforms that the *PS* is not able to operate, four conditions are defined. For the `Liwan 3-1` scenario all these conditions are satisfied. The four conditions are defined as:

- **Weight over 10.000 tons**
  Heavier platforms are more expensive to install, this is a more beneficial environment for advanced installation techniques.
- **Small airgap**
  The *PS* is unable to install/decommission topsides with a small airgap.
- **No maximum dimensions**
  To ensure that this concept can handle all platforms that are not in the scope of *PS*, it is assumed that no maximum dimensions of the topsides are present. Hence, a large platform is used as test scenario.
- **Shallow water**
  The small-airgap and west African platforms are often installed in shallow water. Since the water depth influences the motions of the vessel, shallow water is set as an operational parameter.

To ensure that the **barge** is capable of installing the `Liwan 3-1` topsides, the barge used for the `Liwan 3-1` installation is used for this study: the `HYSY229` barge from the CNOOC. An advantage of this is that the available literature of the `Liwan 3-1` installation contains this barge and topsides configuration. The characteristics of the `HYSY229` are given in Appendix A.2. The scenario used in this thesis is shown during the mating phase in Figure 2.1, however it is placed in swell sea states.

Figure 2.1: The Liwan 3-1 topsides on the HYSY229 barge, just before the mating procedure is started. The heave compensation system will be tested according to this scenario. The main difference is the swell sea which causes more motions of the barge and thus decreases the workability.

2.2.2. HEAVE COMPENSATION DESIGN

The design of the heave compensation system has to be clearly delimited. The aim is to determine the possible gain in workability, thus no detailed design is required. Also, a detailed design is not possible due to the extent of a heave compensation system. Thus, boundary conditions are set for the extent and implementation of the system. The following features are applied in this thesis:

- **The barge is considered as a rigid body**
  This implies that the increased deck loads due to the HCS do not affect the structural integrity of the barge.
- **The HCS must be adjustable for multiple topsides layouts**
  The system must be implementable for all topsides dimensions to ensure that the concept is viable for platforms outside the used setting.
- **The HCS is rigid**
  The assumption is made that the heave compensation system will be able to cope with the loads of the installation. The limiting loads cannot be derived, because no detailed design of a heave compensation system in this order of magnitude is available. Therefore, no structural failure of the heave compensation system is considered.

2.2.3. FLOATOVER APPROACH

The floatover procedure consists out of five stages, each of them containing bottlenecks that affect the workability of the procedure. In this thesis the HYSY229 barge is considered as the basis for the heave compensation design; this barge is proven capable of all five stages of the floatover operation. Therefore, certain demarcations can be set to focus on the main goal of this thesis.

- **Only the mating stage considered**
  In the mating stage the topsides is installed on the substructure. This is the stage where heave compensation is used to decrease the loads on the structures. Hence, it is the most valuable stage for heave compensation implementation. These settings greatly determine the used criteria for the workability determination, therefore, a substantiating is given in the next chapter.
- **Mooring analysis not included**
  Docking in floatover operations is often done with a mooring operation. During the mating stage these mooring lines are still present in the system. In this thesis these effects are not taken into account.
- **No barge surge, sway and yaw motions considered**
  The barge is moored in the slot of the substructure, hence the motions in the horizontal plane are limited. To limit the scope of the thesis these motions are considered insignificant in relation to the heave, roll and pitch of the barge.

2.3. METHODOLOGY

In this section the process and reasoning behind the thesis is described. During the process a lot of sidesteps were made in order to understand the different elements of the problem. These sidesteps were useful for the understanding of the different elements of the system, in this report only the relevant steps are considered.

After the literature study, the possible concepts for the heave compensation system are gathered. The out-of-the-box ideas are listed and their expected performance is assessed. From this assessment a single concept is chosen for the rest of the research.

To assess the workability, limiting conditions need to be determined. This is done by analysing the floatover operation. In this analysis the focus is put on finding a single most critical load, from this the limiting condition is specified. Using this limiting condition the heave compensated scenario can be tested with the `Liwan 3-1` installation to find the gain in workability.

Knowing the limiting case, the heave compensation system can be detailed. This is done by extracting the important elements, these elements are used in the model. The kinematics of the procedure are assessed, thereby identifying the strengths and weaknesses concerning these kinematics. With this information the heave compensation system contains enough detail to assess the workability.

After this stage, a model to identify the response of the vessel in the interface between the barge and topsides is made to analyse the motions. The frequency domain is used to analyse the response with a simplified linear system. With this model the optimal values for the characteristics of the heave compensation system are determined and basic dimensions for the system are determined.

With the model the workability can be calculated for different sea states. These results can be compared for different settings and compared with the conventional techniques. From these results the thesis is finalized with conclusions and recommendations.

3

FLOATOVER LIMITS

In this chapter the floatover procedure is analysed. Herewith, the critical installation stages are determined. From these critical stages, criteria are derived that are used as maximum values in the workability calculations. By comparing results for the base case model with results for the heave compensated model the possible improvement of the heave compensation system can be found. The mating stage is considered to be the limiting stage, this chapter starts by detailing the different stages of the floatover operation. Secondly, the main components during the floatover mating operation are examined, where the weakest component is identified. Thirdly, the derivation of the limit for the mating stage is given based on the weakest component. Where attention is given to the modelling approach for this limit.

3.1. OVERVIEW OF THE METHOD

The floatover installation contains a lot of limiting factors. For the comparison between the `Liwan 3-1` installation and the heave compensated installation, the most governing loads are used as installation criterion. The governing loads are determined by analysing the different floatover stages. The components of the most critical stage are then examined. The limiting loads are found by detailing this most critical component. This process is illustrated in Figure 3.1.

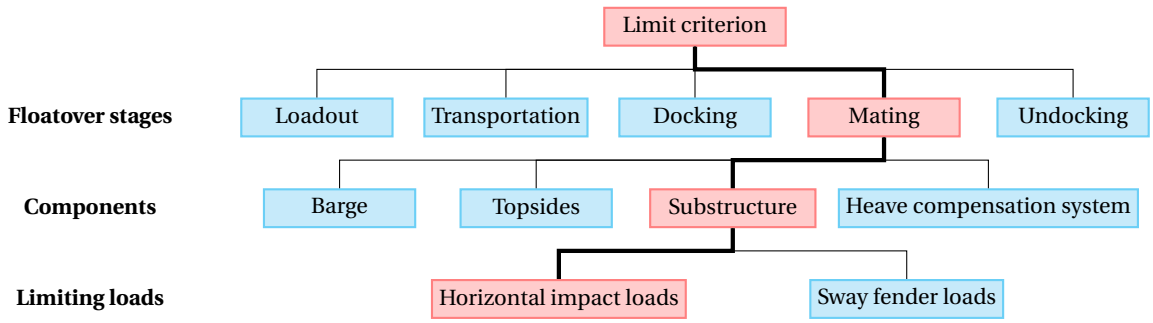

Figure 3.1: Flowchart that illustrates the derivation of the installation limit. The red square indicates the most critical elements. First, the floatover stages are considered, afterwards the components of the most critical stage are examined. This leads to the identification of the limiting loads of the most critical component.

3.2. THE FLOATOVER STAGES

A floatover installation/decommissioning operation contains five stages, these stages are given in Section 1.2.1. To improve the workability of the operation there are two possibilities: decrease the required operation time or increase the maximum allowable sea state.

The critical stages for the operation time are the transport and mating stage, the allowable sea state differs for all stages. The allowed sea state in the transport phase is much higher than during the mating phase. For the load-in stage the allowed sea state is low, but the operation can be done in sheltered waters and is thus not critical. Because of these reasons, the best progression can be made in the docking, mating and undocking stage. When considering the function of the heave compensation system, the mating stage is the only stage, of these three, where the operation is significantly influenced. Therefore, the focus is on the mating stage and the limiting factors of the other stages are not taken into account.

3.2.1. THE MATING STAGE

In this section the mating procedure is described. During the mating stage the topsides load is transferred from the barge to the substructure. The procedure starts when the barge is positioned correctly in the slot of the substructure, the mating lines are tensioned and the barge is correctly ballasted. From this point ballasting continues, causing a draft increase of the barge, and the topsides are lowered on the substructure legs. During the load transfer some characteristic effects take place.

Firstly the characteristic effects of the `Liwan 3-1` mating are given. Then the `UNIDECK` technique is analysed to see how the mating stage is effected by high-tech techniques.

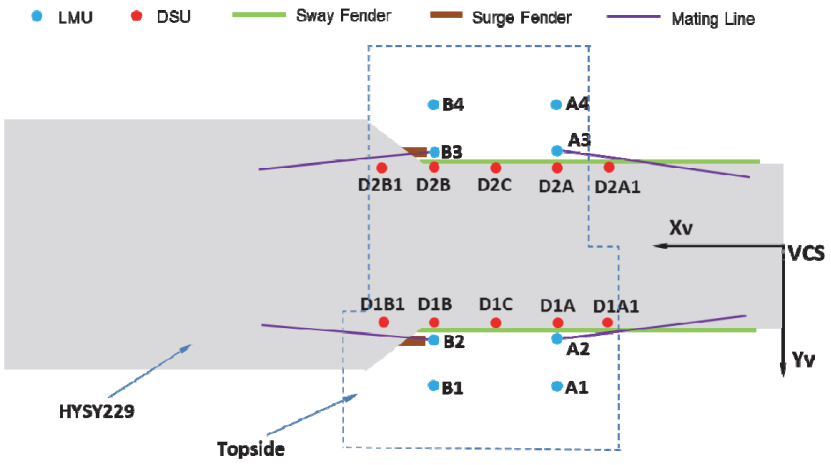

Figure 3.2: The overview of the `Liwan 3-1` floatover operation. The sway fenders leave a gap between the barge and substructure and the surge fenders are kept against the substructure with the mating lines. Additionally mooring lines are used to keep the barge in position, these are not shown in the figure.

LIWAN 3-1 MATING PROCEDURE

For the `Liwan 3-1` operation the mating procedure consists of three main topics: the barge horizontal motions and position, the ballasting procedure and the mating loads. Each of these elements is detailed in the following paragraphs.

The horizontal motions of the barge

The final position of the `HYSY229` during the `Liwan 3-1` installation is shown in Figure 3.2. This figure also includes the substructure leg positions, the fenders and mating lines. This arrangement decreases the impact loads on the substructure and restricts the barge from (significant) movements in surge sway and yaw directions. The allowable motions of the barge depend on the gap between the barge and fenders and the stiffness of the fenders and mooring lines. In Hamilton et al. (2008) the effect of the gap between the fenders and the barge on the loads is investigated. This research shows that a bigger gap leads to higher impact forces. Hence the gap of the barge in the horizontal plane should be minimized in the design phase. However, for the docking operation a bigger gap is favourable since this increases the feasibility of the docking stage. A trade-off between these two criteria must be made for the fender gap. In the thesis the gap is assumed small enough to neglect the motions of the barge in surge sway and yaw direction.

The ballasting procedure

Ballasting the barge is the most time consuming part of the operation. Yuan et al. (2014a) reports that the original ballasting operation for the Liwan 3-1 operation takes 6 hours and 14 minutes. Decreasing the ballasting duration also decreases the chance on critical waves. Hence, increases the workability.

The draft increase due to the added ballast weight creates multiple stages in the ballasting procedure. In the first stage, illustrated in Figure 3.3a, the ballast causes the draft to increase, this decreases the distance between the topsides and the substructure legs. During this phase collisions between the topsides and substructure occur occasionally, due to the wave induced motions. As this phase proceeds the collisions become more frequent.

If the barge is ballasted enough continuous contact between topsides and substructure occurs, Figure 3.3b. The ballasting still continuous, the loads of the topsides are being transferred onto the substructure. This also decreases the loads on the barge. During this stage the barge and substructure move as a single body.

When enough ballast is pumped in the barge the topsides load is fully transferred onto the substructure. Once this is completed the deck support frame uncouples from the topsides and collisions between the deck support frame and topsides can occur, due to the wave induced motions. Ballasting continuous until enough clearance is created to avoid these collisions, finally the position of Figure 3.3c is reached.

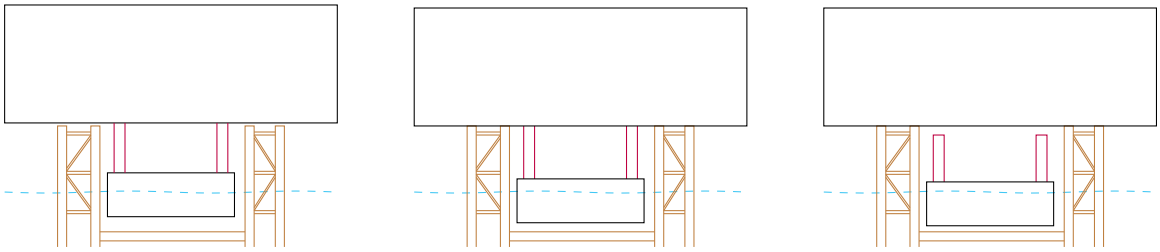

(a) Start of the mating operation. Ballasting sequence starts when the barge motions are in the allowable range.

(b) Middle of the mating operation the barge and topsides now move as a single body. The topsides loads are partially transferred. Ballasting of barge continues.

(c) Final stage of the mating operation. Topsides load fully transferred, barge is now filled with ballast. If the clearance is sufficient the undocking procedure starts.

Figure 3.3: Schematic overview of the mating phase. Ballasting of the barge increases the draft, that leads to contact between the topsides and the substructure. When the ballasting sequence is completed the topsides weight is fully transferred and the undocking phase commences.

Loads in the mating phase

The most critical phase of the mating operation is the first part, where occasional collisions between topsides and substructure take place (Yuan et al., 2014a). During this collisions the topsides can have a large impact that lead to significant loads. In Yuan et al. (2014a) is found that the maximum loads on the substructure are the horizontal loads on the substructure legs. More precisely, the total horizontal loads acting on all the substructure legs. The impact loads of the topsides can cause large forces on the substructure legs. Therefore, these impact forces are found as a limiting load case in the mating stage.

Once the topsides is in continuous contact with the substructure, the horizontal forces decrease and the motions of the barge decrease due to the semi-rigid connection with the substructure. Until this continuous contact occurs, the chance on bouncing effects of the topsides is significant. The bouncing effect implies that the connection between the topsides and substructure legs is lost and a new impact scenario can occur. These bouncing effects can occur until sufficient weight of the topsides is transferred onto the substructur, which takes a significant amount of time. This makes it probable that a large motion occurs during this part of the mating stage. Therefore, there is a high probability on large impact loads.

UNIDECK TECHNIQUE

Technip has created the UNIDECK technique that significantly reduces the installation time and increases the allowable sea states during the topsides installation procedure. They have successfully installed a 18,000 ton topsides using this technique. As explained in the introduction the UNIDECK technique consists of a hydraulic system that lowers the topsides. This enables the topsides to engage with the substructure in a couple

of seconds. Additionally, the probability on high impact forces is reduced, because the bouncing effects (as explained in the previous paragraph) are omitted with the fast load transfer of the hydraulic stroke. Consequently, the stroke is used to decrease the total amount of ballasting time. The effect on the total workability thus works at both ends, making it an effective method.

The UNIDECK technique is further evaluated based on two topics: the effects of the lowering the topsides and reduced impact that can be obtained by timing the stroke correctly.

Lowering the topsides
The fast load transfer is realised by positioning the barge such that the stroke is greater than the clearance, hereafter the full stroke is used to lower the topsides. The extra length of the stroke causes the LMU's to compress such that enough load is transferred to keep continuous contact between topsides and LMU. The effect of this increased touchdown speed is that the motions of the barge can be used, if timed correctly, to decrease the maximum loads during installation.

Reduced impact method
To clarify the latter, the scenario of touch down is sketched for a barge with a sinusoidal heave motion. When the conventional procedure is used, the first impact will most likely occur during the lowest point of the barge's motion. When the barge moves upwards the LMU's disconnect and another impact occurs when the barge is close to the lowest point. These impacts are not critical since the velocity of the topsides is close to zero at the lowest point of the sinusoidal motion. The critical impacts will take place when the barge draft increases and the touch down occurs during the 'zero-crossing' point of the sinusoidal motion, this point contains the maximum velocity of the topsides. When using the UNIDECK technique this can be omitted; the possible stroke of the system is greater than the amplitude of the barge movement. Thus when timed correctly, the stroke can be used to minimise the velocity of the impact by stroking whilst the barge is in upwards motion. This decreases the maximum impact forces and thus increases the workability of the mating operation.

3.2.2. THE OTHER STAGES

In order to assess the feasibility of the final solution, the limiting factors of the full operation are assessed. In the literature study it is found that for the different stages (except the mating) the limiting factors are defined as:

Loadout
The workability of the loadout is not dependent on the wave height. Since the loadout occurs in sheltered waters. In Seij and de Groot (2007) is stated that the requirements for the load out stage are governed by:

- Integrated deck weight
- Tidal range
- Quayside dimensions

These governing factors are only related to the geographical location and not to the present sea state. Therefore, the workability in this stage can not be improved with this solution. Also, it is assumed that this stage already has a high workability.

Transportation
For the transportation phase the limits are governed by the stability of the barge, which is highly correlated to the presence of the topsides since the centre of gravity of the topsides is above mean sea level. Due to the large weight of the topsides, eccentrically positioned on the barge, the structural integrity of the barge is the main concern. Seij and de Groot (2007) states that the ship stability is determined by the width and depth of the barge. However, these parameters also determine the required space in the substructure for the mating procedure. Therefore, an optimum has to be found between the dimensions of the barge and the required stability.

The stresses in the HYSY229 barge during the transport phase are analysed in Li et al. (2013). They concluded that the modified design of the HYSY299 is able to withstand the impact forces of the topsides up to a significant wave height of 7.4 m in beam seas, which is much higher than the swell waves in Africa. However, no period of this wave is given, therefore, a precise comparison cannot be made. Despite this lack of information the transportation phase is still not considered a limiting phase, because the wave height is much higher than the African swell.

Docking
During the docking procedure the barge is placed between the substructure. This is a very critical phase since lateral movements of the barge can cause high loads on the substructure legs. The resistance of the substructure to lateral loads above the sea water level is limited, because the need for a slot in the substructure causes a low resistance to these loads. In Seij and de Groot (2007) is found that the following principles need to be closely monitored during the docking phase:

- Alignment of vessel stern with jacket slot
- Lateral impact loads on the jacket not to exceed limit loads of jacket and fendering arrangement
- No vertical impact loads between deck legs and jacket legs
- Control over the movement of the vessel in longitudinal direction as well as control over the alignment of the vessel

During this phase the fendering arrangement and lateral resistance of the substructure are critical for the allowed sea state. The maximum sea state in this stage is in the same order of magnitude as the mating phase, because the barge impact on the substructure during the mating phase is comparable. In the demarcations of this thesis it is stated that the mooring and fendering arrangement of the installation will not be taken into account. This demarcation is made since the analysis of this arrangement in combination with the docking procedure is too extensive and will not significantly contribute to the research question. This analysis is very important for the workability calculations of the operation but will not be implemented in this thesis. It is important to reflect to the importance of the docking phase when concluding on the effectiveness of the heave compensation system.

Undocking
In the undocking stage the same criteria should be taken into account as the docking stage. However, the topsides is already installed, thus the loading conditions are different. In addition, the clearance between deck and topsides should be sufficient. This stage is still comparable to the docking stage and is subjected to the same reasoning as presented in the previous paragraph.

3.2.3. THE DOCKING ALTERNATIVE

This research focusses on the mating stage. In order to increase the operation workability, the installation should also be able to withstand higher sea states during the docking and undocking procedure. This topic is not thoroughly investigated, however, some ideas are considered that should be able to increase the workability during these stages. The classic floatover overview looks like Figure 3.2 from which can be seen that severe sea states will cause large forces on the jacket legs due to the combined surge, sway and yaw motions of the barge.

Assuming the topsides is kept in the correct position with the heave compensation system, the installation can be done without the use of fenders. This requires the substructure to be designed with a wider slot and the barge to be equipped with a dynamic positioning system, this probably leads to the usage of a vessel. A dynamic positioning system is required to prevent contact of the barge with the substructure. This scenario is expensive and the dynamic positions system might provide a new set of problems. However, this solution has the potential to greatly improve the overall workability of the system.

3.3. COMPONENT LIMITS

The different components of the `Liwan 3-1` mating operation are the barge, topsides, substructure and the interface. The interface in the `Liwan 3-1` installation is the deck support frame, designed to carry the topsides load. The heave compensation system replaces the deck support frame. In this section the expected limits of the components are given.

Each body has different limiting characteristics, therefore, the bodies are evaluated individually in this section. The barge and topsides are assumed not to contain limiting factors and the substructure and interface are considered the critical bodies. The derivations of these conclusions are listed in this section.

The barge
The barge is continuously subjected to the forces of the waves and the topsides. This dynamic loading case, where a large mass accelerates over a large distance from the center of gravity of the barge, leads to large stresses in the hull of the barge. As stated before the structural integrity of the barge is checked by Li et al. (2013), for high beam sea conditions ($H_s = 7.4m$). Unfortunately, the paper does not include the period at which this wave height is tested. Thus it is not possible to compare the motions of the barge to the possible motions of the African swell. Since the African swell is unidirectional it is assumed that the significant roll motions can be omitted. Therefore, the remaining motions and correlated stresses should be comparable to the tested beam sea conditions.

During the mating procedure to barge is subjected to the spring forces from the fendering arrangement. These loads are evenly distributed over the hull of the barge. The weak objects in the fendering arrangement are the substructures legs, which will fail before the hull of the barge does. Therefore, the barge does not contain relevant limiting values.

The topsides
During the operation, the topsides load is transferred to the substructure. The topsides is designed for this final, installed, position. Due to the shape of the topsides, the stiffness of the topsides is large relative to the stiffness of the substructure, especially in the horizontal plane. The forces of the topsides are transmitted through the jacket via the interface. Consequently, the jacket and interface are subjected to much higher deformations and thus the topsides can be assumed rigid.

The substructure
When the platform is in place the horizontal loads on the substructure are determined by the wind and wave loading. Wave loading can be very high and thus the bottom of the structure is designed to withstand large loads. The part of the structure above water is only subjected to wind loads that are, usually, significantly lower. Thus the upper part of the substructure is not designed to cope with very high loads. These loads can occur during the installation, especially on the top of the legs where the Leg Mating Units (LMU) are placed.

In Yuan et al. (2014b) the maximum value of the total horizontal loads on the substructure is given as 800 tons. In their analysis of the float-over installation, the maximum total horizontal loads where 623 tons, in a mild sea state. The second element of the substructure are the sway-fender loads in the docking stage of the float-over installation, this is found in Yuan et al. (2014a). The loads on the fender during docking exceed the maximum value during the beam sea with long wave lengths. Therefore, the substructure is expected to be the leading element in the float-over workability improvement.

The barge-topsides interface
In this research a heave compensation system is placed between the barge and topsides. This leads to relative motions between the barge and topsides which in their turn lead to forces in the heave compensation system. These forces cannot lead to failure of the system or affect the stability. Besides the structural strength, the interface has to provide the required compensation, thus the reaction speed and accuracy of the interface is important. So, the interface element contains failure conditions and kinematic conditions, whenever the kinematic conditions are not met the workability does not increase as expected. However, these conditions are dependent on the detailed design of the heave compensation system. This is not the aim of this study.

Therefore, the heave compensation system limits are not taken into account. Additionally, since the design is not yet made, the assumption is made that the design can be altered to deal with the potential limits of the system.

In the `Liwan 3-1` procedure the interface is the deck support frame. The support frame consists of a steel frame structure that is skidded onto the barge in the load out stage. The topsides is placed onto deck support units that act as springs during the load transfer of the topsides. The deck support units are used to decrease the impact loads during the uncoupling of the topsides and deck support frame. The deck mating units are the limiting factor of the deck support frame, specifically the horizontal loads. However, failure of these units can only occur when the topsides is already installed. Even though this is still unacceptable it is not considered a design criterion for this thesis, since the stroke of the `UNIDECK` technique can be used to bypass these impact loads.

3.4. SUBSTRUCTURE LIMIT

The different elements of the floatover operation are analysed. The installation limits are most significant in the mating stage and on the substructure component. In Yuan et al. (2014a) is found that the substructure in the mating phase contains two critical loading conditions: the horizontal loads on the substructure legs and the sway fender loads. This research does not incorporate the horizontal motions of the barge, as determined in this chapter. Additionally, a heave compensation system does not effect these loads. Therefore, the horizontal loads on the substructure legs are taken as the governing loads. The derivation of the limiting value of this loading condition is done in two steps: by looking into the leg mating units and determining the substructure characteristics. Finally, the approach to derive the limiting loads is summarised.

3.4.1. LEG MATING UNITS

Leg mating units(LMU) are placed on the substructure, or topsides, legs to decrease the impact forces during the installation procedure. The second function is to guide the leg to the correct position, this is done with the cone and receptacle design. LMU's consist of stiff elastomeric units that are designed to deflect under the static topsides load. The elastomeric units in a LMU are shown in Figure 3.4. The elastomer works as a highly non-linear spring in vertical direction, depending on stroke, and is often modelled as a linear spring in the horizontal plane (Yuan et al., 2012).

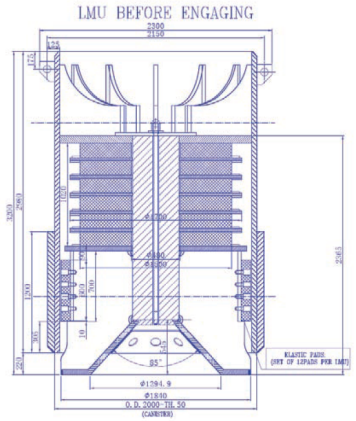

(a) Leg mating unit, in unloaded state. Hence, the elastomeric elements are not compressed, these elements are shown with the cross striped blue lines.

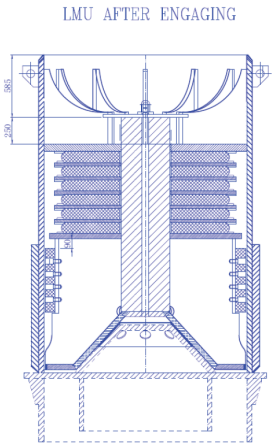

(b) Leg mating unit, in fully loaded condition. Indicating the compression in the vertical elastomeric elements. When the LMU's are fully compressed the topsides and substructure are in steel to steel contact.

Figure 3.4: A typical leg mating unit design, including vertical and horizontal elastomeric units. The stroke in the horizontal plane is small and only possible when the vertical elastomers are not fully compressed (Yuan et al., 2012).

Failure of the leg mating units leads to failure of the topsides installation. The limiting case for the LMU's is determined with the horizontal loading capacity. This is found in Yuan et al. (2012) where the possible failure mechanisms of the LMU's are determined. Furthermore, it is found that the horizontal motions slowly decrease during the installation. This is due to the connection between barge and topsides, which constrains the barge from moving sideways. Thus the loads are highest during the initial impact phase, which coincides with the previous findings.

For the `liwan 3-1` scenario the LMU's stiffnesses are found in Yuan et al. (2014a) and presented in Figure 3.5. The total maximum horizontal loading on a LMU is 980 tons, this is in the order of magnitude of impact conditions. The vertical elastomers are able to cope with 160% of the topsides load, which corresponds to 38,000 tons, thus this is not a failure criterion.

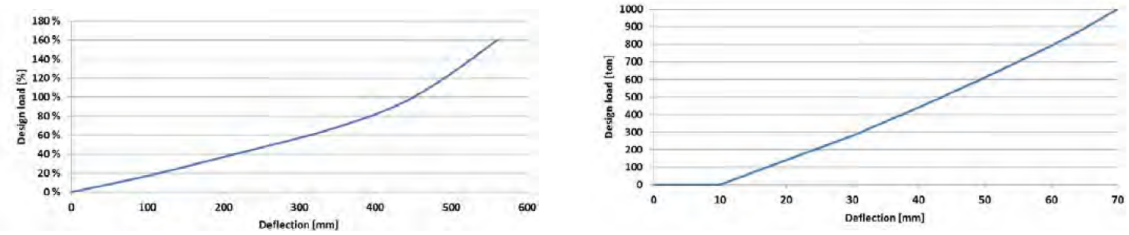

(a) Vertical stiffness curve. The deflection is shown as a function of the design load. Where 100 % coincides with the topside static weight.

(b) Horizontal stiffness curve. The deflection is shown as a function of the horizontal load.

Figure 3.5: The loading curve of a `Liwan 3-1` leg mating unit (Yuan et al., 2014a).

In the same paper a schematic drawing of the LMU is given that leads to a, relatively blunt, receptacle angle(α) of 30 degrees. The angle is measured from the horizontal plane upwards. The installation limit is highly dependent on this angle since the impact loads are transferred over the working line, as is elaborated on in the following paragraphs.

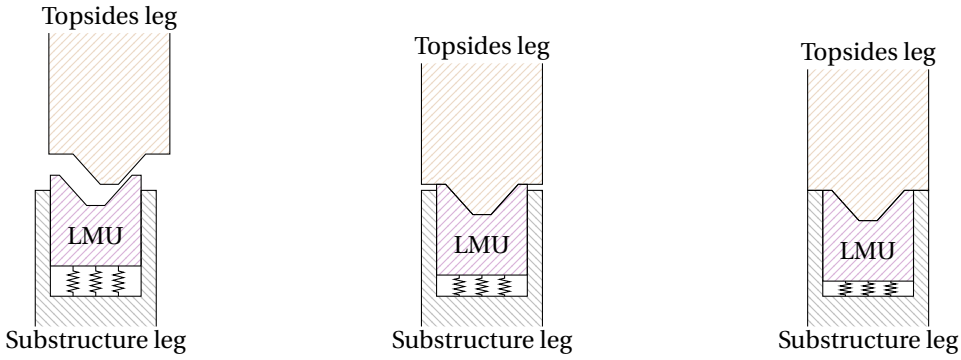

(a) The pre-stabbing phase. The cone has lowered in the receptacle. Only occasional contact between the topsides and LMU occurs due to the motions of the barge. The receptacle guides the topsides leg, during the ballasting, to prevent misalignment. The cone and receptacle are partially engaged

(b) The stabbing phase. Cone and receptacle are aligned and the load is partially transferred. When enough load is transferred no bouncing effects take place. The loads are transferred through the LMU on the jacket leg. The cone and receptacle are now fully engaged.

(c) The installed phase. The elastomeric units are fully compressed, due to a part of the topsides load. The rest of the topsides load is taken by the steel to steel contact of the topsides and substructure legs. The loads of the topsides are no longer directed through the LMU.

Figure 3.6: Different load cases in the mating phase. These drawings are sketched to indicate the different loads acting on the leg mating unit (LMU and the substructure during the different phases of the mating stage.

During the mating phase the LMU's are subjected to multiple load cases. The different load cases are schematically drawn in Figure 3.6. The largest impact loads will take place during the pre-stabbing phase, due to the possible high topsides velocity. During the stabbing phase the horizontal loads of the topsides are directly

transferred onto the horizontal springs of the LMU that can cause an overload. These horizontal springs are not drawn in the illustrations. During the final installation phase the loads are directly transferred onto the substructure. The magnitude of the pre-stabbing LMU loads is found in Yuan et al. (2014a) and the stabbing and installation phase LMU loads are found in Yuan et al. (2014b). When these loads are compared it is concluded that the pre-stabbing loads are the most significant and that the loads in the stabbing and installation phase are not critical. Therefore, the installation limit is based on the pre-stabbing phase loading condition.

The impact scenario on the LMU's is derived by using the schematic representation of Figure 3.7a. Ideally the topsides leg, that is drawn brown, is aligned and moves with a vertical motion onto the receptacle. Realistically , the leg is eccentric and also moves in the horizontal plane. When looking into the eccentric scenario the reaction forces consist of the normal force and friction force of the LMU surface. For the limit the worst probable scenario should is considered.
The friction force is considered as a coulomb friction. The static and dynamic friction coefficients are 0.1 according to (Yuan et al., 2014a). This low estimated coefficients suggest that the surfaces are greased to decrease the friction force, aiding slipping effects. Friction forces are also undesired because stick-slip effects can cause larger impacts. The low friction coefficient causes slip for angle of 6 degrees or more from the perpendicular, LMU surface, orientation. Slip causes upward or downward motions, the downward motions are favourable because the system aligns for the stabbing phase. The upwards motions are undesired since these will cause extra deflections in the LMU.

This worst probable scenario is represented in Figure 3.7b, where the topsides leg impact is given eccentrically on point P. For the limiting scenario the topsides will have the maximum probable velocity, based on the time window of the installation. For the impact calculations the assumption is made that slip will occur. However, the slip will not cause alignment of the LMU and topsides leg. This means that the impact point will stay on the inclined surface. In addition, the energy losses due to the dynamic friction are not taken into account. By using this assumption, the deflections work perpendicular to the receptacle plane, as shown in the figure with the blue dashed line.

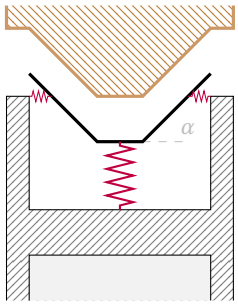

(a) Modelled representation of the LMU based on the literature and the schematics of Figures 3.4a and 3.4b. This is used as an input to derive the model for the impact conditions.

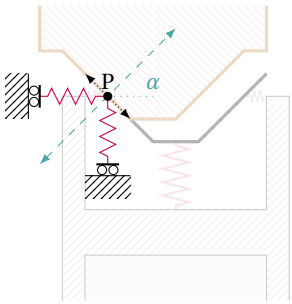

(b) Modelled LMU for eccentric impact conditions at point P. The surface is taken smooth, hence, point P slides over the black dotted line. Therefore, the impact loads are transferred over the blue dashed line. This line also indicates the path of the deflection, working perpendicular on the LMU receptacle plane. The two horizontal springs represent the vertical and horizontal elastomer respectively.

Figure 3.7: Drawings of the maximum impact loads derivation for the leg mating units. These are used to derive the modelling approach for the leg mating units.

In reality this approach is not applicable, because the friction forces will cause changes in the working line and slip effect can cause engagement or disconnection of the cone and receptacle. The modelling of these effects is too elaborate for this thesis.

3.4.2. SUBSTRUCTURE

The substructure is the combination of the jacket and the eight LMU's on top of each of the jacket legs. The jacket has to deal with the loads of the eight LMU's, at least, if all the legs are subjected to the impact forces. In

the previous section it is determined how the impact loads of the LMU's are taken into account. This section elaborates on how the jacket deals with the combined load case of the LMU's. This is done by assessing the scenario for 1,2,4 and 8 jacket legs subjected to the pre-stabbing impact loads.

The amount of legs in contact during the impact assessment is irregular, since the impact probably takes place with a combination of heave roll and pitch motions of the barge. During beam waves impact is likely to occur on either the port side or starboard legs and for quartering waves the added pitch might cause the impact to occur on a one or two jacket legs. To keep the installation maximum unrelated to the wave direction the choice is made to assess the limits of four scenarios being: 1, 2, 4 and 8 legs under topsides impact.

For the substructure the stiffness is found in Yuan et al. (2014a), for the vertical and horizontal directions. In this paper the vertical spring stiffness for a leg is assumed linear and independent of the deflection of the other legs. The stiffness in this case is found by taking the average of the eight legs from Yuan et al. (2014a) that becomes 463 MN/m. The horizontal stiffness of the legs is found to be dependent on the number of legs. However, once the amount of legs is known the corresponding stiffness can be translated to the leg stiffness to determine the individual deflection. Hence the deflections due to the impact can be derived for all individual legs when the number of legs in contact is known. This stiffness in relation to the amount of legs is found as:

Table 3.1: The substructure stiffness, from Yuan et al. (2014a). The stiffness is related to the amount of legs subjected to the loads.

Impact case	Total stiffness [ton/m]	Stiffness per leg
Single leg	7,500	7,500
Four legs	12,200	3,050
Eight legs	16,900	2,113

The scenario found in Figure 3.7b can be combined with the substructure effects to find the deflections of each leg. The model is thus combined to Figure 3.8. From the deflections over the working line, the horizontal force of each leg is derived to compile the total force on the substructure. As previously mentioned, the total maximum horizontal force is 800 tons (Yuan et al., 2014a). Since the allowed horizontal force in a single LMU is larger than 800 tons the failure condition is solely related to the substructure element.

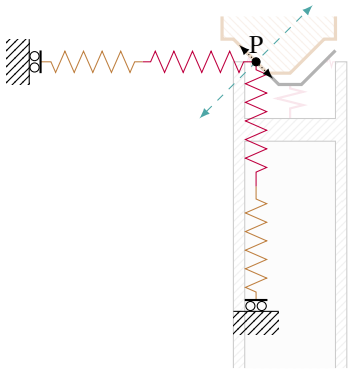

Figure 3.8: Model of a substructure leg with the combined leg mating unit and substructure springs. This approach is used in the model, the deflection of each leg is modelled independent from the other legs. The horizontal substructure stiffness is correlated to the number of legs in contact.

3.4.3. MODEL APPROACH

The limiting installation loads are determined by looking at the mating stage and focussing on the substructure elements. With this scope it is found that the impact case is the most critical loading condition. Within the different impact case possibilities, the impacts during the pre-stabbing phase (Figure 3.6a) are the highest. During this phase the worst probable conditions are assessed. Combining this with the substructure elements lead to a combined model as shown in Figure 3.8. From this the limiting impact conditions will be derived for the impact case on 1, 2, 4 and 8 of the substructure legs to find a limit is suitable for all sea states.

4

HEAVE COMPENSATION SYSTEM

Several heave compensation principles can be used to perform a floatover mating operation. This research takes a single principle into account. This chapter focusses on the heave compensation system and the used approach to implement the system in the floatover mating operation.

Firstly, the passive lift principle is explained, the actuation principle of the concept. Followed by the idea and key elements of the used concept. The third section discusses the kinematics of the `Liwan 3-1` installation and the `UNIDECK` technique considering the heave compensation system, followed by an alternative to improve the kinematic case. Lastly, the approach used to model the system is elaborated.

4.1. PASSIVE LIFT PRINCIPLE

The proposed system uses passive actuation, which implies that energy stored in the system is used and no energy needs to be added. The passive compensation principle is chosen as the best actuation concept for this research, the reasoning behind this can be found in Appendix E. The concept uses pneumatic energy stored in pressure vessels to control the behaviour of the hydraulic cylinder. This passive principle is key to the compensation process, therefore, it is further discussed in this section.

Pneumatic passive actuation is based on the compression characteristics of gas, in this case air. When pressurized air is enclosed, it exerts a pressure force on the hull. When the volume of the confined space decreases, the pressure increases because the air is compressed, thus the exerted force of the pressure is higher. This principle is further elaborated using Figure 4.1.

In Figure 4.1a an enclosed volume V, with pressure p is sketched. The piston, illustrated as a gray block, is free to move in the horizontal direction. For this explanation friction is neglected. A static load (F) is added to keep the piston steady at the dotted line position. Thus, the force due to the pressure is equal to the static load. Figure 4.1b the piston is displaced whilst the static load is the same. The volume has decreased, leading to an increased density of the air, that corresponds to a higher pressure. Therefore, the force also increased. The force of the pressurized air is now larger than the static force. Hence, the piston accelerates towards the equilibrium location (dotted line). Figure 4.1c shows the opposite situation, the displacement of the piston causes an increase of the enclosed volume. The air expands causing the density and pressure of the air to decrease. This creates a lower pressure force and the static force has not changed. Hence, the piston moves towards the equilibrium position.

The passive actuation is realised by connecting pressure vessels to an accumulator. This accumulator is an interface between hydraulic cylinders and pneumatic storage. An accumulator is described as a pressure vessel with a piston inside, separating two different volumes. Relative pressure difference between the two volumes causes the piston to move. By connecting the other side with the hydraulic cylinders, movements of the cylinder rod relate to movements of the accumulator piston.

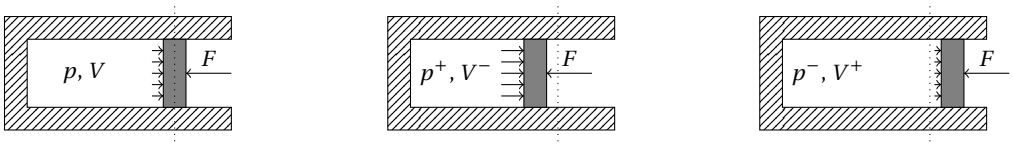

(a) Equilibrium condition of the enclosed air, the air pressure in the confined space exerts an equal force as the static load (F).

(b) The decreased volume causes the air to compress; leading to a higher pressure. The increased force is now larger than the static load, due to the pressure increase.

(c) The increased volume leads to expansion of air. The corresponding lower pressure influences the pressure force, the static force is now larger than the pressure force.

Figure 4.1: Illustration to explain the passive actuation principle. The compressibility of gas in a confined space is used to control the forces on the piston. The figure sketches the effect of the changing volume on the piston force, the force on the piston is related to the pressure of the gas.

To keep the topsides steady, the motions of the barge have to be cancelled. The barge motions are caused by the wave forces; these forces are inevitable. The topsides is subjected to wind loads and the connected heave compensation forces. The wind loading on the topsides is not significant, this is determined in Section 4.4.2. Therefore, the wind is neglected and the main aim of the compensation is to eliminate the motions of the barge.

The passive actuation can be modelled as a spring, with properties of the air volume and pressure. This aspect is used to control the topsides behaviour. A large volume and high pressure of compressed air make the stiffness of the system very low. Because the relative compression due to the accumulator stroke is low. Thus, the change in force of the pressure is small. In this case displacement of the rod causes almost no accelerations towards the equilibrium. This is used as an advantage, because in this case it is not the rod that displaces but the casing. In Figure 4.1 the rod displaces causing large force variations because of the relatively large compression. When this volume is very large, the force on the rod due to a displacement is only slightly altered, causing low acceleration on the rod. Hence, when the casing represents the barge and the rod the topsides the barge movements will cause low accelerations on the topsides due to the relatively low compression factor of the passive system.

Using this principle, the displacement of the barge causes almost no extra forces in the cylinder and thus the acceleration of the topsides is small. This also counts for the forces on the topsides, since these forces will not lead to increased forces of the cylinders. The advantage of this passive system is therefore that motions of the barge can be cancelled. Though, it has to be taken into account that when the topsides is in motion, these are also subjected to the same passive actuation principle.
Fortunately, the cylinders are not only modelled as a spring, the viscous friction of the fluid and the friction of the cylinder seals cause additional (frictional) forces in the system. Thus, the passive system can be seen as a large spring damper system, where the stiffness is related to the volume of pneumatic air and the damping is caused by viscous friction forces.

4.2. THE CONCEPT SYSTEM

The passive concept is based on pneumatics. The used concept combines pneumatics with hydraulics, because the force that lifts the topsides is supplied with an hydraulic cylinder. The passive actuation is given by pressure vessels. To combine the lift force with the actuation source, an accumulator is used. These three items are combined as shown in Figure 4.2. This is the basis of the heave compensation system.

To control the motions in the `Liwan 3-1` scenario the heave compensation system, or interface, consists of four separate passive compensation systems, one for each corner of the topsides. Each system consists of separate components and works independent. The locations of the hydraulic cylinders on the barge and topsides are shown in Figure 4.3, these locations are the points of engagements for the modelling of the heave compensation system.

Four separate systems are required to keep the topsides stable in the three dimensional plane. The amount of elements in the total system is schematically shown in Figure 4.4. All different systems each contain the three main components, this creates an extensive system with multiple unknowns. Therefore, the model is

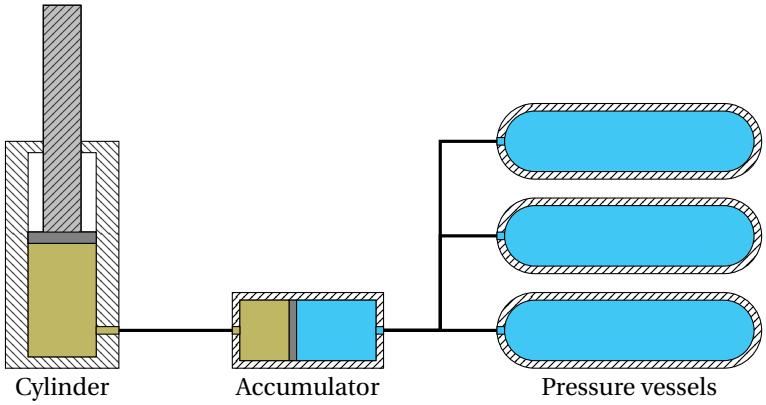

Figure 4.2: The heave compensation concept. Illustrating the three main components: hydraulic cylinder to lift the topsides, pneumatic pressure vessels to provide passive actuation and an accumulator to connect the cylinder with the pressure vessels. The hydraulic fluid is brown and the pneumatic flow is blue. The cylinder stroke causes the piston in the accumulator to compress the air of the pneumatic side. Hence, the passive actuation is realized.

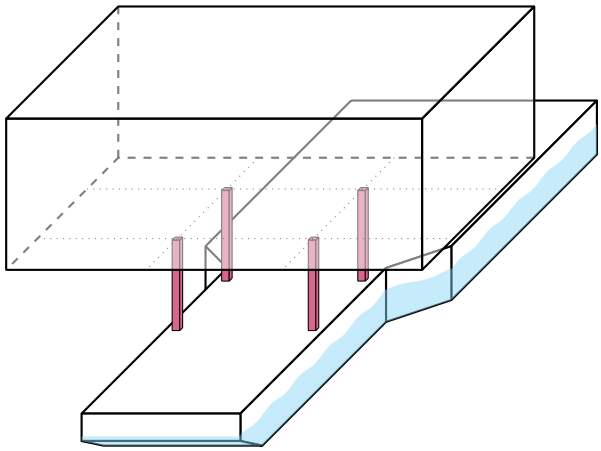

Figure 4.3: The four locations of the hydraulic cylinders are shown in red, the other components are not considered in this sketch. Each of these locations contains a passive heave compensation system. The locations indicate which cylinders can be used to compensate different motions of the barge. The cylinders are not designed the cover this height, in reality a deck support frame is installed to bridge the majority of the height.

made uniform, implying that the forces on each interface are equal. This way four identical systems are used, creating a feasible scope for this research.

The hydraulic fluid is incompressible and no pressure losses are considered. Hence, the pressure is assumed equal in the cylinder and accumulator. The force in the cylinders is thereby related to the pressure in the accumulator. The pressure in the pneumatic side is determined by the initial pressure of the air. The fluctuations relate to the volume connected with the accumulator, the pressure changes relatively to the change in volume. When using a large volume, the change in volume is relatively low. Thus, the change in force is relatively low, which is linked to the stiffness of the system. For very small volumes the change is large and thus the stiffness will be high.

In the calculations the connection between the cylinders and the accumulator is assumed lossless and instantaneous, so no friction forces and flow velocities are taken into account. The same yields for the connection between the accumulator and the pressure vessels.

The `Liwan 3-1` topsides weighs 26,300 tons. The hydraulic cylinders in this concept must be able to carry the static and dynamic loads of the topsides, whilst adjusting their stroke to maintain a fixed topsides height. To lift a quarter of the topsides, which is what each group of cylinders is required to do, a large area is required. Cylinders with areas in that order of magnitude are unusual. Therefore, the concept is based on a group of cylinders that are all connected to the same accumulator. All cylinders must be supplied with the same

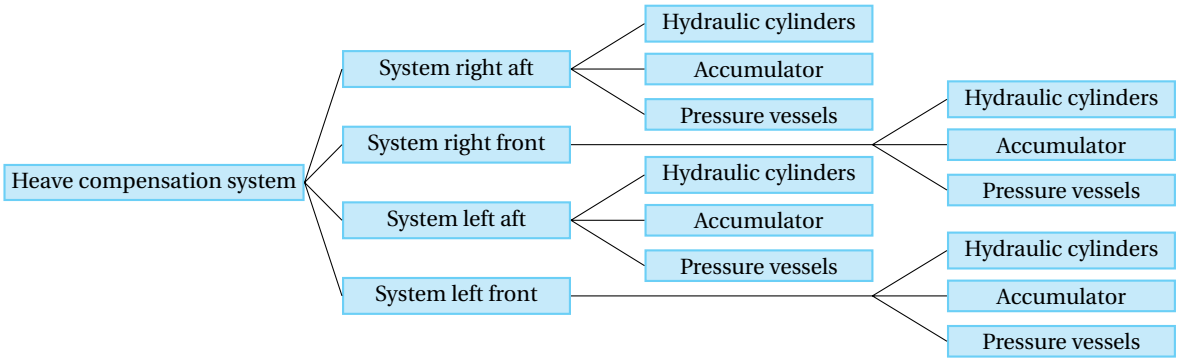

Figure 4.4: A representation of the heave compensation system layout. For the design of the heave compensation system a large amount of components are required. The heave compensation system is built of four separate systems that each lift a quarter of the topsides. Each system consists of the same components, which leads to this composition of the required components.

pressure to ensure that the total force is correct, this is one of the functions of the accumulator. The cylinders are, individually, compared to the *PS* topsides lift cylinders that are designed for comparable loads. The topsides lift system consists of 32 hydraulic cylinders installed with 1,000 tons lifting capacity each.

Each of the passive heave compensation systems is modelled as a spring-damper system. The spring coefficient is dependent on the volume of the used pneumatic storage and the damper corresponds to the hydraulic and pneumatic friction of the system.

During the stroke of the cylinders the hydraulic fluid flows from the accumulator through the connection pipes to/from the cylinders, this process is coupled with viscous damping. The stroke also leads to friction forces of the cylinder seals against the shell of the cylinder. These forces can cause stick-slip effects. Another effect is the pressure loss due to leakage of the cylinder seals. All these effects are related to the final design of the cylinders and the influence of these effects is attempted to be minimal. This is done by working at high pressure to reduce the stick-slip effects. Pressure losses are assumed to be controllable by the pump network, this network is not considered. Finally, the viscous damping as considered is a variable in the system, this is further detailed in Section 4.4.3.

For this concept a simple single acting hydraulic cylinder is studied, which is shown in Figure 4.5. The cylinder contains a casing, piston and rod. The casing is the shell that contains the hydraulic fluid (dashed lines, white fill). The rod is the element that connects the cylinder with the point of engagement (dashed lines, gray fill). Finally, the piston is placed at the end of the rod and subjected to the pressure of the hydraulic oil, shown in solid gray. The accumulator and pressure vessels are taken as shown in Figure 4.2, thus, the accumulator contains a piston and a shell and the pressure vessels are shaped with the cylindrical shell.

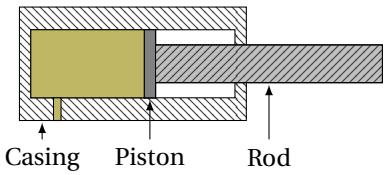

Figure 4.5: Nomenclature of a simple single acting cylinder. Three parts are distinguished; the casing, rod and piston. The casing contains the hydraulic fluid and is mounted, or hinged, to the surface. The rod is moving element used to transfer the loads, usually hinged. The piston is the elements that transfers the hydraulic force to the cylinder rod.

4.3. KINEMATICS

The kinematics of the proposed principle are discussed, to see how the heave compensation system effects the movements of the barge and topsides. The kinematics are assessed using the `Liwan 3-1` scenario as well as the `UNIDECK` installation technique. The latter is done since this technique also uses hydraulic cylinders to perform the lift.

The first section describes both the Liwan 3-1 and the UNIDECK scenario, where the proposed heave compensation system is tested to see the kinematic effects on the scenarios. In the second section an alternative approach for the kinematic scenario is introduced.

4.3.1. THE LIWAN 3-1 AND UNIDECK KINEMATICS

The Liwan 3-1 topsides is installed by the classic floatover layout, which consists of a fixed deck support structure and Deck Support Units (DSU's). This layout is presented in Figure 4.6a where the deck support structure is placed on the skid beams and the DSU's are placed on top of the structure connected to the topsides. In the same figure the possible movements of the barge are illustrated, the sway fenders prevent the barge from large sideways motions whilst there is enough freedom for vertical movements and rotations.

DSU's are stiff elastomeric units that are installed for the gradual progression of the load transfer. The design and working principle is comparable to LMU's, where the main difference is that DSU's are flat and do not contain a cone/receptacle design. In the Liwan 3-1 scenario the elastomers of the DSU's are designed to carry 30% of the load with a corresponding deflection of 250 mm (Yuan et al., 2014b). The outer steel edge of the DSU will take the resulting 70% of the load. This means that until 70% of the load is transferred, the stiffness only relates to the deck support structure. Like the LMU's, the DSU's can also be modelled as a 3 DOF spring. The paper also mentions that the topsides and deck support structure are in steel to steel contact when the loads exceed the 30%. This implies that the horizontal spring stiffness has the same relation as the vertical stiffness. When the loads are above the 30% design load then the horizontal stiffness is also solely related to the horizontal stiffness of the deck support structure.

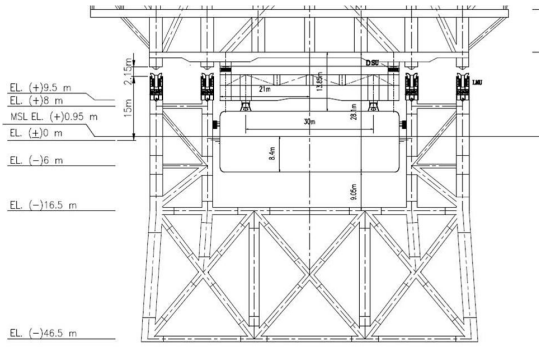

(a) Frontview the Liwan 3-1 installation, just before the mating commences. The deck support frame rests on the skid beams, the topsides are supported with deck support units. On the legs the leg mating units are illustrated. The clearance between the topsides and leg mating units is 2.15 m. It is visible that the gap between the barge and the substructure is small.

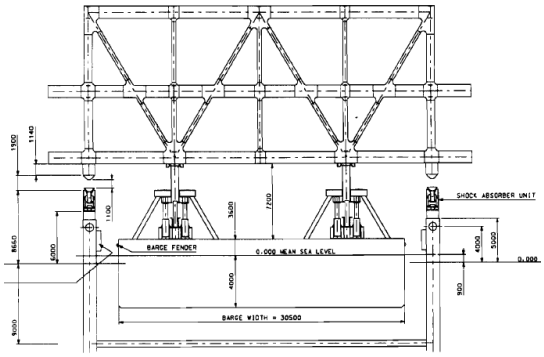

(b) A UNIDECK layout (Sigrist et al., 1998), of a 7,500 tons platform. The deisgn shows that no deck support frame is required. The clearance between the topsides leg and leg mating unit is 1.1 m. In the literature is found that the stroke of this system is 1.3 meters. Hence, the system is capable of bridging the clearance in a single stroke.

Figure 4.6: Two typical floatover barge layouts. The positions shown are prior to the mating procedure. The figures illustrate the clearances between the different elements of the barge, topsides and substructure.

The UNIDECK principle uses the stroke of hydraulic cylinders to bring the topsides down vertically, a typical layout for a light topside is given in Figure 4.6b. The principle differs from the classical floatover deck layout due to difference in transverse forces of the topsides. The main difference is that the deck structure is not horizontally connected and the DSU's are replaced with hydraulic cylinders. Remarkable is also that the barge is allowed to move in sway direction. In the early days of the technique a lot of uncertainties lead to low allowable sea states for the installation. More recent data of the 18,000 tons UNIDECK technique installation of the EAP GN Topsides is not available, pictures indicate that a similar layout of the technique is used.

When deriving the kinematic relations for the Liwan 3-1 and UNIDECK installation the same model can be used. For both scenarios the deck support is assumed rigid, since this has a very high stiffness in relation to the LMU's and DSU's. However, the hydraulic cylinders are less favourable for horizontal loading than DSU's. This has to be taken into account when looking into the installation procedure. When taking the pre-

installed situation both layouts can be modelled as Figure 4.7a. The stiffness in vertical direction comes from the deck support structure and hydraulic cylinders for the `Liwan 3-1` and `UNIDECK` technique, respectively. In this figure the effects of roll motions are shown, the angle is exaggerated but the principle also occurs for small angles. Roll motions of the barge create sway motions of the topsides due to the rigid connection and large vertical distance between the topsides and barge. The same effect occurs for pitch rotations, then the topsides will translate in surge direction.

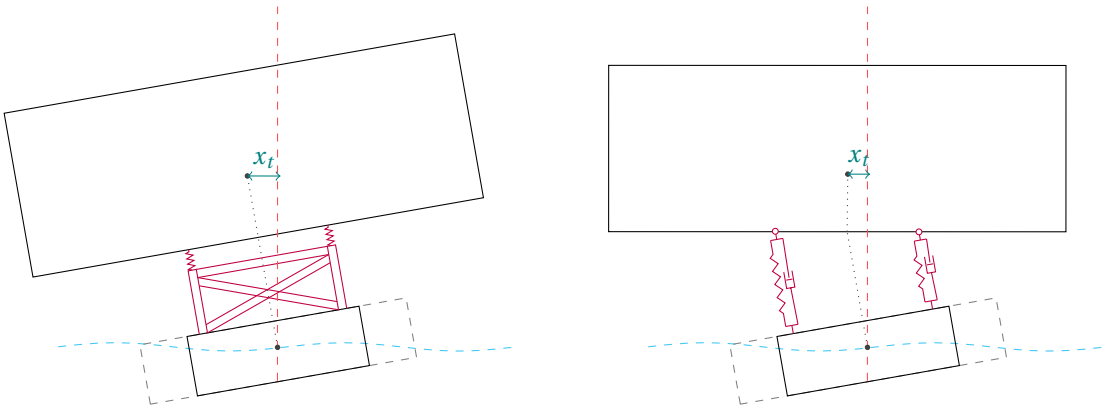

(a) The kinematic model for the classical and `UNIDECK` installations. The rotations of the barge directly influence the rotations of the barge, resulting in a sway component for the topsides. The sway depends on the distance between the two center of gravity locations.

(b) Kinematic scenario of an ideally heave compensated system. The topsides is perfectly horizontal due to the stroke of the heave compensation system. This reduces the effects of the sway motions in relation to the classical model. However, the system is not capable of cancelling the sway motions.

Figure 4.7: Sketches of the difference in kinematics between the classical floatover installation and an ideally heave compensated installation. Indicating the the sway component of the topsides is only slightly reduced. The angle is exaggerated to indicate this effect.

In the previous chapter it is found that transverse forces on the substructure legs are the limiting loads for the installation procedure. Therefore, this kinematic relation is an important factor for the limiting loads. When implementing a heave compensation system with the same kinematic constraints, the ideal heave compensation can perform as shown in Figure 4.7b. The sway motion due to the roll is still present. This situation is still considered because the topsides can be held horizontal which might lead to simultaneous impact on all jacket legs. This can create an advantage with respect to impact on a single or two legs as might occur during installation with the conventional roll kinematics. Additionally, the impact energy in the vertical direction is decreased, thus the total energy of the topsides is expected to decrease.

4.3.2. THE REVERSE HINGE APPROACH

The heave compensated floatover procedure can be modelled as shown in Figure 4.7b. This kinematic relation is caused by the fixed position of the heave compensation system at the barge deck. The large height amplifies small rotation in significant translations. The model does assume that rotation is possible in the connection between interface and topsides, the connection is hinged.

When the hinged connection is reversed, thus the heave compensation system fixed on the topsides and hinged on the deck, the translations of the topsides are reduced significantly. The kinematic scenario is shown in Figure 4.8. With these minimised horizontal motions, the impact is expected to reduce significantly. However, this scenario is far from ideal. The hinged connection at the bottom will lead to high forces at the top of the system. The topsides connection has to be strong to stay fixed perpendicular to the topsides. During installation horizontal forces are exerted on the topsides due to the design of the LMU's. These forces result in an unwanted loading condition, transverse loads on the hydraulic cylinders. Therefore, for this scenario to be feasible, a solution for the horizontal forces has to be implemented and an estimation of the forces due to eccentricity of the topsides has to be estimated.

The reversed hinge system is not capable of processing the horizontal loads from the LMU's. These horizontal loads will be directly transferred as shear forces on the cylinder rods, which means that a large overturning

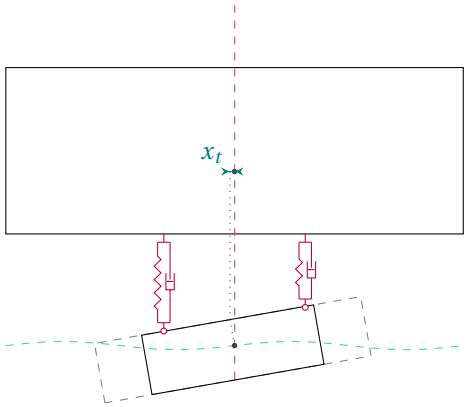

Figure 4.8: Kinematic model of the proposed reversed hinge scenario. This concept also compensates the majority of the sway motions. The sway motions are now caused by the distance between the center of gravity of the barge and the deck height. The angle is exaggerated to illustrate the roll effects.

moment will occur in these cylinders. These loads can cause deformation of the cylinder seals that lead to higher friction forces and larger pressure losses. If these loads are high, instant failure of a cylinder can also occur.

The hinges in this reversed kinematic model are difficult elements, because they should be able to rotate in two degrees of freedom without stick-slip effects. The loads acting on the hinge are big and no information on ball bearings is available for these type of high loads. However, information can be found for regular bearings with 1 DOF. A superposition of the 1 DOF bearings can be used to approximate a ball bearing with these loading characteristics. This could be a feasible way to approach the forces acting on the bearings.

4.4. MODELLING APPROACH

This section presents the modelling approach of the heave compensation system. Firstly, the implementation of the kinematic model is discussed and afterwards the approach is detailed.

4.4.1. KINEMATICS

The model of the heave compensation system can be based on the `Liwan 3-1` kinematics or the reversed hinge approach. The choice is made to use only the `Liwan 3-1` kinematics.
The aim of this research is to find the added value of a heave compensation system, thereby focussing on the possible increase in workability. For this first indication it is better to look at the possible improvements with the basic system, than starting with a more complex solution. Additionally, with an extensive system the workability improvement must be larger to create a viable system. To get an idea of the possibilities with heave compensation, the focus is put on the simple system. Therefore, it is decided to work out the kinematic using the `Liwan 3-1` scenario. Considering the reversed hinge scenario, this is advised when this system turns out not to give a significant gain in workability.

4.4.2. WIND LOADS

In this research the wind loads on the topsides are neglected, the reasoning behind this is briefly discussed in this subsection.

An estimation of the extent of the wind loads is made to check the order of magnitude of the force. This is done by calculating the drag force of the most probable wind velocity. The drag force is given by:

$$F_D = \frac{1}{2}\rho v^2 C_D A \tag{4.1}$$

Where ρ is the density of the air, v the velocity of the air, C_D the block coefficient of the shape and A the area subjected to the drag.

The wind velocity is found in the internal environmental database. For the Nigerian location the maximum ten minute averaged wind velocity, ten meters above mean sea level, is measured as 7.9 m/s. The internal database provides a method to extrapolate this value. For the topsides a more interesting velocity is the 3 sec averaged, 25 meters above mean sea level velocity, found as 9.7 m/s. The corresponding wind load for the long side of the topsides is found as 254 kN (block coefficient = 1) for the 3 second gust. In other words, 26 tons. The maximum horizontal load on the substructure is found as 800 tons, as derived in Section 3.4. The wind loads are thus insignificant in relation to the maximum horizontal loads.

4.4.3. IMPLEMENTED METHOD

The modelling of the system is done by approximating the system as a spring and damper element. The four systems are independent and are thus modelled as separate spring damper systems. Simplification of the system is done by assuming that the topsides center of gravity is centred between the spring-damper element locations. The final configuration of the model is shown in Figure 4.9.

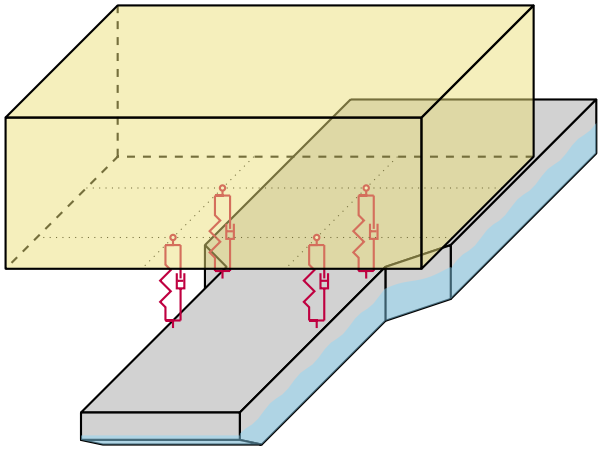

Figure 4.9: The 3D over view of the model. Showing the final interpretation of the barge and topsides for the modelling. Four separate spring damper systems are modelled, using the shown locations. Different settings of the spring and damper are used to analyse the behaviour of the barge and topsides.

The spring and damper characteristics determine the behaviour of the model. So a good approximation of these values is important. The method for determining both values is given in the following two subsections.

STIFFNESS DERIVATION

The passive actuation system determines the stiffness. The volume and pressure in the pneumatic part are key to the stiffness to the system. This subsection gives the stiffness derivation.

The pneumatics are approximated using the adiabatic compression law. This means that the pressure losses are not taken into account, the gas behaves as an ideal gas and the process is considered reversible. Under these assumptions the polytropic process equation becomes valid, that is given as:

$$p \cdot V^{\kappa} = \text{constant} \tag{4.2}$$

Where p is the pressure, V the volume and κ the heat capacity ratio. This ratio is related to the temperature, pressure and type of gas. In this thesis air is used and the working temperature for the gasses is put on 350 Kelvin. The pneumatic system of the *PS* uses this value, the value is assumed valid for this concept. With a set working temperature a direct link between the pressure and the heat capacity ratio is obtained.

Due to the large volume required for the passive compensation the compression factor becomes small. In other words, the non-linearity of the air compression can be neglected. Therefore, the stiffness of the cylinders is linearized around x=0, where x represents the mean stroke of the cylinder. Using the basic relations of: $F = p \cdot A$, the relation from Equation (4.2): $p_0 \cdot V_0^{\kappa} = p_1 \cdot V_1^{\kappa}$ and for the volume change in the cylinder:

$V_1 = V_0 - Ax$. The linearized stiffness is found with:

$$k_{\text{cyl}} = \frac{dF_{\text{cyl}}}{dx} \tag{4.3}$$

$$F_{\text{cyl}} = \frac{p_0 \cdot A \cdot V_0^{\kappa}}{(V_0 - A \cdot x)^{\kappa}} \tag{4.4}$$

$$k_{\text{cyl}} = \frac{\kappa \cdot p_0 \cdot A^2}{V_0} \tag{4.5}$$

$$k_{\text{cyl}} = \frac{\kappa \cdot m_t^2 \cdot g^2}{16\, p_0 \cdot V_0} \tag{4.6}$$

Where p_0 and V_0 are the pressure and volume at zero stroke. The pressure acting on the cylinder is taken equally to the pneumatic part of the system. The volume is the combination of all pressured air in the vessels, tubes and passive side of the accumulator. k_{cyl} is the stiffness of a cylinder group and the total weight that is supported by four of these groups.

The derivation from Equation (4.5) to Equation (4.6) can be made because A is related to p_0 this leaves only two variables since κ is a function of p and m_t and g are known. And thus an increase in p_0 as well as V_0 will lead to a lower stiffness factor. Though an increase in p_0 is counteracted with an increase of κ which has a slightly negative effect. It can be seen that higher pressure and larger volumes relate to a lower stiffness coefficient. For the relation between κ and p table is Table 4.1 is used, from Sychev et al. (1978). The stiffness of the cylinders it thus related to the volume and pressure of the heave compensation system.

Table 4.1: The values of κ for different pressures. Derived for a working temperature of 350 K. This table is used to derive the stiffness related to the settings of the heave compensation system. From Sychev et al. (1978).

p [bar]	0	50	100	150	200	250	300	350	400	450	500
κ	1.4	1.47	1.56	1.66	1.78	1.91	2.04	2.17	2.29	2.42	2.54

DAMPING CONSIDERATIONS

For the modelling stage the system is considered as a linear spring damper system. The damper forces are based on the friction forces in the concept. In reality, these forces are not linear. In this study the forces are assumed linear to be able to analyse the system in the frequency domain. This section details the forces and gives an insight in the assumption and simplifications required for a linear damper model. This is done firstly detailing the viscous friction. Afterwards the piston friction is discussed. At the end the approach is explained.

Viscous friction

In the hydraulic part of the heave compensation system, friction due to the fluid flow is present. This is called the viscous friction. It takes place in all elements where the fluid moves. This means that the viscous friction takes place in the accumulator, cylinders and all elements in between. The viscous friction is dominant in the piping of the system. Hence, the forces in the pipes are discussed in this section.

The viscous friction is dependent on the Reynolds number, a well-known dimensionless parameter in fluid mechanics. The number is used to indicate in what regime the flow is located. The regimes indicate if a flow behaves laminar or turbulent. The viscous friction in pipes is found with the Darcy-Weisbach equation, from White (2011) given in Equation (4.7).

$$\Delta p = f_D \cdot \frac{L}{D} \cdot \frac{\rho v^2}{2} \tag{4.7}$$

Where Δp indicates the pressure loss, f_D is the Darcy friction factor, which is explained later. L and D indicate the length and diameter of the pipe respectively. ρ is the density of the fluid and finally v is the flow velocity of the fluid.

The Darcy friction factor (f_D) is related to the flow regime and is based on the Reynolds number. The different formulae for this friction factor are not relevant since the viscous friction is not going to be calculated.

Equation (4.7) indicates two effects. First, the head loss due to the friction is dependent on the velocity squared and thus non-linear. Secondly, the factor $\frac{L}{D}$ determines the amount of friction. This factor is dependent on the detailed design, this is not the aim of the concept study. Hence, both of this effects indicate that the viscous friction can not be implemented in the model.

Piston friction

The heave compensation concept contains pistons in the cylinders and accumulators. Friction forces arise between the walls and the piston seals, the force is dependent on the design and characteristics of the walls and cylinder seals. The friction of the seal can be modelled using the Coulomb model of friction, this is given as:

$$F = F_c \cdot \text{sign}(v) \tag{4.8}$$

$$F_c = \mu \cdot F_n \tag{4.9}$$

Where v is the velocity of the piston, F_c the coulomb friction, μ the friction factor and F_n the normal force of the wall.

The friction coefficient is dependent on the design of the seal, the diameter, the material of the seal and the smoothness of the wall surface. The normal force on the wall contains two components: the forces required to prevent the seals from leaking and the force due to the bending moment on the rod. The latter is only present for the cylinders. Hence, the friction force in the cylinders relates to the eccentric loads on the cylinder rod.

The friction force depends on the sign of the velocity. Hence, the force is non-linear around zero. The friction coefficient is dependent on the piston seals and the bending moment is related to the detailed design. Thus, this force can also not be taken into account for the same two reasons as the viscous friction.

The piston friction can also cause stick-slip effects. This occurs when the force difference does not exceed the friction force. The stick slip is not considered in this research, since the effects can not be approached in a linear model.

Damping approach

The previous two sections conclude that all friction forces are non-linear. Still the model contains a linear damper component. This linear damper is used to approximate the behaviour of the viscous friction, even though this friction is related to the velocity squared in reality. The reason for this is that the design of the heave compensation system can be done such that a large or small viscous friction is present, by tweaking the $\frac{L}{D}$ ratio from Equation (4.7).

Friction in heave compensation is used to damp out motions by dissipating energy, mostly by generation of heat. This property can be used to control the motions. Therefore, the damping is taken as a linear component of the piston velocity, which represents the required fluid flow. The value is taken as a percentage of the critical damping of the system, a term often used in dynamics. The critical damping of the system is given with:

$$\zeta_{cr} = 2\sqrt{m \cdot k} \tag{4.10}$$

Where ζ_{cr} is the notation for critical damping, m is the mass subjected to the movements and k represents the stiffness.

The four heave compensations systems carry the static topsides load. Hence, each cylinder carries one quarter. By taking the damping as a percentage of the critical damping the damping per system is found as:

$$\zeta_{\text{cyl}} = \zeta_{\%} \cdot 2\sqrt{\frac{1}{4} m_t \cdot k_{\text{cyl}}} \tag{4.11}$$

Where ζ_{cyl} is the damping value for the cylinder, $\zeta_{\%}$ is the damping percentage used, m_t it the mass of the topsides and k_{cyl} is the stiffness setting of the cylinder.

5

MODEL

In this chapter the model is presented. First, the definition of the system is described, where the heave compensation system definition (interface) is used from Section 4.4. Followed by the equations of motion of the system, derived in the frequency domain. In the third section, the installation limit as described in Section 3.4.3 is rewritten in formulae. Then attention is given to the calculations that derive the workability.

5.1. SYSTEM DEFINITION

This section explains how the heave compensated `Liwan 3-1` scenario is interpreted in the model. This is done by firstly elaborating the basic view of the model. In the second subsection the force of the heave compensation system are derived. Then attention is paid to the kinematics, explaining the effects of the kinematics on the equations. At last, the used viscous force is briefly elaborated.

5.1.1. MODEL BASICS

A model is made of the `Liwan 3-1` operation to find the effects of the heave compensation system, in the modelling this is often referred to as interface. The system is analysed for the degrees of freedom particularly influenced by the heave compensation system. The model represents the mating stage, thus certain degrees of freedom are not taken into account. The fenders of the substructure and the mooring line arrangement of the barge prevent motions in the surge, sway and yaw direction. Therefore, these barge motions are not included, the model is built on the heave, roll and pitch motions.

The heave compensation system is installed on the deck of the barge, consequently the cylinders stroke perpendicular to the deck. The cylinders are able to stroke in their longitudinal direction and are considered rigid in the transverse directions. At the top of the interface the connection is assumed hinged, as defined in Section 4.4. The wind forces on the topsides are not taken into account, this creates the scenario where the topsides surge and sway is solely dependent on the barge roll and pitch, because the interface is rigid in transverse directions. Thus the topsides model is made for the heave, roll and pitch directions, the surge and sway motions are derived from the barge pitch and roll rotations respectively.

The model is based on six degrees of freedom, three for the topsides and three for the barge. These are noted in the array x shown in Equation (5.1), where subscript t and b indicate topsides and barge respectively. Between the barge and topsides four compensation systems are used. The compensation system is modelled using a spring-damper interface. The locations of the system and the interpretation of the degrees of freedom is illustrated in Figure 5.1.

$$x = \begin{bmatrix} z_t & \phi_t & \theta_t & z_b & \phi_b & \theta_b \end{bmatrix}^T \tag{5.1}$$

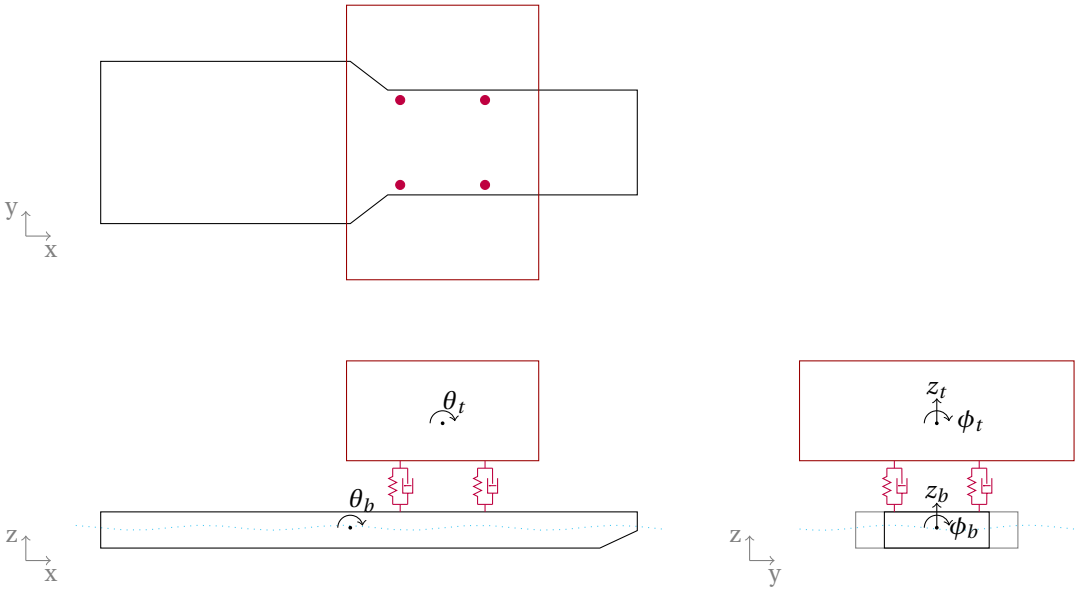

Figure 5.1: Sketch of the model, this is the general input for the derivation of the model. The key elements are: The topsides, the barge, the interface and six degrees of freedom of the model . The heave compensation system is considered a spring-damper system.

All degrees of freedom in the model, as defined in Equation (5.1), influence the displacement of the interfaces. This implies that the forces of the interface involves all 6 degrees of freedom, the effect of the forces on the behaviour of the barge is expected to be significant.

The topsides is subjected to the interface forces and the gravitational force, no other forces on the topsides are taken into account to derive the equations of motion. For the modelling of the mating phase the sub-structures reaction forces can be added to this model. For the barge, four different forces are distinguished: the interface force, the radiation force due to the displacement of water related to the displacement of the barge, a viscous force due to the friction effects of the water on the hull of the vessel and a restoring force which is a combination of buoyancy and gravity. This is shown for heave degree of freedom z, for the barge and topsides, in Equation (5.2). These forces are also applied on the other degrees of freedom.

$$m_t \ddot{z}_t = F_{\text{int}} + F_z \tag{5.2}$$

$$m_b \ddot{z}_b = F_{\text{int}} + F_{\text{rad}} + F_{\text{visc}} + F_{\text{res}} + F_{\text{wave}} \tag{5.3}$$

Where, F_{int} is interface force, F_z the gravitational force, F_{rad} the radiation force, F_{visc} represents the viscous force, F_{res} equals the restoring force and F_{wave} the wave force on the barge.

The radiation, restoring, wave and viscous force are all related to the shape of the barge. These forces are the hydrodynamic properties of the barge. To find these properties the barge is modelled as a finite element model in `Ansys` this model is then used in `AQWA` to find the corresponding hydrodynamic properties. `AQWA` computes the radiation, restoring and wave forces. The `Ansys` and `AQWA` models are detailed in Appendix A.3. The viscous force is determined using the method given in Section 5.1.4.

5.1.2. THE INTERFACE FORCE

The interface force links the topsides to the barge, as can be see in Equations (5.2) and (5.3). All six degrees of freedom in the model have an effect on this force, thus all degrees of freedom influence each other. In this section these relations are elaborated.

The displacements are taken positive upwards and rotations are positive clockwise. The model is thus defined as in figure 5.2. Using this figure the effect of each degree of freedom on the interfaces displacement is found by analysing the increase/decrease in force due to the motions.

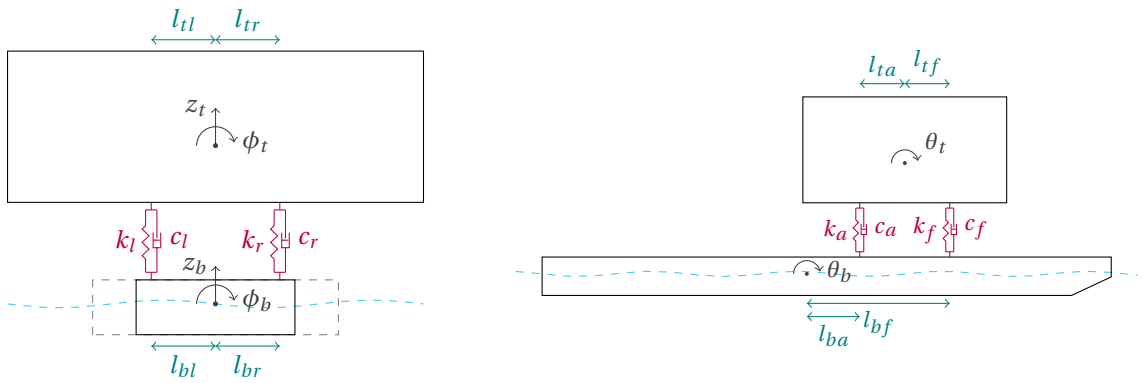

(a) Front view of the model, showing the yz-plane. Used to derive the deflections of the left and right location of the heave compensation system.

(b) Side view, showing the xz-plane. Used to derive the deflections of the front and aft location of the heave compensation system.

Figure 5.2: Cross-sections of the model, used to determine the relations between the degrees of freedom and the interface deflections. The lengths (shown in blue) use the subscripts that links to the topsides or barge, using t and b respectively, and to the left, right, front or aft location with l, r, f and a respectively. The latter is also used to identify the locations of the interfaces.

The force of the spring increases when the relative distance between the topsides and barge decreases, for the damper the same relation is valid for the relative velocity. Thus positive movements for the barge heave and negative movements of the topsides heave increase the force of the interface. Using this principle and the two views from Figure 5.2 the relations between the barge degrees of freedom and the relative displacement of the interfaces is derived.

The relative displacement is used to derive the forces of the interface. The relative displacement (δ) represents the compression or extension of a heave compensation system with relation to the equilibrium position. This displacement is derived four the four locations of the system. From the YZ view, Section 5.1.2, the relative displacement for the left (δ_l) and right (δ_r) side are constructed, where z_t, ϕ_t, z_b and ϕ_b are included, this leads to Equations (5.4) and (5.5). It is assumed that the rotations are small and therefore all equations are linearised. The effect of θ_t and θ_b is captured for the front and aft interfaces with the XZ view and named δ_f and δ_a respectively. This results in Equations (5.6) and (5.7).

$$\delta_l = z_b - z_t + \phi_b\, l_{bl} - \phi_t\, l_{tl} \tag{5.4}$$
$$\delta_r = z_b - z_t - \phi_b\, l_{br} + \phi_t\, l_{tr} \tag{5.5}$$
$$\delta_f = -\theta_b\, l_{bf} + \theta_t\, l_{tf} \tag{5.6}$$
$$\delta_a = -\theta_b\, l_{ba} - \theta_t\, l_{ta} \tag{5.7}$$
$$\delta_{la} = \delta_l + \delta_a = z_b - z_t + \phi_b\, l_{bl} - \phi_t\, l_{tl} - \theta_b\, l_{ba} - \theta_t\, l_{ta} \tag{5.8}$$
$$\delta_{lf} = \delta_l + \delta_f = z_b - z_t + \phi_b\, l_{bl} - \phi_t\, l_{tl} - \theta_b\, l_{bf} + \theta_t\, l_{tf} \tag{5.9}$$
$$\delta_{ra} = \delta_r + \delta_a = z_b - z_t - \phi_b\, l_{br} + \phi_t\, l_{tr} - \theta_b\, l_{ba} - \theta_t\, l_{ta} \tag{5.10}$$
$$\delta_{rf} = \delta_r + \delta_f = z_b - z_t - \phi_b\, l_{br} + \phi_t\, l_{tr} - \theta_b\, l_{bf} + \theta_t\, l_{tf} \tag{5.11}$$

To identify the displacements in each interface, the displacements of Equations (5.4) to (5.7) are combined to four displacements for the interface locations. The notation used to identify each interface is shown in Figure 5.3. Where each interface is given a k and c value, for stiffness and damping respectively. The displacements for the locations of the interface are given the same subscripts and are derived by super positioning the displacements, shown in Equations (5.8) to (5.11).

The displacements of the interfaces are found. In each interface a spring and a damper are situated, the spring forces are related to the displacements and stiffness k whilst the damper forces are related to the velocity and damping c. This system is considered linear, therefore, the damping is also considered linear with the velocity. The interface force is thus derived for each cylinder using:

$$F_{ij} = k_{ij}\,\delta_{ij} + c_{ij}\,\dot{\delta}_{ij} \quad \begin{cases} i = l, r \\ j = a, f \end{cases} \tag{5.12}$$

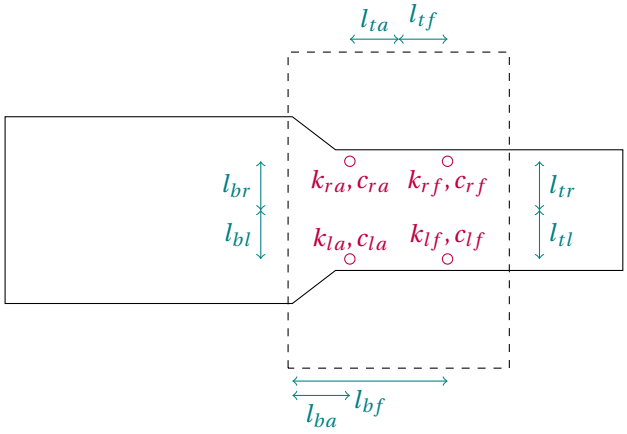

Figure 5.3: Model overview in the XY plane, presenting the notation to identify the four different spring-damper systems. The lengths used to identify the relations correspond to the notation of Figure 5.2

5.1.3. KINEMATICS

The kinematic situation creates a model where phenomena take place that are not directly incorporated in the force balance of Equations (5.2) and (5.3). These phenomena occur because the model is based on two masses, barge and topsides, while in reality these masses are only uncoupled in the heave direction. When considering the pitch/roll motion of the barge the rigid interface assumption causes the pitch/roll to cause sway/surge motions of the topsides. Since the interface can stroke in heave direction and is assumed rigid in transverse directions. This effects the inertial properties of the barge.

For the inertial properties the pitch and roll motions of the barge are adjusted. Figure 5.4 shows roll of the barge with a fully rigid interface connection, the figure shows the effect of barge roll on the topsides sway translation. This movement will also occur when the interface is designed to compensate the motions in the vertical plane of the barge. Therefore, the inertial properties of the topsides should be added to the barge using Steiner's theorem for both pitch and roll rotations. The inertia of the barge is then given as Equations (5.13) and (5.14), the vertical distance between the barge and topsides is noted as l_z.

$$J_{44} = J_{b_{xx}} + J_{t_{xx}} + \quad l_z^2\, m_t \tag{5.13}$$

$$J_{55} = J_{b_{yy}} + J_{t_{yy}} + \underbrace{l_z^2\, m_t}_{\text{Steiner's term}} \tag{5.14}$$

For the inertia (J) the used subscripts are $_{44}$ and $_{55}$ for roll and pitch of the barge, respectively. This notation correlates to the degrees of freedom of the barge as explained in Appendix A.1. The added Steiner terms lead to an significant raise in the barges inertia. The elaboration on the values for barge and topsides inertia's is given in Appendix B.2.

Taking the same roll motion another effect is observed. The topsides is translated and rotated while the barge is only rotated, hence the center of gravity of the topsides is no longer in the same vertical position. This effect will not be translated through the interface forces since the translation does not affect these values. This force creates an overturning moment that is incorporated in the hydrodynamic data from `AQWA`.

5.1.4. THE VISCOUS FORCE

The viscous force is an additional damping force for the roll motions of the barge. The viscous damping in the other barge degrees of freedom is not taken into account because the potential part of the damping, which is gathered in the radiation force, is dominant. However, for roll the contribution of the viscous force is often significant. There are a lot of different methods for the determination of the viscous roll damping, varying from relatively direct methods to very complex methods. An indication of the roll damping is sufficient for this research because the aim is to model the effects of the interface on barge and topsides.

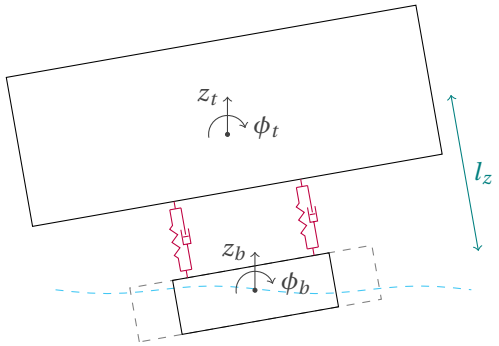

Figure 5.4: The effects of the rigid body assumption in the barge equations, rotation is not compensated creating an overturning moment of the topsides on the barge due to the roll motions. Additionally sway of the topsides occurs, this is taken into account in the rotational inertia of the barge. The sway relates to the height of the topsides center of gravity above the center of gravity of the barge, indicated with l_z.

The method used to determine the viscous roll damping is based on the manual of SEAWAY (Journeé, 2007). Here a derivation is made to obtain the non-dimensional roll damping coefficient, κ. A empirical formula is found by (Journeé, 1991) to determine the κ for rectangular barges. This method has two downsides: the `HYSY229` is not rectangular and the formula is based on a COG on the waterline, that is also not the case. However, no better approximation is found thus this is considered sufficient.

The non-dimensional damping coefficient:

$$\kappa = \frac{B_{44} + B_{44v}}{2\sqrt{(I_{xx} + A_{44}) \cdot C_{44}}} \tag{5.15}$$

And the empirical formula:

$$\kappa = 0.0013 \left(\frac{B}{d}\right)^2 + 0.5 \cdot \phi_a \tag{5.16}$$

The Equation (5.15) is valid for the natural roll frequency of the system, solved iteratively. The values A_{44},B_{44} and C_{44} are obtained from the model with `AQWA`, starting with no viscous damping. This creates an initial damping value which is added to the `AQWA` model, slightly changing the parameters. After three iterations a converged value is obtained. The results of the damping iterations are included in the hydrodynamic model and presented in Appendix A.3.

5.2. THE EQUATIONS OF MOTION

The equations of motion are derived for the six degrees of freedom from Equation (5.1). These equations are transformed to the frequency domain for the analysis of the system. However, the transformation to the frequency domain is only valid when the system contains a fully linear set of equations, this is detailed at the end of this section.

In this section the forces of Equations (5.2) and (5.3) are detailed. Firstly, the equations of motion for the topsides (Equation (5.2)) are presented, followed by the equations for the barge (Equation (5.3)). Afterwards the equations are combined and transformed in the frequency domain formulation, with attention to the final set of equations.

5.2.1. TOPSIDES EQUATIONS

The equations of motion are derived using free body diagrams, as shown in Figure 5.5. As mentioned, no environmental loads on the topsides are taken into account. Therefore, the three degrees of freedom are only subjected to the forces of the interface connections and the gravitational force. These equations are time dependent, where $\dot{x}$ means the time derivation of x. The translation from the time to the frequency domain is done in the last subsection.

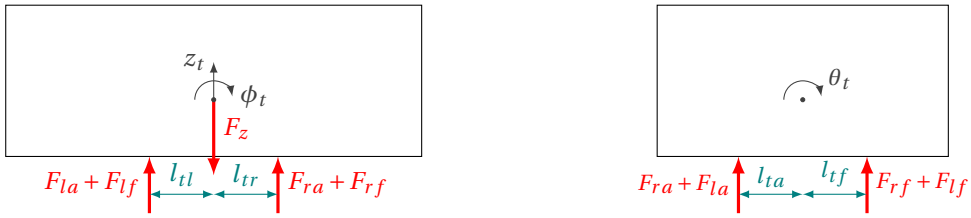

(a) Front view, yz-plane.

(b) Side view, xz-plane.

Figure 5.5: Free body diagram of the topsides, the degrees of freedom are defined as shown in this figure. Used to derive the equations of motion.

The equation of motion for the topsides are:

$$\sum F_z \uparrow: \qquad m_t \ddot{z}_t = F_{la} + F_{lf} + F_{ra} + F_{rf} + F_z \tag{5.17}$$

$$\sum F_\phi \curvearrowright: \qquad J_{t_{xx}} \ddot{\phi}_t = (F_{la} + F_{lf}) \cdot l_{tl} - (F_{ra} + F_{rf}) \cdot l_{tr} \tag{5.18}$$

$$\sum F_\theta \curvearrowright: \qquad J_{t_{yy}} \ddot{\theta}_t = (F_{ra} + F_{la}) \cdot l_{ta} - (F_{rf} + F_{lf}) \cdot l_{tf} \tag{5.19}$$

Where m_t is the topsides mass, the topsides inertial values are given with $J_{t_{xx}}$ and $J_{t_{yy}}$, for roll and pitch rotations respectively. The forces (F) and lengths (l) the subscripts match the description of Figure 5.5.

The inertia of the topsides is derived in Equations (B.9) to (B.15). In this derivation the topsides is assumed to contain eccentric center of gravity in the vertical plane.

5.2.2. BARGE EQUATIONS

The barge equations of motions are derived from Equation (5.3), the barge is subjected to five forces: $F_{\text{int}}, F_{\text{rad}}, F_{\text{visc}}$, F_{res} and F_{wave}. The interface force (F_{int}) and viscous force (F_{visc}) are identified in Sections 5.1.2 and 5.1.4 respectively. The radiation force is the combination of the added mass and radiation damping, these forces are frequency dependant and obtained with the 3D-panel method in `AQWA`. The `AQWA` model is also used for the restoring force (F_{res}) and wave force (F_{wave}), the latter is also frequency dependant.

The radiation force and restoring force contain coupling elements, due to the symmetry and anti-symmetry of the barge. In hydrodynamic calculations three degrees of freedom are coupled due to symmetry: surge, heave and pitch. The anti-symmetric degrees are also coupled: sway, roll and yaw. The symmetric and anti-symmetric motions are uncoupled. Therefore, in this model only the heave and pitch motions are coupled. This leads to the following force matrices for the barges degrees of freedom:

$$F_{\text{rad}} = -\begin{bmatrix} a_{33}(\omega) & 0 & a_{35}(\omega) \\ 0 & a_{44}(\omega) & 0 \\ a_{53}(\omega) & 0 & a_{55}(\omega) \end{bmatrix} \cdot \begin{bmatrix} \ddot{z}_b \\ \ddot{\phi}_b \\ \ddot{\theta}_b \end{bmatrix} - \begin{bmatrix} b_{33}(\omega) & 0 & b_{35}(\omega) \\ 0 & b_{44}(\omega) & 0 \\ b_{53}(\omega) & 0 & b_{55}(\omega) \end{bmatrix} \cdot \begin{bmatrix} \dot{z}_b \\ \dot{\phi}_b \\ \dot{\theta}_b \end{bmatrix} \tag{5.20}$$

$$F_{\text{res}} = -\begin{bmatrix} k_{33} & 0 & k_{35} \\ 0 & k_{44} & 0 \\ k_{53} & 0 & k_{55} \end{bmatrix} \cdot \begin{bmatrix} z_b \\ \phi_b \\ \theta_b \end{bmatrix} \tag{5.21}$$

$$F_{\text{wave}} = \begin{bmatrix} F_{\text{wave}_3}(\omega) & M_{\text{wave}_4}(\omega) & M_{\text{wave}_5}(\omega) \end{bmatrix}^T \tag{5.22}$$

Where the subscript notation is based on the degree of freedom as used in common literature. These matrices relate to the forces of Equation (5.3).

The free body diagrams of Figure 5.6, the definitions from Equation (5.3) and the kinematic relations from Section 5.1.3 lead to the equations of motions for the barge, presented in Equations (5.23) to (5.25).

$$\sum F_z \uparrow: \quad (m_b + a_{33}(\omega))\,\ddot{z}_b + b_{33}(\omega)\,\dot{z}_b + k_{33}\,z_b + a_{35}(\omega)\,\ddot{\theta}_b + b_{35}(\omega)\,\dot{\theta}_b + k_{35}\,\theta_b = -F_{la} - F_{ra} - F_{lf} - F_{rf} + F_{\text{wave}_3}(\omega) \tag{5.23}$$

$$\sum F_\phi \curvearrowright: \quad (J_{44} + a_{44}(\omega))\,\ddot{\phi}_b + (b_{44}(\omega) + b_{44v})\,\dot{\phi}_b + k_{44}\,\phi_b = -(F_{lf} + F_{la})\,l_{bl} + (F_{rf} + F_{ra})\,l_{br} + M_{\text{wave}_4}(\omega) + F_{om_\phi} \tag{5.24}$$

$$\sum F_\theta \curvearrowright: \quad (J_{55} + a_{55}(\omega))\,\ddot{\theta}_b + b_{55}(\omega)\,\dot{\theta}_b + k_{55}\,\theta_b + a_{53}(\omega)\,\ddot{z}_b + b_{53}(\omega)\,\dot{z}_b + k_{53}\,z_b = (F_{la} + F_{ra})\,l_{ba} + (F_{lf} + F_{rf})\,l_{bf} + M_{\text{wave}_5}(\omega) + F_{om_\theta} \tag{5.25}$$

(a) YZ view (b) XZ view

Figure 5.6: Free body diagram of the barge, the degrees of freedom are defined as shown in this figure. Used to derive the equations of motion.

The used mass and inertia of the barge are given in Appendix B.

5.2.3. THE FREQUENCY DOMAIN

The frequency domain is derived with a Fourier analysis of the time dependent equations. The equations of motion derived in the previous sections are valid in the frequency domain. In fact they are only valid when translated to the frequency domain (or when looking at a single sinusoidal function). When writing the equations with the time dependant x the frequency domain relations are derived with the Fourier transformation.

The equations of motion derived in the previous sections contain frequency dependant parameters in with time dependant displacements. The terms are gathered as:

$$\big(M + A(\omega)\big)\,\ddot{x}(t) + B(\omega)\,\dot{x}(t) + K\,x(t) = F(\omega, t) \tag{5.26}$$

Where:

M = mass matrix	K = restoring matrix
$A(\omega)$ = added mass matrix	x = displacement vector
$B(\omega)$ = damping matrix	$F(\omega, t)$ = combined wave forces

This equation is only valid when the system acts on a single frequency. Thus, the time domain is transformed in the frequency domain to be able to analyse the response independent of time.

The Fourier transformation of $g(t)$ is defined as:

$$G(\omega) = \int_{-\infty}^{\infty} g(t)\,e^{-i\omega t}\,dt \tag{5.27}$$

The Fourier transformation of Equation (5.26) is found as:

$$\Big(-\omega^2\big(M + A(\omega)\big) + i\,\omega\,B(\omega) + K\Big)X(\omega) = F(\omega) \tag{5.28}$$

From this equation the response of the system is derived. For this the equations of motions are written into the six degrees of freedom of the model and all the terms are gathered in the A, B and K matrices, what is left is

the force vector containing the wave force and gravitational force. The displacement vector in the frequency domain is given in Equation (5.29).

$$X(\omega) = \begin{bmatrix} z_t(\omega) & \phi_t(\omega) & \theta_t(\omega) & z_b(\omega) & \phi_b(\omega) & \theta_b(\omega) \end{bmatrix}^T \tag{5.29}$$

The matrices obtained for the vector X are characterised in the following way:

$$\left[\begin{array}{c|c} \text{Topsides terms} & \text{Coupling terms} \\ \hline \text{Coupling terms} & \text{Barge terms} \end{array}\right] \tag{5.30}$$

The mass matrix is found by combining the second derivatives from the Equations (5.17) to (5.19) for the topsides and Equations (5.23) to (5.25) for the barge. These are then rewritten into:

$$(M + A(\omega)) = \left(\begin{bmatrix} m_t & 0 & 0 & 0 & 0 & 0 \\ 0 & J_{t_{xx}} & 0 & 0 & 0 & 0 \\ 0 & 0 & J_{t_{yy}} & 0 & 0 & 0 \\ 0 & 0 & 0 & m_b & 0 & 0 \\ 0 & 0 & 0 & 0 & J_{44} & 0 \\ 0 & 0 & 0 & 0 & 0 & J_{55} \end{bmatrix} + \begin{bmatrix} 0 & 0 & 0 & 0 & 0 & 0 \\ 0 & 0 & 0 & 0 & 0 & 0 \\ 0 & 0 & 0 & 0 & 0 & 0 \\ 0 & 0 & 0 & a_{33}(\omega) & 0 & a_{35}(\omega) \\ 0 & 0 & 0 & 0 & a_{44}(\omega) & 0 \\ 0 & 0 & 0 & a_{53}(\omega) & 0 & a_{55}(\omega) \end{bmatrix} \right) \tag{5.31}$$

The damping is gathered using the same principle as the masses, rewritten as:

$$B(\omega) = \begin{bmatrix} c_{lf} + c_{la} + c_{rf} + c_{ra} & c_{lf} l_{tl} + c_{la} l_{tl} - c_{rf} l_{tr} - c_{ra} l_{tr} & c_{la} l_{ta} - c_{lf} l_{tf} - c_{rf} l_{tf} + c_{ra} l_{ta} \\ c_{lf} l_{tl} + c_{la} l_{tl} - c_{rf} l_{tr} - c_{ra} l_{tr} & c_{lf} l_{tl}^2 + c_{la} l_{tl}^2 + c_{rf} l_{tr}^2 + c_{ra} l_{tr}^2 & c_{la} l_{tl} l_{ta} - c_{lf} l_{tf} l_{tl} + c_{rf} l_{tf} l_{tr} - c_{ra} l_{tr} l_{ta} \\ c_{la} l_{ta} - c_{lf} l_{tf} - c_{rf} l_{tf} + c_{ra} l_{ta} & c_{la} l_{tl} l_{ta} - c_{lf} l_{tf} l_{tl} + c_{rf} l_{tf} l_{tr} - c_{ra} l_{tr} l_{ta} & c_{lf} l_{tf}^2 + c_{la} l_{ta}^2 + c_{rf} l_{tf}^2 + c_{ra} l_{ta}^2 \\ -c_{lf} - c_{la} - c_{rf} - c_{ra} & c_{rf} l_{tr} - c_{la} l_{tl} - c_{lf} l_{tl} + c_{ra} l_{tr} & c_{lf} l_{tf} - c_{la} l_{ta} + c_{rf} l_{tf} - c_{ra} l_{ta} \\ -l_{br}\left(c_l b + c_{la} - c_{rf} - c_{ra}\right) & -l_{br}\left(c_l b l_{tl} + c_{la} l_{tl} + c_{rf} l_{tr} + c_{ra} l_{tr}\right) & l_{br}\left(c_l b l_{tf} - c_{la} l_{ta} - c_{rf} l_{tf} + c_{ra} l_{ta}\right) \\ c_{lf} l_{bf} + c_{la} l_{ba} + c_{rf} l_{bf} + c_{ra} l_{ba} & c_{lf} l_{bf} l_{tl} + c_{la} l_{ba} l_{tl} - c_{rf} l_{bf} l_{tr} - c_{ra} l_{ba} l_{tr} & c_{la} l_{ba} l_{ta} - c_{lf} l_{bf} l_{tf} - c_{rf} l_{bf} l_{tf} + c_{ra} l_{ba} l_{ta} \end{bmatrix} \cdots$$

$$\cdots \begin{bmatrix} -c_{lf} - c_{la} - c_{rf} - c_{ra} & c_{rf} l_{br} - c_{la} l_{bl} - c_{lf} l_{bl} + c_{ra} l_{br} & c_{lf} l_{bf} + c_{la} l_{ba} + c_{rf} l_{bf} + c_{ra} l_{ba} \\ c_{rf} l_{tr} - c_{la} l_{tl} - c_{lf} l_{tl} + c_{ra} l_{tr} & -c_{lf} l_{bl} l_{tl} - c_{la} l_{bl} l_{tl} - c_{rf} l_{br} l_{tr} - c_{ra} l_{br} l_{tr} & c_{lf} l_{bf} l_{tl} + c_{la} l_{ba} l_{tl} - c_{rf} l_{bf} l_{tr} - c_{ra} l_{ba} l_{tr} \\ c_{lf} l_{tf} - c_{la} l_{ta} + c_{rf} l_{tf} - c_{ra} l_{ta} & c_{lf} l_{bl} l_{tf} - c_{la} l_{bl} l_{ta} - c_{rf} l_{br} l_{tf} + c_{ra} l_{br} l_{ta} & c_{la} l_{ba} l_{ta} - c_{lf} l_{bf} l_{tf} - c_{rf} l_{bf} l_{tf} + c_{ra} l_{ba} l_{ta} \\ b_{33}(\omega) + c_{lf} + c_{la} + c_{rf} + c_{ra} & c_{lf} l_{bl} + c_{la} l_{bl} - c_{rf} l_{br} - c_{ra} l_{br} & b_{35}(\omega) - c_{lf} l_{bf} - c_{la} l_{ba} - c_{rf} l_{bf} - c_{ra} l_{ba} \\ l_{br}\left(c_l b + c_{la} - c_{rf} - c_{ra}\right) & b_{44}(\omega) + c_{rf} l_{br}^2 + c_{ra} l_{br}^2 + c_{lf} l_{bl} l_{br} + c_{la} l_{bl} l_{br} & -l_{br}\left(c_l b l_{bf} + c_{la} l_{ba} - c_{rf} l_{bf} - c_{ra} l_{ba}\right) \\ b_{53}(\omega) - c_{lf} l_{bf} - c_{la} l_{ba} - c_{rf} l_{bf} - c_{ra} l_{ba} & c_{rf} l_{bf} l_{br} - c_{la} l_{bl} l_{ba} - c_{lf} l_{bf} l_{bl} + c_{ra} l_{br} l_{ba} & b_{55}(\omega) + c_{lf} l_{bf}^2 + c_{la} l_{ba}^2 + c_{rf} l_{bf}^2 + c_{ra} l_{ba}^2 \end{bmatrix} \tag{5.32}$$

The stiffness is found as:

$$K = \begin{bmatrix} k_{lf} + k_{la} + k_{rf} + k_{ra} & k_{lf} l_{tl} + k_{la} l_{tl} - k_{rf} l_{tr} - k_{ra} l_{tr} & k_{la} l_{ta} - k_{lf} l_{tf} - k_{rf} l_{tf} + k_{ra} l_{ta} \\ k_{lf} l_{tl} + k_{la} l_{tl} - k_{rf} l_{tr} - k_{ra} l_{tr} & k_{lf} l_{tl}^2 + k_{la} l_{tl}^2 + k_{rf} l_{tr}^2 + k_{ra} l_{tr}^2 & k_{la} l_{tl} l_{ta} - k_{lf} l_{tf} l_{tl} + k_{rf} l_{tf} l_{tr} - k_{ra} l_{tr} l_{ta} \\ k_{la} l_{ta} - k_{lf} l_{tf} - k_{rf} l_{tf} + k_{ra} l_{ta} & k_{la} l_{tl} l_{ta} - k_{lf} l_{tf} l_{tl} + k_{rf} l_{tf} l_{tr} - k_{ra} l_{tr} l_{ta} & k_{lf} l_{tf}^2 + k_{la} l_{ta}^2 + k_{rf} l_{tf}^2 + k_{ra} l_{ta}^2 \\ -k_{lf} - k_{la} - k_{rf} - k_{ra} & k_{rf} l_{tr} - k_{la} l_{tl} - k_{lf} l_{tl} + k_{ra} l_{tr} & k_{lf} l_{tf} - k_{la} l_{ta} + k_{rf} l_{tf} - k_{ra} l_{ta} \\ -l_{br}\left(k_{lf} + k_{la} - k_{rf} - k_{ra}\right) & -l_{br}\left(k_{lf} l_{tl} + k_{la} l_{tl} + k_{rf} l_{tr} + k_{ra} l_{tr}\right) & l_{br}\left(k_{lf} l_{tf} - k_{la} l_{ta} - k_{rf} l_{tf} + k_{ra} l_{ta}\right) \\ k_{lf} l_{bf} + k_{la} l_{ba} + k_{rf} l_{bf} + k_{ra} l_{ba} & k_{lf} l_{bf} l_{tl} + k_{la} l_{ba} l_{tl} - k_{rf} l_{bf} l_{tr} - k_{ra} l_{ba} l_{tr} & k_{la} l_{ba} l_{ta} - k_{lf} l_{bf} l_{tf} - k_{rf} l_{bf} l_{tf} + k_{ra} l_{ba} l_{ta} \end{bmatrix} \cdots$$

$$\cdots \begin{bmatrix} -k_{lf} - k_{la} - k_{rf} - k_{ra} & k_{rf} l_{br} - k_{la} l_{bl} - k_{lf} l_{bl} + k_{ra} l_{br} & k_{lf} l_{bf} + k_{la} l_{ba} + k_{rf} l_{bf} + k_{ra} l_{ba} \\ k_{rf} l_{tr} - k_{la} l_{tl} - k_{lf} l_{tl} + k_{ra} l_{tr} & -k_{lf} l_{bl} l_{tl} - k_{la} l_{bl} l_{tl} - k_{rf} l_{br} l_{tr} - k_{ra} l_{br} l_{tr} & k_{lf} l_{bf} l_{tl} + k_{la} l_{ba} l_{tl} - k_{rf} l_{bf} l_{tr} - k_{ra} l_{ba} l_{tr} \\ k_{lf} l_{tf} - k_{la} l_{ta} + k_{rf} l_{tf} - k_{ra} l_{ta} & k_{lf} l_{bl} l_{tf} - k_{la} l_{bl} l_{ta} - k_{rf} l_{br} l_{tf} + k_{ra} l_{br} l_{ta} & k_{la} l_{ba} l_{ta} - k_{lf} l_{bf} l_{tf} - k_{rf} l_{bf} l_{tf} + k_{ra} l_{ba} l_{ta} \\ k_{33} + k_{lf} + k_{la} + k_{rf} + k_{ra} & k_{lf} l_{bl} + k_{la} l_{bl} - k_{rf} l_{br} - k_{ra} l_{br} & k_{35} - k_{lf} l_{bf} - k_{la} l_{ba} - k_{rf} l_{bf} - k_{ra} l_{ba} \\ l_{br}\left(k_{lf} + k_{la} - k_{rf} - k_{ra}\right) & k_{44} + k_{rf} l_{br}^2 + k_{ra} l_{br}^2 - g l_z m_t + k_{lf} l_{bl} l_{br} + k_{la} l_{bl} l_{br} & -l_{br}\left(k_{lf} l_{bf} + k_{la} l_{ba} - k_{rf} l_{bf} - k_{ra} l_{ba}\right) \\ k_{53} - k_{lf} l_{bf} - k_{la} l_{ba} - k_{rf} l_{bf} - k_{ra} l_{ba} & k_{rf} l_{bf} l_{br} - k_{la} l_{bl} l_{ba} - k_{lf} l_{bf} l_{bl} + k_{ra} l_{br} l_{ba} & k_{55} + k_{lf} l_{bf}^2 + k_{la} l_{ba}^2 + k_{rf} l_{bf}^2 + k_{ra} l_{ba}^2 - g l_z m_t \end{bmatrix} \tag{5.33}$$

Finally, the force vector :

$$F(\omega) = \begin{bmatrix} F_z & 0 & 0 & F_{\text{wave}_3}(\omega) & M_{\text{wave}_4}(\omega) & M_{\text{wave}_5}(\omega) \end{bmatrix}^T \tag{5.34}$$

Where F_z is not affected by the transformation and in the frequency domain the wave force is dependant of the wave spectrum. This implies that the wave force is dependant of H_s, Ω and ω. Where H_s is the significant wave height and Ω stands for the wave direction.

In the model the topsides COG is assumed centered in the horizontal plane. This is done to be able to design four equal heave compensation systems that all cope with an equal share of the topsides loads. Thus the stiffness and damping of the four cylinders can be taken equal and the topsides length are also symmetrical. This leads to the following simplifications: $k_{la} = k_{lf} = k_{ra} = k_{rf} = \frac{k}{4}$, $c_{la} = c_{lf} = c_{ra} = c_{rf} = \frac{c}{4}$, $l_{bl} = l_{br}$, $l_{tl} = l_{tr}$ and $l_{ta} = l_{tf}$. Then the simplified B^* and K^* matrices of the model become:

$$B^*(\omega) = \begin{bmatrix} c & 0 & 0 & -c & 0 & \frac{c}{2}\left(l_{bf}+l_{ba}\right) \\ 0 & c\,l_{tl}^2 & 0 & 0 & -c\,l_{bl}\,l_{tl} & 0 \\ 0 & 0 & c\,l_{tf}^2 & 0 & 0 & -\frac{c\,l_{tf}}{2}\left(l_{bf}-l_{ba}\right) \\ -c & 0 & 0 & \mathrm{b}_{33}(\omega)+c & 0 & \mathrm{b}_{35}(\omega)-\frac{c}{2}\left(l_{bf}+l_{ba}\right) \\ 0 & -c\,l_{bl}\,l_{tl} & 0 & 0 & \mathrm{b}_{44}(\omega)+\mathrm{b}_{44v}+c\,l_{bl}^2 & 0 \\ \frac{c}{2}\left(l_{bf}+l_{ba}\right) & 0 & -\frac{c\,l_{tf}}{2}\left(l_{bf}-l_{ba}\right) & \mathrm{b}_{53}(\omega)-\frac{c}{2}\left(l_{bf}+l_{ba}\right) & 0 & \mathrm{b}_{55}(\omega)+\frac{c}{2}\left(l_{bf}^2+l_{ba}^2\right) \end{bmatrix} \tag{5.35}$$

$$K^* = \begin{bmatrix} k & 0 & 0 & -k & 0 & \frac{k}{2}\left(l_{bf}+l_{ba}\right) \\ 0 & k\,l_{tl}^2 & 0 & 0 & -k\,l_{bl}\,l_{tl} & 0 \\ 0 & 0 & k\,l_{tf}^2 & 0 & 0 & -\frac{k\,l_{tf}}{2}\left(l_{bf}-l_{ba}\right) \\ -k & 0 & 0 & \mathrm{k}_{33}+k & 0 & \mathrm{k}_{35}-\frac{k}{2}\left(l_{bf}+l_{ba}\right) \\ 0 & -k\,l_{bl}\,l_{tl} & 0 & 0 & \mathrm{k}_{44}+k\,l_{bl}^2-g\,l_z\,m_t & 0 \\ \frac{k}{2}\left(l_{bf}+l_{ba}\right) & 0 & -\frac{k\,l_{tf}}{2}\left(l_{bf}-l_{ba}\right) & \mathrm{k}_{53}-\frac{k}{2}\left(l_{bf}+l_{ba}\right) & 0 & \mathrm{k}_{55}+\frac{k}{2}\left(l_{ba}^2+l_{bf}^2\right)-g\,l_z\,m_t \end{bmatrix} \tag{5.36}$$

In these matrices the uncoupled roll equations are visible and the coupling between the heave and pitch variables is shown. With this equations the steady state solution on regular waves is found for all frequencies.

To derive the motions of the system on a given sea state the Response Amplitude Operator (RAO) is used. The RAO's can be used the find the amplitude of the response based on the energy density for each wave frequency. This method is given in the next section. The RAO's of the system can be derived for the different values of k and c and the effects to varying this value on the Eigen frequencies of system can be found.

The RAO's are found for the six degrees of freedom of the model with the following formula:

$$R(\omega) = \frac{F(\omega)}{\left(-\omega^2\left(M+A(\omega)\right)+i\,\omega\,B^*(\omega)+K^*\right)} \tag{5.37}$$

Where R represent the RAO's. This formula is practically equal to Equation (5.28), only than the displacement vector X is replaced with the RAO representation (R). This is done for the elaboration on the leg displacement in Section 5.4. Note, that the simplified matrices for damping and stiffness are used.

For the heave compensation system the stiffness and damping are inserted as:

$$k = 4 \cdot k_{\text{cyl}} \tag{5.38}$$

$$c = 4 \cdot \zeta_{\%} \tag{5.39}$$

To represent the `Liwan 3-1` installation the stiffness is put on very large value.

5.3. INSTALLATION LIMITS

The installation limits are derived with the method as described in Chapter 3. In this method the limit is set on the total horizontal force on the substructure, during the pre-stabbing phase of the mating stage. To determine the workability, the maximum force is translated to a maximum velocity of the topsides. How this velocity aids the workability calculations, is explained in the next section.

The maximum installation velocity is derived using the kinetic energy of the topsides and the energy storing capacity of the LMU and substructure. The energy storage is assumed ideal, thus no losses are taken into account. There are eight substructure legs on the `Liwan 3-1` substructure, in the mating phase the substructure is positioned as illustrated in Figure 5.7a. For each of this legs the model derived in Section 3.4 can be applied, for convenience the model is re-posted in Figure 5.7b. The installation limit is assessed for 1, 2, 4 and 8 legs subjected to impact loads.

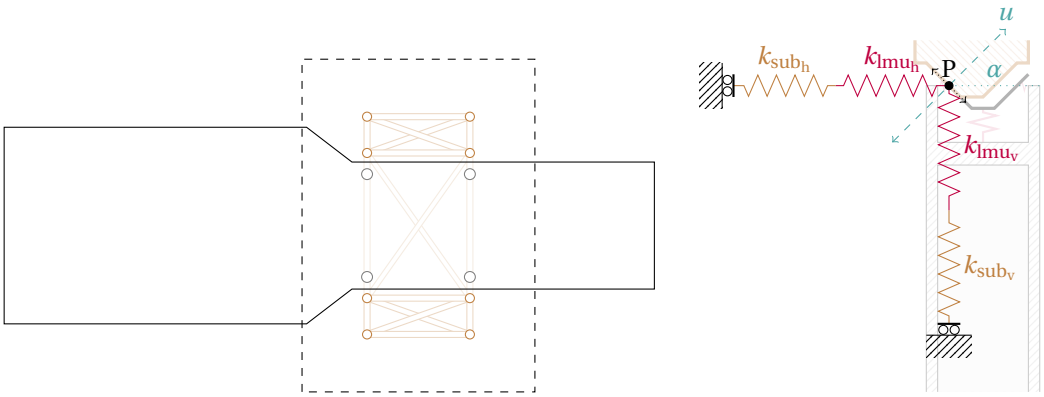

(a) The configuration of the substructure legs during mating position with the barge and topsides aligned.

(b) The model representing the substructure and LMU. Where the deflection (u), due to impact of point p, take place perpendicular to the LMU surface, this is represented in with the blue line. This model is derived in Section 3.4.

Figure 5.7: The basis of the installation limit model. Eight legs positioned as in the left figure are subjected to the model of the right figure. In other words, the model as shown in the right is applied on each of the eight substructure leg locations as shown in the left figure.

The stiffness information for the four springs is gathered in Section 3.4. The LMU stiffness is given in Figures 3.5a and 3.5b, these figures contain the deflection curve of the LMU's in horizontal and vertical direction. For both directions the gradient is derived which is used as linear LMU stiffness. The section also gives the substructure vertical stiffness and the horizontal stiffness is found for 1, 4 and 8 legs, the stiffness for 2 legs is derived with a linear interpolation of this data. From the four springs only the horizontal substructure stiffness is scalable with the number of legs.

The LMU and substructure springs are connected in series, Figure 5.7b. The individual legs are combined as parallel springs to get the total stiffness of the substructure. The equivalent stiffness for the substructure is written as a function of the number of legs as:

$$k_{eq_h}(N) = N \cdot \frac{1}{\left(k_{\text{lmu}_\text{h}}^{-1} + k_{\text{sub}_\text{h}}^{-1}(N)\right)} \tag{5.40}$$

$$k_{eq_v}(N) = N \cdot \frac{1}{\left(k_{\text{lmu}_\text{v}}^{-1} + k_{\text{sub}_\text{v}}^{-1}\right)} \tag{5.41}$$

Where N is the number of substructure legs in the calculation, k_{lmu} is the stiffness for the LMU and k_{sub} is the stiffness of the substructure, which is dependent on the number of considered legs. The subscripts h and v indicate horizontal and vertical direction, respectively.

With the equivalent stiffness the maximum deflection to reach the horizontal force limit is found. The deflection is taken perpendicular to the LMU surface, using α and Figure 5.7b, the relations between the deflection and energy are found as:

$$F_{h_{\max}} = k_{eq_h} \cdot u_{h_{\max}} \tag{5.42}$$

$$u_{v_{\max}} = \frac{u_{h_{\max}}}{\tan(\alpha)} \tag{5.43}$$

$$E_{\text{sub}} = \frac{1}{2} k_{eq_h} \cdot u_h^2 + \frac{1}{2} k_{eq_v} \cdot u_v^2 \tag{5.44}$$

$$E_{\max} = \frac{1}{2} k_{eq_h} \cdot u_{h_{\max}}^2 + \frac{1}{2} k_{eq_v} \cdot u_{v_{\max}}^2 \tag{5.45}$$

Where $F_{h_{\max}}$ is the found maximum horizontal load on the substructure, $u_{h_{\max}}$ is the maximum horizontal deflection corresponding to this load, $u_{v_{\max}}$ is the maximum vertical deflection that correspond to the deflection line assumed in this model, E_{sub} represents the energy absorbed by the substructure and finally $E_{\max}$ is the maximum energy before failure of the substructure.

By comparing the kinetic energy of the topsides with the maximum energy in the substructure springs, the maximum velocity of the topsides impact is found as:

$$E_{\text{kin}} = E_{\max} \tag{5.46}$$

$$\frac{1}{2} m_t \cdot V_{\max}^2 = E_{\max} \tag{5.47}$$

$$V_{\max} = \sqrt{\frac{\left(k_{eq_h} + \frac{k_{eq_v}}{\tan^2(\alpha)}\right) u_{h_{\max}}^2}{m_t}} \tag{5.48}$$

The maximum velocity is derived for the four different leg contact scenarios; 1, 2, 4 and 8 legs. This is done to find a limit for all possible the impact scenarios. From which the installation maximum will be derived. The aim is to work with a single maximum value. In reality the number of legs changes during the impact scenario, this creates a complex setting which is unique for each impact case. The lowest velocity found with this method incorporates all possible impact cases, due to the changing number of legs in contact. Therefore, this lowest value will be used. This method is conservative, but for the comparison of two scenarios a conservative benchmark value is adequate.

5.4. WORKABILITY CALCULATIONS

For the workability calculations the model, as described in sections Sections 5.1 and 5.2, is used to find the velocity of the topsides caused by different sea states. To determine which motions are allowed the velocity of the model on the substructure leg locations is analysed and compared with the installation limit velocity.

The velocity of the topsides is assessed by combining the surge, sway and heave components of the topsides. The surge of the topsides is related to the roll of the barge, as visualised in Figure 4.7. Whilst the sway motions of the topsides are caused by pitch of the barge. For the heave of the topsides the combination of the topsides heave, roll and pitch motions is compiled. The surge and sway components are equal for all topsides leg locations and the heave is calculated for the outer leg positions.

The section firstly explains how the motions at the topsides leg locations are obtained, followed by the details of the used wave spectra. After that the velocity derivation is presented. Finally, the method to derive the workability from the velocity is described.

5.4.1. DETERMINE MOTIONS AT THE LEG LOCATIONS

The frequency domain model is used to determine the motions at the leg locations. At the leg locations the topsides is subjected to surge, sway and heave motions. The horizontal motions are caused by the rotations of the barge and the vertical motions are a result of the topsides degrees of freedom.

The model is built on the kinematics as explained in Section 4.4, hence the roll of the barge is directly linked to sway of the topsides, this is also illustrated in Figure 5.8. The same applies to the pitch motions of the barge, that cause surge motions of the topsides. By linearising the equations the effect of the topsides roll and pitch on the topsides surge and sway motions is not taken into account. The same counts for the rotations of the barge on the topsides heave motion. Therefore the RAO's of the topsides displacement at the leg location are given as:

$$R_{x_{\text{leg}}}(\omega) = R_{\phi_b}(\omega) \cdot l_z \tag{5.49}$$

$$R_{y_{\text{leg}}}(\omega) = R_{\theta_b}(\omega) \cdot l_z \tag{5.50}$$

$$R_{z_{\text{leg}}}(\omega) = R_{z_t}(\omega) + R_{\phi_t}(\omega) \cdot l_y + R_{\theta_t}(\omega) \cdot l_x \tag{5.51}$$

Where R indicates an RAO. z, ϕ and θ represent the heave, roll and pitch respectively, l_z is the height from the center of gravity of the barge to the bottom of the topsides, l_x is the distance over the x-axis from the center of gravity of the topsides towards the location of the leg and l_y equals the distance over the y-axis from the center of gravity of the barge to the location of the leg. The subscripts b and t represent the barge and topsides respectively.

The length of l_z is considered fixed, in reality the vertical motions of the topsides effect the value of l_z. For small angles the influence of the rotations on l_z can be neglected. The heave of the barge and topsides will directly influence this length. This effect is considered insignificant, because the heave motions are much smaller than l_z. Hence, the change in length is relatively small.

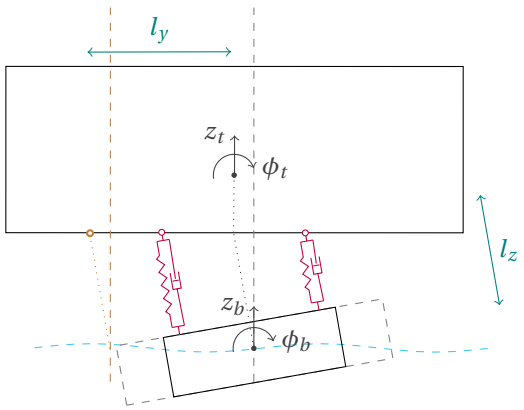

Figure 5.8: Illustration of the topsides displacement due to roll of the barge, with heave compensated topsides. This figure illustrates that the sway is equal at all locations of the topsides bottom. The leg position is drawn as a circle on the topsides. The original location is represented by the dashed brown line. The displacement of the leg is equal to the sway of the topsides, at height l_z.

The three directional RAO's are then combined into a single displacement vector. From this vector the velocities will be derived for each wave spectrum. This combination is done to assess the motions due to the combination of movements, thus taking the phases into account. When the motions are not combined the maximum values of the three directions would lead to a very conservative approach. The displacement at a single leg location thus becomes:

$$R_{u_{\text{leg}}}(\omega) = \sqrt{R^2_{x_{\text{leg}}}(\omega) + R^2_{y_{\text{leg}}}(\omega) + R^2_{z_{\text{leg}}}(\omega)} \tag{5.52}$$

This displacement vector is derived for the four outer leg locations, the leg locations are shown in Figure 5.7a. These vectors are all subjected to the derivation of the velocity, explained in the next subsection. From these four vectors the maximum velocity is used for the workability calculations.

5.4.2. WAVE SPECTRA

In this research the sea state of Nigeria is used. The Nigerian sea states are found in internal documentation, which provided information regarding the method of the used wave spectrum for the data analysis.

In this particular case the JONSWAP spectrum with a peak enhancement factor of 8 is used. This is odd since the west African sea is often considered as a fully developed sea and thus the logical fit would be the Pierson-Moskowitz spectrum. Since the data from the internal file is used, the peak enhancement factor of 8 is considered. The JONSWAP spectrum is obtained from the DNV guidelines as (DNV-RP-C205, 2010):

$$S_{\text{JONSWAP}}(\omega) = A_\gamma \cdot S_{\text{PM}}(\omega) \cdot \gamma^{\exp\left(-0.5\left(\frac{\omega-\omega_p}{\sigma_s \omega_p}\right)^2\right)} \tag{5.53}$$

$$S_{\text{PM}}(\omega) = \frac{5}{16} \cdot H_s^2 \cdot \omega_p^4 \cdot \omega^{-5} \exp\left(-\frac{5}{4}\left(\frac{\omega}{\omega_p}\right)^{-4}\right) \tag{5.54}$$

Where the following parameters are used:

$$\begin{aligned} S_{\text{PM}} &= \text{Pierson} - \text{Moskowitz spectrum} \\ \gamma &= \text{Non dimensional peak shape parameter} \\ \sigma_s &= \text{Spectral width parameter} \\ \sigma_s &= 0.07 \text{ for } \omega \leq \omega_p \\ \sigma_s &= 0.09 \text{ for } \omega > \omega_p \\ A_\gamma &= 1 - 0.287 \ln \gamma \\ \omega_p &= \frac{2\pi}{T_p} \end{aligned}$$

The value γ corresponds to the peak enhancement factor, here set on 8. The two variables that are used to determine a spectrum are H_s and T_p, the significant wave height and peak period respectively. Based on the scatter diagram of Nigeria, given in Table A.2, the peak period varies between 2 and 22 seconds. This values are also used to determine the wave spectra. The significant wave height varies from 0.5 to 3.0 meters, it is chosen to interpolate to the correct wave height. The method used for this interpolation is given in the last subsection.

5.4.3. DETERMINE VELOCITY

The wave spectrum and the RAO's at the leg locations are used to find the response of the system. The response is found using the formulation as given in Journeé and Massie (2001). Using the symbols of this research this leads to:

$$S_u(\omega) = S_{\text{JONSWAP}}(\omega) \cdot |R_u(\omega)|^2 \tag{5.55}$$

Where S_u is the displacement response spectrum on the leg location. This displacement spectrum is then converted to the velocity spectrum using:

$$S_v(\omega) = S_u(\omega) \cdot \omega \tag{5.56}$$

Where S_v is the velocity response spectrum. The last step is to convert this spectrum into the most probable maximum velocity during the installation period. This most probable maximum is based on the number of waves that, typically, occur during the time period. The approach from Journeé and Massie (2001) is used, this is given as:

$$n = \frac{T_{\text{mating}}}{T_p} \tag{5.57}$$

$$\text{m}_0 = \int_0^\infty S_v(\omega) \cdot \text{d}\omega \tag{5.58}$$

$$V_{\text{mpm}} = \sqrt{(2 \cdot \text{m}_0 \cdot \log(n)} \tag{5.59}$$

Using the steps elaborated in this section the final V_{mpm} can be compared with the V_{max} found with the installation limit methodology. The V_{mpm} depends on the wave height, wave peak period, wave direction, interface stiffness, interface damping and installation time.

5.4.4. WORKABILITY DERIVATION

The workability numbers are derived based on the maximum impact velocities of the topsides, in the mating stage, when the barge is subjected to the Nigerian sea states. Knowing the Nigerian sea states, Table A.2, and the probability correlated to the wave heights and peak period the workability number is derived for all settings of the barge interface stiffness and damping.

The Nigerian scatter is linearly interpolated. This way the maximum wave height is not dependent on the 0.5 meters steps and the discrepancies in the results are lower. Using this interpolated table a convenient property of the response velocity can be used. The velocity scales linearly with the significant wave height. This means that for given values of the interface stiffness the maximum wave height per peak period can be found by dividing the most probable maximum velocity of the topsides (based on a significant wave height of 1 meter) with the maximum velocity limit of the installation. In a formula this becomes:

$$H_{\max} = \frac{V_{\text{mpm}}}{V_{\max}} \tag{5.60}$$

The value of $H_{\max}$ can than be linked to the scatter table to obtain the workability percentage. Adding these percentages for all peak periods leads to the workability percentage.The Nigerian data table is based on year round values, hence the workability will indicate the percentage in time that the installation is possible.

6

RESULTS

In this chapter the results of the model are presented. The results are split in three sections. Firstly, the results of the hydrodynamic model are detailed, where the characteristic behaviour of the barge and topsides with and without heave compensation system is given. Secondly, the installation method outcome is presented, combined with the preliminary workability estimations. Finally, these results are used to find the workability for realistic parameters of the heave compensation system, in this section the parameters used to approximate the dimensions are set and the corresponding characteristics are given.

6.1. BARGE AND TOPSIDES RESPONSE

The response is derived via the Response Amplitude Operator (RAO) formulation, see Section 5.2.3. The RAO indicates the response amplitude for a 1 meter significant wave height at each frequency. The response scales linearly with the amplitude of the significant wave height. Hence, an RAO for a 1 meter significant wave is used to derive the response for all wave heights.

The equations derived in Chapter 5 are used to calculate the RAO's of the barge and topsides, based on the frequency domain and the different heave compensation settings. The RAO's for the different heave compensation stiffness characteristics are given in Figures 6.1 and 6.2, where a constant damping is assumed (10 percent of the critical damping). The figures show the uncompensated situation with the 'fixed' notation (very high stiffness). For the heave compensation system stiffness different order of magnitudes are used, the stiffness represents a single heave compensation system. From these different stiffness settings the characteristic behaviour of the barge and topsides is found, this information is used the derive the aim for the heave compensation settings. The results are shown with 10.2 meters draft and a 160 degree wave heading. The draft is based on the average mating draft. The wave direction is used because more than 90% of the Nigerian waves are northbound (based on the internal documents of Allseas). 160 degrees is the maximum angle of these northbound waves, if the substructure slot is orientated ideally.

The barge RAO's (Figure 6.1) show that the heave and pitch motion are only slightly effected by the stiffness settings. However, the effect of the heave compensation on the roll motion is significant. For all motions is clear that the stiff solution of 1 MN/m has the largest effect on the motions of the barge, the reason for this is discussed further on in this section.

For the topsides RAO's (Figure 6.2) the effect of the variable stiffness is dominantly present. The first observation is that excitation occurs with the high stiffness settings. In other words, the motions of the topsides increase due to the presence of the heave compensator. The 10 MN/m causes a high roll and pitch response and the 1 MN/m alters the heave and pitch motions significantly. The second effect is that a low stiffness clearly causes minimal motions as the response approaches to zero for 10 kN/m solution. Note that the used stiffness values are arbitrary and purely indicate the effects of the system, a 10 kN/m stiffness is not realistic.

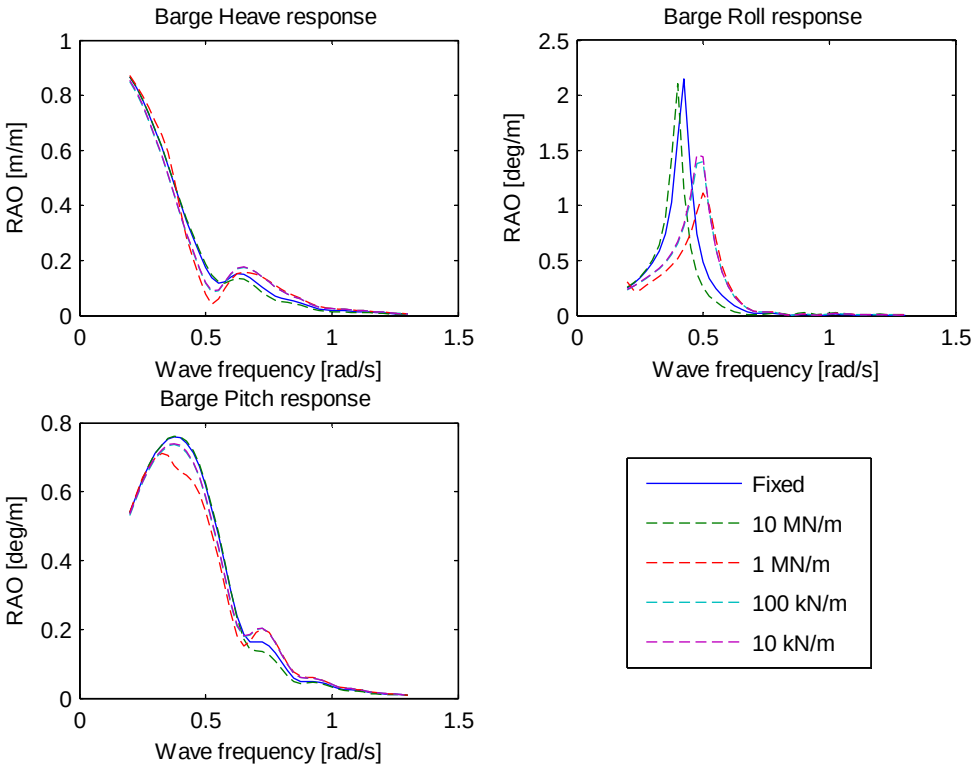

Figure 6.1: The response of the barge for different settings of the heave compensation system stiffness. Results are based on a 160 degree incoming wave and a stiffness of ten percent of the critical value for the system.

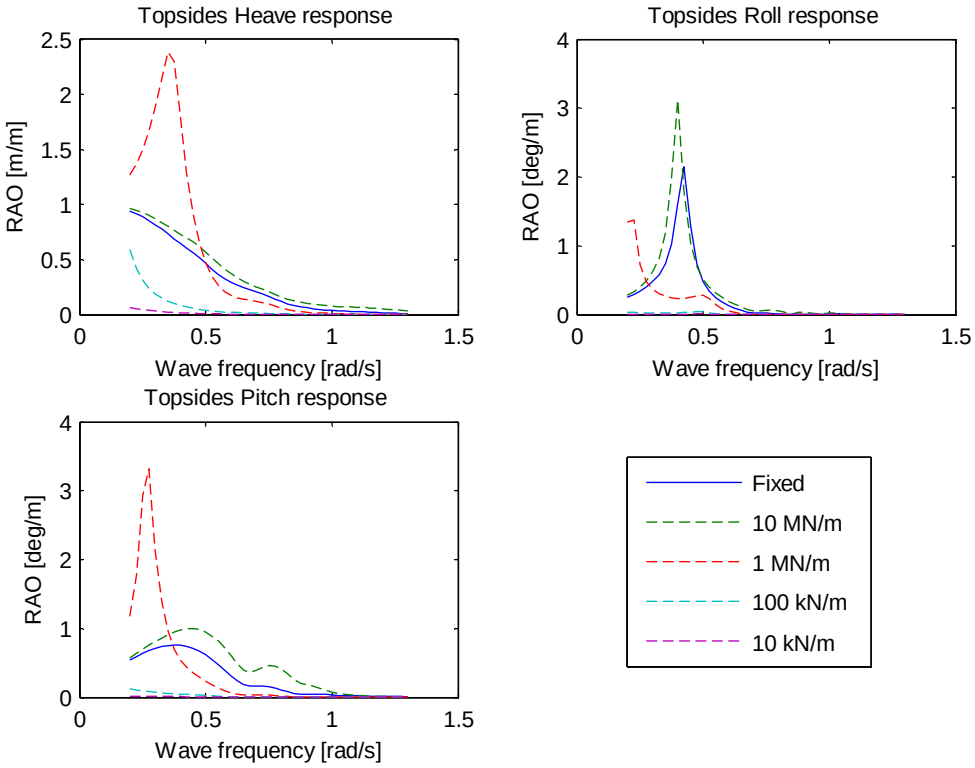

Figure 6.2: The response of the topsides for different stiffness settings of the heave compensation system. Results are based on a 160 degree incoming wave and a stiffness of ten percent of the critical value for the system.

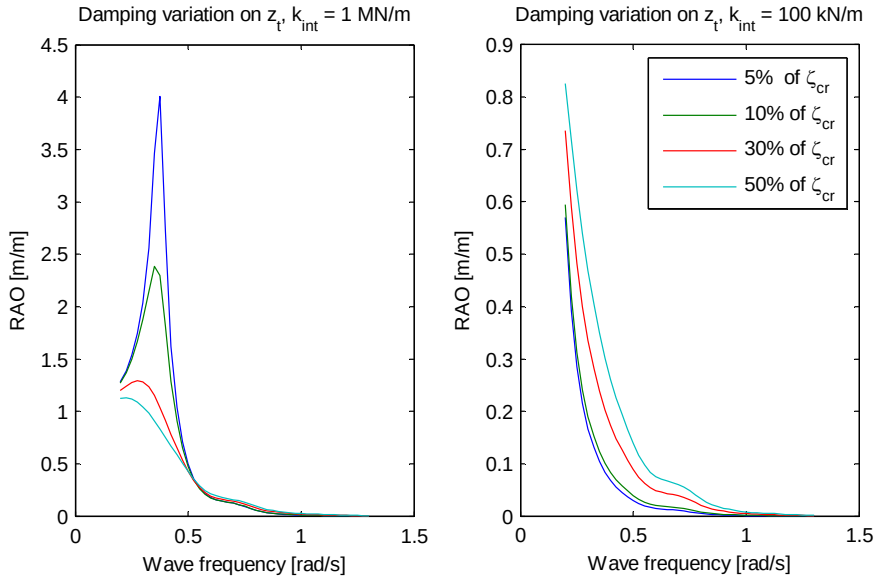

Figure 6.3: Influence of the damping on two different stiffness settings. Both for the topsides heave motions, based on a 160 degree incoming wave. In the left figure the damping cancels the excitation of the stiff spring whilst the damping has a negative effect on the right figure where a soft spring is used.

The combination of the barge and topsides motions show that an amplification of the topsides motions relates to a decrease in barge motions, for all cases except 1 MN/m roll motions. For the lower stiffness values a decrease in barge and topsides motions is found, this implies that the low stiffness creates an overall positive effect on the motions. Thus, the heave compensation system should aim for a low stiffness value.

The heave compensation damping influence is shown in Figure 6.3, the figure shows the damping influence on the topsides heave RAO for two different stiffness settings. The damping is given as a percentage of the critical damping of the cylinders, as explained in Section 4.4.3. With a high stiffness, high damping values are positive for the response, as can be seen in the left figure of Figure 6.3. A low stiffness requires a low damping coefficient for better results, Figure 6.3 on the right side. The damping effects are highly dependent of the stiffness settings. Therefore, it can not be determined which damping setting is most favourable without the final stiffness value. Hence, the damping is defined simultaneously with the stiffness characteristics.

The RAO's show the sensitivity of the system to certain frequencies. For example, the roll of the barge with the 'fixed' setting has a peak on 0.4 rad/s, thus the maximum response of the barge occurs due to 0.4 rad/s waves. The African swell spectra are narrow banded, so each spectrum can cause different motions of the system. To assess these differences a table is compiled with three typical African swell periods, this table can be found in Appendix C.1. To show the order of magnitude of the motions the response on sea state with a T_p of 14 seconds and a H_s of 1 meter is given in Table 6.1. This period is the highest common value in Nigeria, the Nigerian sea state is given in Table A.2.

Table 6.1 shows the motions at the center of gravity of the barge and topsides. The COG of the barge is not vertically above the COG of the barge. Hence, the heave motions of the topsides are caused by a combination of heave and pitch motions of the barge. Therefore, the topsides and barge heave motions are not equal for the fixed scenario. The roll and pitch motions are equal for the barge and topsides in the fixed scenario.

To understand the roots of this behaviour, the RAO's of Figures 6.1 and 6.2 are compared to the 3 hour most probable maximum amplitudes of the three characteristic sea states(of Table C.1). The 3 hour most probable amplitudes indicate the maximum expected motions for the degrees of freedom based on the sea state. From this information some clear correlations are observed:

- The effects of the peak shift for the barge roll RAO is visible. For the lower period spectra ($T_p < 10$ s) the roll value is higher for the lower stiffness values, even though the peak of the fixed scenario is higher. This indicates that the frequency of the excitation is important for the behaviour of the barge.

- For the heave and pitch of the barge the RAO's for all values are comparable, except the 1 MN/m pitch RAO which is clearly lower. Thus the responses of all values should be more or less equivalent for each spectrum, this effect is visible in the amplitude table since the maximum difference is 0.04 meters for heave and 0.08 degrees for pitch, where the low pitch value is reached with the lower RAO of the 1 MN/m RAO. Hence, the effect of the low peak is not that large.
- The 1 MN/m stiffness has a high response characteristic for the topsides heave and pitch. However, this excitation will only take place at low frequencies, especially for the pitch motions. The most probable maximum amplitudes shows this effect. For the low T_p spectrum the response of the topsides due to the 1 MN/m is lower than the fixed scenario, for both heave and pitch motions. For the medium T_p spectrum the excitation for the heave motion takes place whilst the pitch is still damped. Looking into the high T_p response excitation take place in the heave and pitch motions.
- For the very low stiffness values, 100 kN/m and 10 kN/m, the topsides RAO's are very low for all degrees of freedom, thus the corresponding responses should also be very low. The table shows a clear decrease in topsides motions for the low stiffness values. For the 10 kN/m stiffness the topsides motions are almost completely cancelled.

Table 6.1: The three hour most probable maximum amplitudes, using the RAO's from Figures 6.1 and 6.2. This represents the expected motions in the installation procedure. Results are based on 160 degree wave and ten percent of the critical damping.

Three hour most probable maximum amplitudes

For T_p= 14s, H_s= 1m							
	DOF	Unit	Fixed	10 MN/m	1 MN/m	100 kN/m	10 kN/m
Barge	Heave	[m]	0.25	0.25	0.20	0.21	0.21
	Roll	[deg]	1.08	0.71	0.66	0.88	0.91
	Pitch	[deg]	0.57	0.58	0.50	0.55	0.55
Topsides	Heave	[m]	0.46	0.54	0.89	0.05	0.01
	Roll	[deg]	1.08	1.11	0.21	0.03	0.01
	Pitch	[deg]	0.57	0.82	0.34	0.03	0.01

6.2. INSTALLATION MAXIMA AND WORKABILITY

The installation procedure consists of two elements, identifying the maximum allowable velocity and calculating the velocity of the topsides. First, the identification is done and a design maximum is obtained. Secondly, the system velocity is derived by translating the motion of the COG's towards the leg positions of the topsides.

6.2.1. INSTALLATION LIMIT

Using the methodology from Section 5.3, the maximum velocity for the topsides is found for different leg configurations. In this method the energy balance between the kinetic energy of the topsides and the maximum energy absorption of springs representing the LMU's is solved. For this approach, the assumption is made that the kinetic energy of the topsides is fully transferred onto the substructure, which is valid when the stiffness of the substructure is high in relation to the stiffness of the LMU's. The latter is the case in the heave compensated scenario. Also, the friction force on the LMU is not taken into account, as explained in Section 3.4. The method is based on the limit for four different leg impact scenarios, being 1, 2, 4 and 8 legs. From these four scenarios a single limiting value is obtained. To derive the limits Equation (5.46) is solved, for which all variables are known. The maximum velocities are shown in Table 6.2.

Table 6.2 shows that the impact on more legs causes a lower installation maximum. The reason for this is: the maximum deflection decreases linearly with a higher stiffness, the energy storage capacity of a spring is determined by the deflection squared times the stiffness, the influence of the squared term is higher. Hence, the installation limit decreases for smaller allowed deflections and smaller allowed deflections are caused by higher stiffness. More legs cause a higher stiffness, therefore, the limit is lower.

Table 6.2: The maximum allowable impact velocity of the topsides, for the different amount of legs considered.

N_{legs}	V_{max} [m/s]
1	0.459
2	0.455
4	0.431
8	0.411

The maximum is set to cover all impact scenarios, this has the advantage that no research to the actual amount of legs during impact is required. Since the friction on the LMU is neglected the maximum velocity is taken as a conservative minimum of Table 6.2. Hence, the maximum velocity for the installation procedure is set as: $V_{max} = 0.40 \frac{m}{s}$.

6.2.2. MOTIONS AT LEG POSITIONS

The motions at the leg positions are found using the method of Section 5.4. This method derives the most probable maximum velocity, for a given time period and wave spectrum. The results show the most probable maxima based on variation of the peak period and constant wave height (H_s is 1 meter).

The velocity results are shown in Figure 6.4, where the same settings are used as the barge and topsides RAO's plots. Thus, the waves are head on and the average mating draft is used, a constant damping value and an order of magnitude variation of the heave compensation stiffness as shown in the figure. The found installation limit is added to see when the velocity exceeds this value. The figure shows that a low stiffness corresponds to a much lower velocity of the topsides.

It is pointed out that the 1 MN/m stiffness has a lower maximum velocity until a peak period of 14.5 seconds whilst the RAO data, Figures 6.1 and 6.2, gives reason to believe that this settings would lead the largest response. The low velocity is explained by the topsides roll RAO that is much lower, therefore, the sideways (sway) velocity is low enough to keep the energy level within the limit.

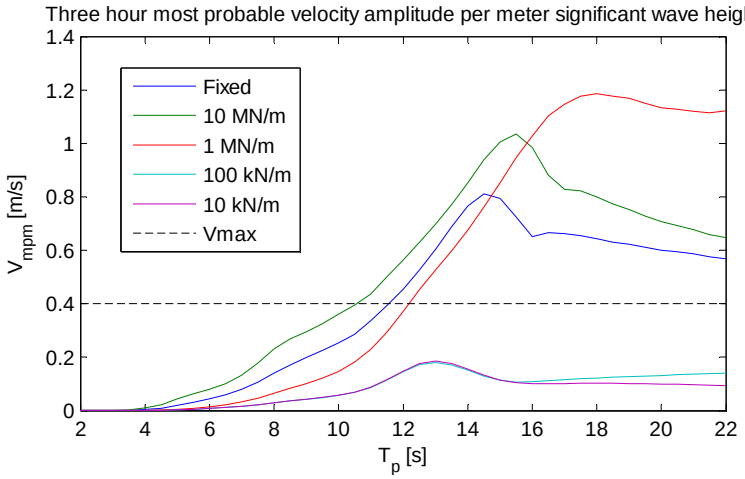

Figure 6.4: The most probable maximum velocity at the topsides leg locations, related to the peak period of the wave spectrum, based on a period of three hours, a significant wave height of 1 meter, 160 degree incoming wave and ten percent critical damping. The maximum impact velocity limit is shown with the black dashed line.

For the response due to different wave heights, the linear relation between wave height and velocity is used. This means that the maximum significant wave height corresponding to the installation limit per peak period is determined as:

$$H_{max}(T_p) = \frac{V_{3H}(T_p)}{V_{max}} \tag{6.1}$$

With the maximum significant wave height value known for all peak periods, the workability number is obtained for the Nigerian sea comparing the maximum wave height to the probability table for the Nigerian sea, A.2. This data table is interpolated for the wave height. The corresponding workability numbers for the mating phase of the floatover operation are shown in Table 6.3.

Table 6.3: The workability numbers for the different stiffness settings using the Nigerian environmental data table. Based on the most probable maximum velocity data as presented in Figure 6.4.

Stiffness	Workability [%]
Fixed	45.2
10 MN/m	20.9
1 MN/m	50.1
100 kN/m	99.8
10 kN/m	99.8

The workability numbers clearly show that the 10 MN/m stiffness decreases the workability and that a large profit in workability can be obtained using a low stiffness solution. This is the theoretical gain of the heave compensation system, now the order of magnitude stiffness values are substituted with the stiffness of the passive heave compensation cylinders.

6.3. HEAVE COMPENSATION CHARACTERISTICS

The heave compensation system is based on four large passive heave compensation cylinders, as detailed in Chapter 4. In the previous section is found that a low stiffness of the system results in a very high workability during the mating phase of the floatover operation. In this section the stiffness of the system is translated into characteristics of the heave compensation system, where a balance between a high workability and a feasible solution is found.

In Section 4.4 the method to approach the system is elaborated, this includes the equations to determine the stiffness. The stiffness is calculated using Equation (4.6), for readability the equation is repeated:

$$k_{\text{cyl}} = \frac{\kappa \cdot m_t^2 \cdot g^2}{16\, p_0 \cdot V_0} \tag{6.2}$$

This equation contains three variables p_0, V_0 and κ, the latter is dependent of p_0. For a low stiffness the denominator has to be high, thus a high pressure and large volume are favourable. The κ factor increases with the higher pressures, thus lowering the effect of increased pressure. However, the κ increase is lower than the pressure increase, the values of κ and relation to the pressure are presented in Table 4.1.

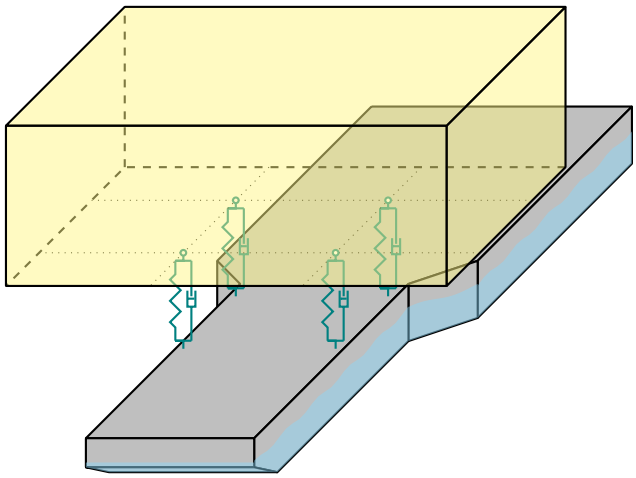

Figure 6.5: A 3D overview of the model. The values for k_{cyl} and ζ_{cyl} are used at four locations of the systems as indicated in this figure.

The *PS* uses a high pneumatic pressure of 300 bar in the topsides lift system, that copes with comparable loads. Therefore, the assumption is made that 300 bar is also applicable in this configuration. Higher working pressures are favourable for the cylinders since stick-slip effects are less likely to occur. It is chosen to dimension the system on two pressure values, 300 bar and 200 bar. The latter is because a large amount of pneumatic energy is going to be stored and a higher pressure requires thicker vessels and stronger pumps, this might lead to a heavier system.

Using this values for the working pressure the formula is solely dependent on the initial volume of the pneumatic reservoirs. To estimate the most efficient heave compensation system, an analysis is performed where the volumes and critical damping values are varied. Eventually the most efficient system is a trade off between complexity (size) and effectiveness of the system (workability).

The results of this variation for the 300 bar setting is given in Figure 6.6 and for the 200 bar in Figure 6.7 (enlarged in Figures C.1 to C.8). In these results a variation of wave headings is used. These wave directions are used to determine the final design values of the heave compensation design. The previous results are based on the 160 degrees direction, the choice for this variation in the last step is based on the large gain in workability that is reached in beam sea conditions. The volume indication in the plots correspond to the required pneumatic volume of a single heave compensation system. The total required volume is thus four times higher. The result of the uncompensated scenario is plotted on the zero volume location.

The workability plots of Figures 6.6 and 6.7 show a significant gain in workability, this figure also provides insight in the contribution of the damping value on the workability. These results show that for the head on waves the workability becomes very high, whilst for the beam seas the workability stays very low for the majority of the settings. From the 90 degrees result the decision is made to evaluate the 300 bar scenario at 500 m^3 and 20% damping. For the 200 bar scenario the values are taken such that the workability almost equal to the 300 bar scenario, this corresponds to a volume of 650 m^3 and 20% damping. The values are displayed for a single system. Hence, the volumes of the total heave compensation system become 2,000 m^3 at 300 bar and 2,600 m^3 at 200 bar.

With the method detailed, it is possible to determine the influence of the peak enhancement factor and the installation duration. The variation of the peak enhancement factor is because the found value did not correspond to the expected value. The results show (Figure C.18) that the effect of this value does not seriously effect the installation characteristic. The duration of the `Liwan 3-1` installation is 6 hours. For this results the 3 hour most probable motions are used for the heave compensated and uncompensated scenario, this is done to compare the solution on equal terms. The effects of the change in installation duration is minimal, shown in Figure C.19. Hence, it is concluded that these two parameters do not influence the choice of the parameters for the heave compensation system.

By choosing these parameters a significant gain in workability is achieved, especially when the beam seas are considered. In beam seas the classic floatover scenario has a very low workability, the heave compensated workability is almost nine times higher. The effects of the workability and the comparison with the classical scenario are made in Table 6.4.

Table 6.4: Workability numbers based on the chosen, most suitable, settings. The 300 bar setting is based on 500 m^3 and 20 % damping and the 200 bar is derived using 650 m^3 and 20 % damping.

	Fixed	300 bar		200 bar	
Wave direction	Workability	Workability	Gain	Workability	Gain
90°	5.5%	42.8 %	x 7.8	43.7 %	x 7.9
135°	10.3%	55.6 %	x 5.4	58.2 %	x 5.7
150°	38.2%	79.9 %	x 2.1	83.0 %	x 2.1
160°	45.9%	86.0 %	x 1.9	87.8 %	x 1.9

The chosen settings correspond to a system stiffness (k_{cyl}) of 0.57 MN/m and a damping value ($\zeta_{\%}$) of 1.1 MN·s/m, for the 300 bar and 200 bar solution these values are equal. Thus, the total heave compensation system is represented with four systems with these characteristic values. With these settings the RAO's are significantly improved in relation to the uncompensated scenario (given in Figures C.9 and C.10), the improvement is also visible when looking at the installation velocity plot (shown in Figure C.11).

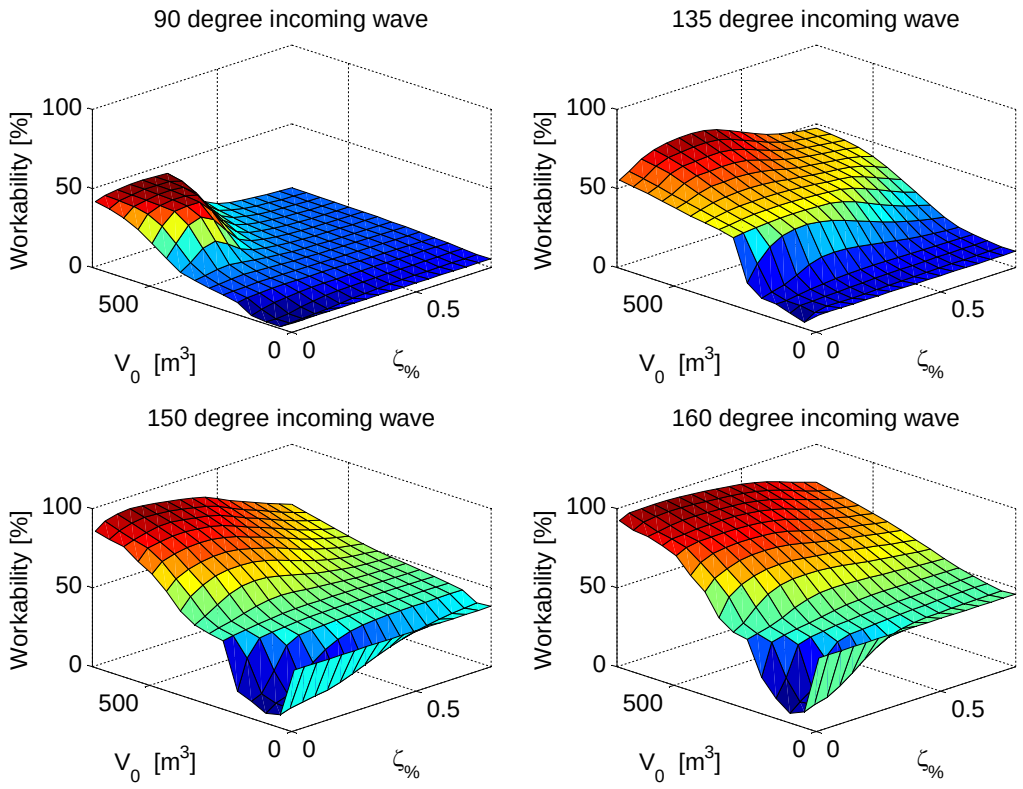

Figure 6.6: **300 bar** workability numbers for different wave directions, based on variation of the total initial volume of pressured air [V_0] and the camping percentage of critical damping value [$\zeta_{\%}$]. The Nigerian sea states are used. The workability of the conventional floatover is plotted on the zero volume line.

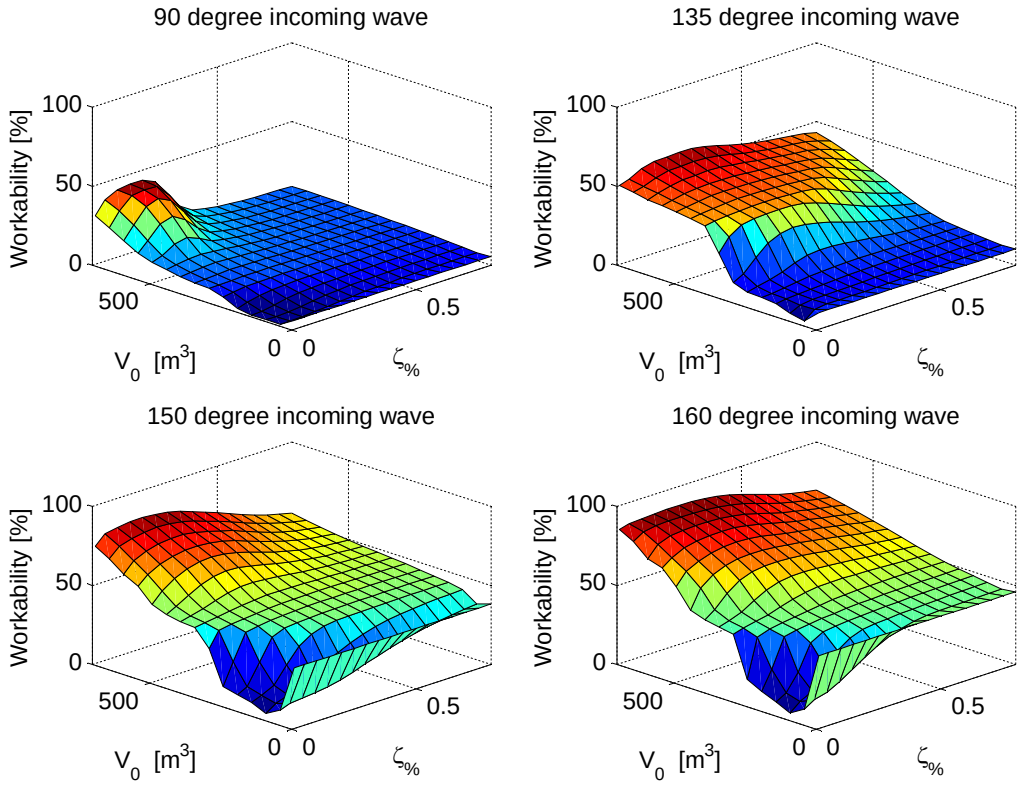

Figure 6.7: **200 bar** workability numbers for different wave directions, based on variation of the total initial volume of pressured air [V_0] and the camping percentage of critical damping value [$\zeta_{\%}$]. The Nigerian sea states are used.The workability of the conventional floatover is plotted on the zero volume line.

7

DIMENSIONING

To conclude on the effectiveness of the heave compensation system an indication of the gross weight and dimensions is requestedrequired. This chapter starts by elaborating the used method for the approximation of the weight and dimensions. Followed by the results of this method with the use of the results from the previous chapter.

7.1. METHOD

The heave compensation system is defined in Chapter 4. This section starts with a brief repetition on the heave compensation system approach, with in addition the considerations for the weight estimations . Afterwards, the methodology and formulae for the calculations of the different components is detailed.

7.1.1. SYSTEM INTERPRETATION

The heave compensation system is developed using the results for the stiffness and damping, with these results the general dimensions and number of elements can be derived . Then, the steel weight per element is approximated and the required deck area for the total system is obtained. With these two parameters a general impression of the magnitude of the system can be made. This magnitude is used to compare the gain in workability to the extensiveness of the system from which the viability of the heave compensation principle is assessed.

The dimensions are derived for the basic elements using a simplified view on these parts, to find a preliminary indication of the system size. More detail is not accurate with the input from the linearised model.

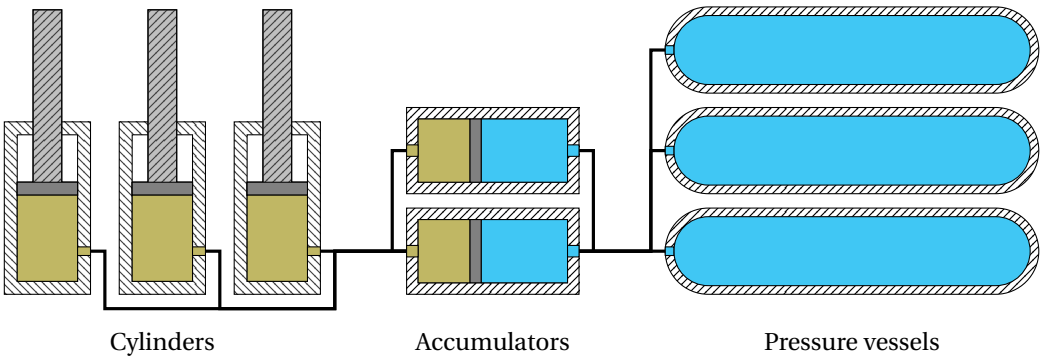

Figure 7.1: The heave compensation system interpretation for the dimensioning process. Using the passive system as described in Chapter 4, the difference is that components are interpreted as a multiplication of a single design.

The dimensioning of the elements takes place for a single system, they are considered equal. The forces of the topsides are split over the four systems. Thus, the force on each system is described as:

$$F_{\text{system}} = \frac{1}{4} F_{\text{topsides}} = \frac{1}{4} m_t \cdot g \tag{7.1}$$

Besides the three components of the heave compensation system an additional component is considered in the dimensioning of the system. The illustrations of the model show that the barge and topsides are connected with the spring damper system. In reality the system can not bridge this distance. Thus, a deck support frame (DSF) is required. Combined with the requirement to minimise the transverse loads of the cylinders and buckling criteria the decision is made to design the DSF to the maximum height. Therefore, the cylinders are mounted at the top of the casing. More information about this mounting position is given in the cylinders subsection. The weight estimation of the DSF is based on the weight of the DSF from the `Liwan 3-1` installation. The model thus looks like Figure 7.2, where the spring damper elements represent the required stroke of the cylinders.

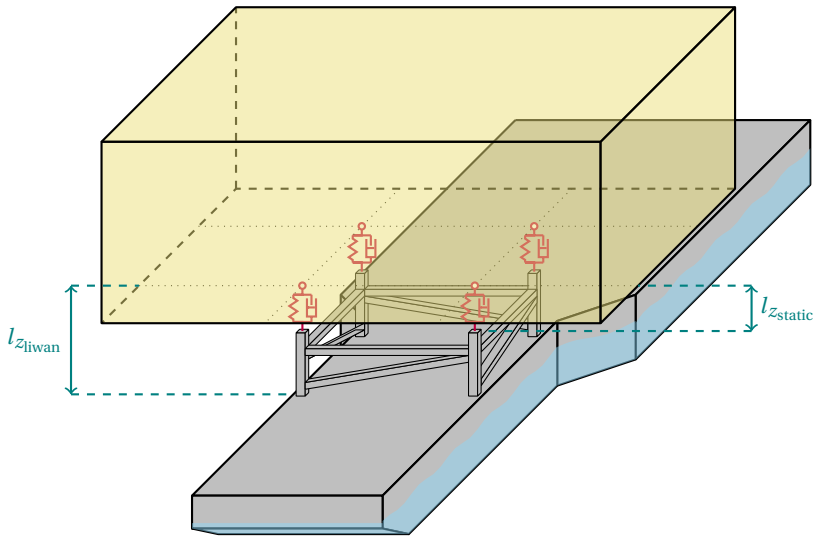

Figure 7.2: Sketch of the implementation of the deck support frame. The spring-damper system has the length of cylinders stroke. The remaining height is filled with a deck support frame to get the correct working height of the system.

The gap between the DSF and the topsides is set as the neutral stroke of the cylinders, being the the neutral position of the cylinder during heave compensation. For safety reasons this length should be as small as possible, to minimize the loads of the bending moment on the cylinder rod. The cylinders are mounted as shown in the left illustration of Figure 7.4, where the ground is taken as the deck support frame top height. To indicate the weight of the used DSF the length ratio between the `Liwan 3-1` DSF height and the new height is used to find the new DSF weight, in the formula:

$$m_{\text{dsf}} = m_{\text{dsf}_{\text{liwan}}} \left(1 - \frac{l_{z_{\text{static}}}}{l_{z_{\text{liwan}}}}\right) \tag{7.2}$$

Where m_{dsf} is the weight estimation of the DSF. The weight of the `Liwan 3-1` DSF is given with $m_{\text{dsf}_{\text{liwan}}}$. $l_{z_{\text{liwan}}}$ the height of the DSF in the `Liwan 3-1` installation. Finally, $l_{z_{\text{static}}}$ describes the length of the cylinder rod in static conditions. This static length is the combination of the installation stroke and the the most probable maximum heave amplitude these values are explained in the next section.

7.1.2. COMPONENT DIMENSIONING PROCESS

The components are dimensioned using the input values from Chapter 6. For each element different methods are derived to find the basic dimensionings of each part. Firstly, the hydraulic cylinder method is given. Followed by the accumulator and lastly the pressure vessels method is detailed.

HYDRAULIC CYLINDERS

The cylinder design is simplified to the dimensioning of the heavy components: the casing, rod and piston. Firstly, the input and design parameters are listed. After this the methodology behind the cylinders is elaborated.

Parameters
The process contains fixed input values and variable design parameters. For a better understanding of the method the fixed and variable parameters are listed.

The input values, which are fixed, are given by:

- Working pressure
- Cylinder group loads
- Required stroke

The design parameters are:

- Length rod
- Casing height
- Diameter rod
- Design pressure
- Design yield strength
- Number of cylinders

Method
The force exerted by the hydraulic cylinder group is the sum of the force exerted by the separate cylinders. The pressure is assumed equal in all cylinders, since the friction is neglected. Therefore, the total force is related to the pressure in the accumulator and the total piston area, given as Equation (7.3). Using the initial pressure, p_0, the required area of the cylinder group is derived by the requirements of the group force and the static loads as Equation (7.1). Combining these equations, the total piston area required in a cylinder group is found by Equation (7.4).

$$F_{\text{system}} = A_{\text{system}} \cdot p_0 \tag{7.3}$$

$$A_{\text{system}} = \frac{\frac{1}{4} \cdot m_t \cdot g}{p_0} \tag{7.4}$$

Here F_{system} corresponds to the static gravitational load of the topsides of Equation (7.1); p_0 is the pressure in equilibrium conditions; A_{system} is the area of the cylinder group; F_{system} is the force of the total cylinder group; g is the gravitational acceleration and m_t is the topsides mass.

The cylinder dimensioning is based on Figure 7.3, where a distinction is made between casing, rod and piston. For these three elements the dimensions are derived, starting with the area and diameter of the piston with:

$$A_{\text{piston}} = \frac{A_{\text{group}}}{n} \tag{7.5}$$

$$d_{\text{piston}} = \sqrt{\frac{4}{\pi} \cdot A_{\text{piston}}} \tag{7.6}$$

Where n is the number of cylinders in the cylinder group, A_{piston} is the area of a single cylinder piston and d_{piston} is the diameter of the cylinder piston.

The inner diameter of the cylinder casing is taken equal to the cylinder piston diameter.

The rod diameter is determined to be smaller than the piston diameter. A smaller rod diameter means that the piston can be actuated from the top using a second actuation system. In a more detailed design this can be used to control the installation stroke. For the determination of the rod diameter setting, the lift cylinders of the *PS* are examined. In that case the rod diameter is significantly smaller than the piston diameter. This is done to be able to control the cylinders pulling force. In this research, the pulling force is less significant because of the passive actuation. However, it was stated before that this function could be used to control the

installation stroke, thus a decreased diameter is used. This decrease is set on 80% of the cylinder casing inner diameter. This value agrees with the following two requirements. The area created with this decrease should be significant enough to use the pulling force and the diameter of the rod must be large enough to cope with the buckling loads. The schematic drawing of Figure 7.3 shows the effects of the 80% assumption, supported by:

$$d_{\text{rod}} = 0.8 \cdot d_{\text{piston}} \tag{7.7}$$

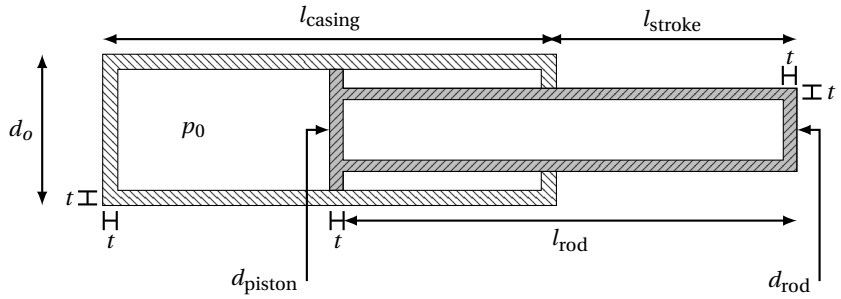

Figure 7.3: Schematic drawing of the dimensioned cylinder.

Now the diameters of the casing, piston and rod are known. The thickness of the wall and height of the elements are required to estimate the weight of the cylinders. The wall thickness is used for the cylinder casing as well as the rod. The wall thickness of the cylinder is calculated using the guidelines from DNV for hydraulic cylinders (5-778.93, 2009). The wall thickness is derived by:

$$t = \frac{p_d \cdot r_i}{10\,\sigma \cdot e - 0.5 p_d} + c_c \tag{7.8}$$

Where:

t = required wall thickness [mm]
p_d = design pressure [bar]
r_i = internal cylinder tube radius [mm]
σ = allowable stress, design stress [N/mm^2]
e = welding factor
c_c = corrosion allowance

The design pressure is set as the maximum pressure the system can be subjected to. The system works with hydraulics thus the pressure fluctuations of impact loads can be significant. The design pressure is taken as 1.5 times the working pressure to cope with these pressure fluctuations.

For the yield strength the value of stainless structural steel S355 is used. However, the design yield strength should consider a safety factor. The hydraulic cylinders cope with huge loads thus failure has extreme consequences. The used yield strength is taken as half the yield strength of steel to guarantee that the material holds. This value is considered conservative.

The welding factor (e) is set as 1, according to the DNV guidelines this value is used for seamless cylinders and the corrosion allowance is set as 0.3 cm, the advised value of DNV.

To determine the height of the cylinder, the stroke length is required. The stroke length is a combination of the design heave of the barge and the installation stroke to avoid unnecessary impact loads. The required stroke due to the heave at the leg locations is extracted from the model. For the installation stroke the value is set on 2.15 meters which is the clearance at the start of the `Liwan 3-1` mating phase. In a formula this becomes:

$$l_{\text{stroke}} = 2 \cdot z_{\text{barge}} + l_{\text{installation}} \tag{7.9}$$

Where z_{barge} is 1 determined as meter, this is the most probable maximum of the vertical displacements of the barge and topsides at the heave compensation locations. The most probable vertical displacements at

the heave compensation location are plotted in Figure C.12. This figure shows that a vertical displacement of 1 meter is required for a spectrum with peak period of 15 seconds and significant wave height of 1 meter. This is chosen as the design point for the stroke requirements.

The height of the cylinders is taken such that the rod is capable of handling the transverse loads at the maximum stroke position. This is achieved by making the length of the rod twice the required stroke length combined with a cylinder casing with the same length, these lengths are illustrated in Figure 7.3. At maximum stroke position the rod still reaches halfway down the cylinder casing, thus the forces induced at the casing top and bottom of the rod location are not subjected to a leverage. No extra research is done regarding the transverse loads on the cylinder, therefore, the cylinders are designed using twice the minimal size for the length of the rod as well as the cylinder casing height. This leads to:

$$l_{\text{rod}} = l_{\text{casing}} = 2 \cdot l_{\text{stroke}} \tag{7.10}$$

To determine the amount of the cylinders, redundancy consideration and the buckling loads are used. Failure of a cylinder may not lead to significant different behaviour of the system. Hence, for redundancy it is better to use multiple cylinders. Additionally, the amount of cylinders influences the diameter of the cylinders, which relates to the buckling strength. The amount of cylinders is determined with the trade-off between buckling strength and redundancy. The effect of the amount of cylinders on the total weight and buckling load is given in Appendix C.2.

The buckling loads also give an indication of the maximum unsupported length of the rod, due to the topsides loading. This is used to check if the stroke height is possible with the cylinders. The buckling load for a hydraulic cylinder is found in Albers (2010), where the formulas of Euler and Tetmayer are used.

The maximum force on the cylinder rod is found with:

$$\text{If:} \quad \lambda \geq 100 \qquad F_{\max} = \frac{\pi^2 \cdot E_{st} \cdot I}{V_f \cdot l_k^2} \tag{7.11}$$

$$\text{If:} \quad \lambda < 100 \qquad F_{\max} = \frac{\frac{\pi}{4} \cdot d^2 \cdot I \cdot \left(Rm - \left(Rm - 210 \cdot 10^6\right) \cdot \left(\frac{\lambda}{100}^2\right)\right)}{V_f} \tag{7.12}$$

Which uses the following formulae:

$$I = \pi \cdot \frac{d^4}{64} \qquad \lambda = \frac{l_k}{i} \qquad i = \sqrt{\frac{I}{\frac{\pi}{4} \cdot d^2}}$$

Using the following parameters:

$$\begin{aligned} E_{st} &= \text{The elasticity modulus of steel} \\ I &= \text{Moment of inertia of the piston rod} \\ V_f &= \text{Safety factor, commonly 3} \\ l_k &= \text{Buckling length} \\ d &= \text{Inner diameter of piston rod} \\ Rm &= \text{Yield strength of steel} \\ \lambda &= \text{Slenderness ratio} \\ i &= \text{Radius of gyration} \end{aligned}$$

The buckling length is determined by the mounting principle of the cylinder. In this case the left example of Figure 7.4 is used, since the cylinders are assumed clamped in the DSF. The right-hand side case can be used to check whether a solution without DSF is possible. It also indicates what happens to the buckling length when different mounts are used.

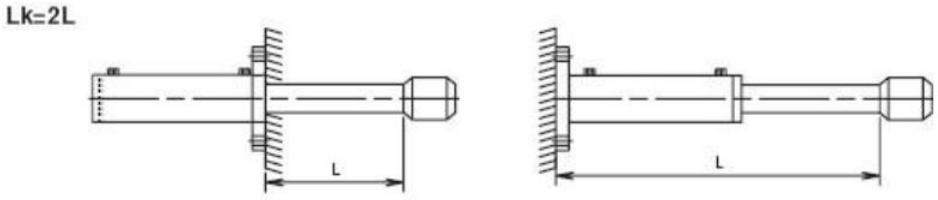

Figure 7.4: Two mounting principles, these are the relevant cases in this study. In the left principle the cylinder is mounted at the rod location, to increase the buckling capacity, this means that the support structure is built around the cylinders. If the right mounting principle is used the maximum loads are lower but the extra support structure is not required. Lk indicates the length that is used in the buckling calculations. . From Albers (2010).

PRESSURE VESSELS

The pressure vessel design is not related to the outcome of the accumulator and cylinder design. The design can thus be done separately from these results. The parameters are given in the next paragraph and the method is elaborated subsequently.

Parameters

The input values for the pressure vessels are given by:

- Required volume
- Working pressure

The design parameters are:

- Maximum internal diameter of vessels
- Length of vessels
- Design pressure
- Design yield strength

Method

The pressure vessels are approximated as shown in Figure 7.5, where the maximum dimensions are set to a fixed value. This is done by fixing the length for each vessel and setting a maximum diameter. These dimensions lead to the number of required vessels. A new internal diameter is then calculated, based on the length and the amount, to ensure that the total volume is accurate. The length (L) is based on the layout possibilities on the barge. A length of 20 meters creates a feasible installation of the pressure vessels in between the cylinders, so this value is used for the calculations. The maximum internal diameter (d_i) is set on 1.5 meters to ensure that the wall thickness does not become too large.

The length and inner diameter settings have a large influence on the footprint and weight of the results, therefore a variation plot is made to see how these parameters influence the total weight of the solution and the number of pressure vessel required. For the 200 bar solution the data is added in Appendix C.2.

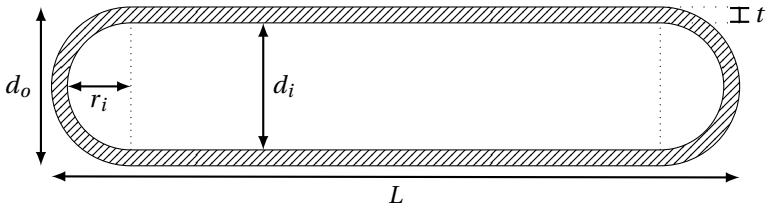

Figure 7.5: The dimensioned pressure vessel. The long stretched cylinder is enclosed by two spherical ends.

The wall thickness (t) of the pressure vessels is based on DNV guidelines for pressure vessels. The guidelines provide a method to determine the minimum wall thickness for the pressure vessels. Assumptions are used for the maximum dimensions of the vessels, in this case the diameter and length. With the pressure, the diameter assumption and the properties of steel the wall thickness is found. With the required volume and

maximum length, the amount of pressure vessels is derived. These properties are combined into the mass calculations.

The DNV guidelines (Machinery and systems, 2011) for wall thickness in cylindrical pressure vessels are found as:

$$t = \frac{p_d \cdot r_i}{10\,\sigma \cdot e - 0.5 p_d} + c_c \tag{7.13}$$

These parameters have an equal description as used in Equation (7.8). Some of these parameter values change for this specific situation.

The vessels are filled with a large volume of pressurized air, the pressure of air is not as sensitive to fluctuations of the pressure as an hydraulic system. The system should still be able to cope with higher pressures than the working pressure. Therefore, the design pressure (p_d) is set as 130% of the working pressure.

For the yield strength the same steel is considered, S355 structural steel. The safety factor is adjusted, because the situation in the pressure vessels is subjected to less dynamic loading. The safety factor is 1.5.

When the pressure exceeds 50 bar, the pressure vessel should be designed as a class I vessel, according to the DNV guidelines. Thus the requirements for a class I pressure vessel are used, in this case that leads to a value for e of 1.

The top and bottom of the cylinder are assumed spherical and the wall thickness is taken equal to the cylindrical shell wall thickness. In the guidelines detailed methods are given to determine the required wall thickness at the ends of the cylinder. These methods are not applied here since an optimised design of the ends does not add value to this dimensioning approximation.

ACCUMULATORS

The accumulators are dimensioned using input from the cylinders. Again the parameters are listed and afterwards the method is stated.

Parameters
The input values for the accumulator are given by:

- Minimum volume
- Working pressure

The minimum volume is provided by summing the casing volumes of the cylinders, this is the amount of hydraulic fluid that is transported with a full stroke of the hydraulic cylinders.

The variable parameters are:

- Number of accumulators
- Design pressure
- Design yield strength
- Volume of accumulator
- Length/diameter of accumulator

Method
The accumulator is the interface between the hydraulic system and the pneumatic system. The accumulator is designed based on the required volumetric flow of hydraulic fluid due to the stroke of the hydraulic cylinders. The accumulator is also taken cylindrical shaped with circular ends and thus Equation (7.13) can be used to determine the wall thickness.

The separation technique is considered as the piston type accumulator, which is favourable for large volumetric requirements. This piston is designed as a circular plate with the wall thickness of the shell. The piston type also enables the possible variation of the pressure between the hydraulic and pneumatic sides. By adding a rod, at the hydraulic part, the effective area of the hydraulic part becomes smaller and the corresponding pressure increases. On the contrary, the accumulator becomes much larger due to the stroke of the rod. The rod also increases the weight of the system. This principle is not used in this thesis, it is mentioned because it can be a very efficient method.

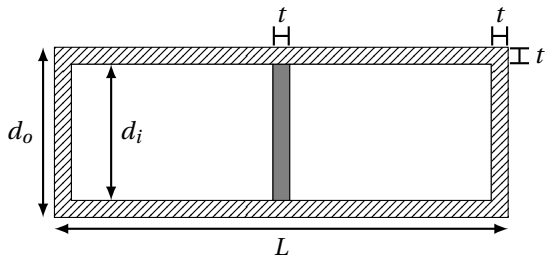

Figure 7.6: A schematic drawing of the considered accumulator. The ends are considered as circular plates with an equal wall thickness as the cylindrical shell. The piston is assumed to have an equal width as the wall thickness.

The number of accumulators is based on redundancy and here set on 2. This way during failure of one accumulator at least the half of the stroke can still be reached.

The design pressure and yield strength are equal to the hydraulic cylinder since the accumulator is also prone to hydraulic pressure fluctuations.

For the accumulator volume the accumulator of the *PS* topsides lift system is analysed. In this case the required volume is found by adding ten percent to the minimum volume, this is applied in this research as well.

To determine the length and diameter of the accumulator, one of these parameters is taken as a fixed value. In this case it is chosen to fix the length of the accumulator, because the accumulator length determines the velocity of the piston. The piston strokes over the length of the accumulator due to the wave motions. To ensure that a feasible velocity is obtained the length is fixed at 7.5 meters, the *PS* lift accumulators contain a stroke of 9 meters. Hence, this length is assumed possible.

A side effect of the relatively small fixed length, is that the diameter of the accumulator becomes larger. This can lead to a large wall thickness. With the length fixed at 7.5 meters a comparable wall thickness of the accumulator and the cylinders is obtained. Thus, this is accepted.

7.2. RESULTS

Using the method stated in the previous paragraph results are found for the two results as derived in Chapter 6. The two results differ in working pressure and required pneumatic volume the effect of this design parameter on the size and weight of the system is shown in the following sections.

7.2.1. 300 BAR

The 300 bar approximation results in 16 cylinders, 8 accumulators and 60 pressure vessels, weighing 38, 27 and 109 tons respectively. The weight contribution of the DSF is 2969 tons. All elements combined give a total weight of 10,240 tons. Each system is a combination of 4 cylinders actuated with 2 accumulators supported with the volume of 15 pressure vessels. Basic information of the elements is presented in Table 7.1, The detailed information is listed in Tables C.2 to C.4.

In Figure 7.7 the dimensioned elements are placed and connected on the barge; this indicates the relation between the available deck space and the area required for the elements. This is a simple configuration in which no other deck equipment is considered, in reality this arrangement is not likely due to the skidding beams. From this illustration the percentage of deck area covered with the heave compensation system is estimated at 41.2%. In this approach no elements are stacked, this could by an option to minimise the required area. This results indicate that the system is extensive and will consume a large amount of the barge. The deck support frame covers around 14.8% of the deck area, the accumulators around 1.2% and the pressure vessels 25.2%.

Table 7.1: Summary of the results of the 300 bar dimensioning. The total weight of the estimation equals 10,240 tons.

Cylinder		Accumulator		Pressure vessel		Unit
Quantity	16	Quantity	8	Quantity	60	[-]
Weight total	38	Weight	27	Weight	109	[tons]
l_{casing}	8.30	L	7.50	L	20.00	[m]
d_o	1.06	d_o	1.17	d_o	1.72	[m]
t	11.90	t	13.10	t	12.90	[cm]

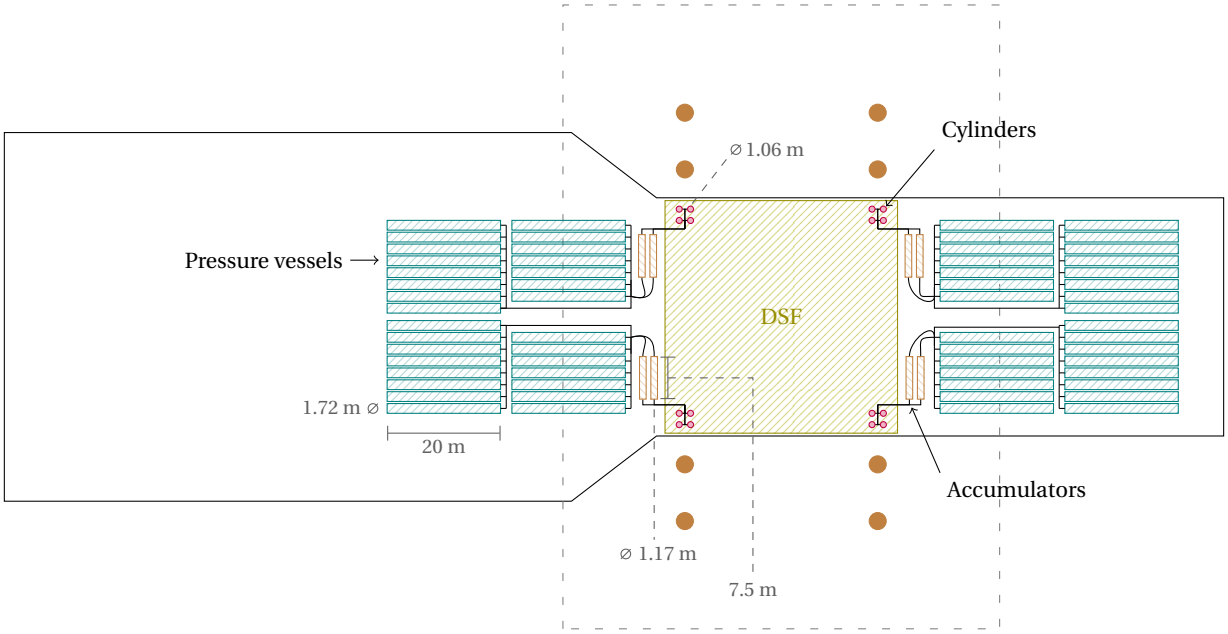

Figure 7.7: The elements of the 300 bar solution, with a total weight of 10,240 tons. From this figure the required deck area is estimated.

7.2.2. 200 BAR

The 200 bar solution uses the same methods as the 300 bar solution. A possible layout for the 200 bar solution is given in Figure 7.8. The main difference is that the 200 bar solution is significantly lighter and uses more cylinders and pressure vessels. The solution contains 24 cylinders, 8 accumulators and 96 pressure vessels. Combined with the DSF this gives a total weight of 9,016 tons. Each group is built using 6 cylinders actuated with 2 accumulators using the volume of 19 pressure vessels. Basic information of the elements is presented in Table 7.2, The detailed information is listed in Tables C.5 to C.7.

The required deck area of the 200 bar is solution is higher than the 300 bar solution, this is due to the higher amount of pressure vessels. The total required deck area is estimated at 46.5% of the total deck, where the contribution of the DSF is also 14.8% and the accumulator area is comparable and leads to 1.2%. The increase is found in the pressure vessels that now incorporate 30.5% of the deck area.

Since the 200 bar approximation is significantly lighter than the 300 bar approximation the 200 bar solution is taken as the better solution in this research. Additionally, the increased footprint is not considered a significant disadvantage. For the conclusions the 200 bar solution is thus considered.

Table 7.2: Summary of the results of the 200 bar dimensioning. The total weight of the estimation equals 9,016 tons.

Cylinders		Accumulators		Pressure vessels		Unit
Quantity	24	Quantity	8	Quantity	96	[-]
Weight	24	Weight	25	Weight	70	[tons]
l_{casing}	8.3	L	7.5	L	20	[m]
d_o	0.98	d_o	1.32	d_o	1.65	[m]
t	7.6	t	10.2	t	9.0	[cm]

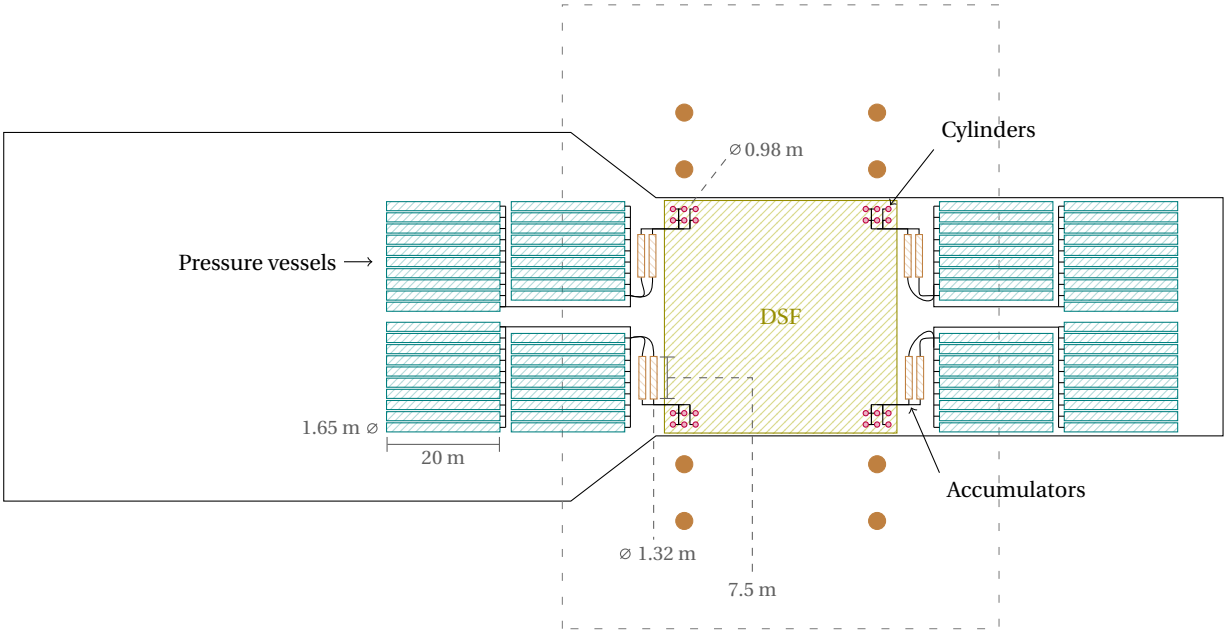

Figure 7.8: The elements of the 200 bar solution, with a total weight of 9,016 tons. From this figure the required deck area is estimated.

8

DISCUSSION

This is a preliminary research on a heave compensated floatover operation. The amount of topics related to the floatover operation exceeds the scope of a graduation study. Hence, the included scope is narrowed by several limitations during the process. The aim is set on the workability improvement with heave compensation. To be able to reach this aim, assumptions and simplifications are made, some of which may have a significant influence on the results. This chapter discusses the findings in twofold. First the demarcations of the thesis are discussed. Secondly, the simplification and assumptions are debated.

8.1. DEMARCATIONS AND SCOPE

The demarcations are divided in four subjects. First, the consequence of focussing on the mating phase is discussed. Followed by an elaboration on the effects of neglecting the horizontal motions of the barge. Thirdly, the influence of the Nigerian sea conditions as basis for the workability is argued. Finally, the expected forces on the heave compensation cylinders are reviewed.

Mating stage
For this study the mating stage is considered for improving the workability for three reasons: it is a time consuming stage, it contains dominant installation limits and it is the stage where heave compensation has the most significant influence. The results of the heave compensated scenario leads to higher allowable sea states in the mating phase. Thus, the workability in the mating stage increases. However, this does not mean that the workability of the total floatover operation is equally increased. In the heave compensated scenario the critical limits shift to the docking phase. It is possible that docking with the increased sea state of the heave compensated scenario is not possible. Thus, it might be necessary to expand the heave compensation system with an improvement for the docking stage to obtain an increased workability for the total floatover operation.

Barge constraints
During the mating phase the barge is moored inside the substructure slot. Fenders are installed to cope with the forces between the barge and substructure. This way the surge, sway and yaw motions are restricted. For this reason the horizontal motions of the barge are considered insignificant. During the limit study it is found that the horizontal forces on the fenders are critical loads in the mating procedure. Since these motions are not considered this limit is not incorporated in this research. Hence, the workability during the mating procedure can be lower.

Nigerian seas
The Nigerian sea is used for the test scenario, because of the high amount of heavy platforms installed by floatover in this region. The workability results are based on this single location. Considering multiple regions might present a more substantiated result of the performance of the heave compensation system. Especially since the peak enhancement factor of the Nigerian data did not correspond to the expected swell value.

Failure of the heave compensation system
When deriving the limits, failure of the heave compensation system is not considered. The concept is based on hydraulic cylinders; most cylinders are designed to carry loads longitudinally. Transverse loads on cylinders cause bending moments in the rod and can eventually lead to leakage of the cylinder seals, due to wear at one side of the cylinder wall. Rotations of the barge cause the heave compensation cylinders to rotate. The topsides load always acts downwards, hence, transverse loads at the top of the cylinders appear. Reaction forces of the substructure during the installation also cause transverse loads on the cylinders. In this conceptual research it is assumed that these forces can be handled by adjusting the design. In this study the lateral forces on the cylinders are only considered in the dimensioning of the heave compensation system. This is done by increasing the safety factors of the cylinders, no failure calculations of the cylinders due to the lateral loads are performed.

8.2. SIMPLIFICATIONS & ASSUMPTIONS

The simplifications and assumptions in this study are split in the simplifications and assumptions due to the limit derivation and due to the hydrodynamic model. First the findings for the limit derivation are discussed followed by the simplifications and assumptions for the hydrodynamic model, where the findings for the heave compensation system are also discussed.

8.2.1. LIMIT DERIVATION

The derivation of the installation limit lead to three important assumptions. Firstly, the amount of legs that are considered in the impact equations is discussed. Afterwards, the influence of the barge on the impact loads is detailed. Lastly, the friction effects on the leg mating unit is examined.

Leg considerations in the impact equations
The methodology to derive the impact load limits was considered sufficient because of two reasons: a detailed impact assessment is not possible in the frequency domain equations and for a comparison in workability a benchmark value is sufficient. The assumption made to obtain the benchmark value, is that the impact occurs on 1, 2, 4 or 8 substructure legs. In reality the number of legs changes through time. The results show that impact on 8 legs has the lowest limit, the benchmark value is based on this case. Impact on eight legs is likely for the heave compensated scenario; when the topsides roll and pitch are low, the impact occurs on 8 legs. However, for the uncompensated scenario the impact always occurs on 1, 2 or 4 legs, because the topsides is subjected to the roll and pitch of the barge. The impact limit incorporates all the impact scenarios, in order not to favour one scenario.

Barge resistance during the impact scenario
The impact model is based on the stiffness of the substructure legs and the leg mating units. The contribution of the barge buoyancy is not considered in this impact model. For the heave compensated scenario this contribution is negligible, because the substructure springs are much stiffer than the heave compensation system. In the uncompensated scenario the barge is rigidly connected with the topsides. Thus, the contribution of the barge forces can be significant. The contribution of this force cannot be taken into account in the used method. A proposed solution is given as: the substructure legs can be added in the hydrodynamic model, using compression only springs. However, this is a non-linear contribution that makes the analysis in the frequency domain impossible. For this reason, the contribution of the restoring force in the uncompensated scenario is not taken into account. Hence, the workability of the barge is conservative. Note that the proposed solution is also applicable for the discussion in the previous paragraph.

Friction on the leg mating units
In the impact model, the working line of the impact force and corresponding deflection is taken perpendicular to the surface of the leg mating unit. This is based on the assumption that no stick-slip effects occur on the lubricated surface of the leg mating unit, because of the low friction coefficient. This assumption has two side effects: firstly, stick-slip can occur, which can cause the leg mating unit and topsides leg to engage. This implies that the topsides leg and leg mating unit align, causing the barge and substructure to act as a single body. Secondly, the friction force acting on the leg mating unit changes the working line of the leg mating unit deflection, this effects the horizontal loads. Both effects change the installation limit. For the first side effect, the assumption is made that engagement of the legs does not occur because the contribution of the horizontal velocity is substantial, especially in the heave compensated scenario. The second effect is not taken into account because the friction force is non-linear and because a benchmark value is more suitable for this study, implementing the friction would lead to an installation maximum that depends on the orientation of the topsides velocity. It is unknown if these effects have a negative or positive influence on the results of the model. The installation maximum is rounded downwards to anticipate on a possible negative contribution of these effects.

8.2.2. MODELLING METHODS

The used model leads to the discussion of six significant topics. Starting with the elaboration on the frequency domain. After this the non-linear forces in the heave compensation system are discussed. Thirdly, the used viscous barge damping approach is explained. Consequently, the effects of the topsides eccentricity is debated. Followed by the discussion of the cylinder stroke possibilities. Lastly, the heat generation is argued.

The frequency domain approach
The largest influence on the assumptions and simplifications is caused by the frequency domain model, which requires that all forces are linear. The frequency domain is a good method to derive the characteristic behaviour of the system. For a conceptual study this method provides sufficient information. The non-linear components of the system are often extensive to implement, because they require detailed information that is often not directly available. A non-linear model will provide a more accurate result of the behaviour of the barge. The frequency domain model can be used to derive most probable values based on probability theories. The time domain model would require a large amount of computations and more complicated post processing.

Non-linear forces in the heave compensation system
The non-linear forces in the heave compensation system are caused by the friction of the pistons and the flow of the fluid. All friction is assumed as a linear friction force. In reality, the pistons friction forces are approximated with coulomb friction and the Stribeck effect. The results of which are non-linear. The pressure loss due to the fluid flow is related to the velocity squared. The behaviour of the system can be significantly influenced by implementing these effects. To incorporate these effect a more detailed model has to be made. The effect of the non-linear forces could be positive on the behaviour of the system. A good design can use the properties of the forces to control the characteristics of the system. Therefore, the results of the linear model in this study can be used as an incentive to study the non-linear model.

Viscous damping
The hull of the barge is subjected to viscous damping of the sea water; this cannot be calculated with the used hydrodynamic software. The viscous damping has a significant effect on the rotations of the barge, especially on the roll motions. To accurately determine this effect, damping experiments or RANSE calculations have to be done. A couple of complex theories exist to approximate the damping. This study uses a relatively simple method of Journee. However, this method is only valid for rectangular barges, with the center of gravity on the waterline. Both of these conditions are not true in this case. The method is used because an approximation of the viscous damping is required. The aim of this thesis lays on the interaction between barge and topsides. Hence, the choice is made not to determine the viscous friction with complex methods.

Topsides eccentricity
The model assumes that the center of gravity of the topsides is located perfectly centred above the four lifting points, with a uniform weight distribution. This is done to assess the heave compensation system as four identical systems, in reality the center of gravity is located eccentrically leading to four different forces on the heave compensation system locations. The systems will have to be altered to reach the same characteristics parameters. For large offsets this might lead to different behaviour of the barge and topsides.

Cylinder stroke
The cylinders can use their stroke to ease the topsides load transfer, this also decreases the maximum impact loads and installation duration. This stroke can not be implemented in the model, because the velocity of the stroke is related to the detailed design of the cylinders. The stroke effect could be included in the mating duration. The choice is made not to decrease the mating period for the heave compensated scenario. The decrease in mating duration is a subjective choice, this choice only favours the heave compensated scenario. Therefore, the durations are taken equal, this way the effect of the heave compensation is shown without subjective factors.

Heat generation
The concept considers a high percentage of damping, 20% of the critical damping per system relates to a damping coefficient of 1.1 MN·s/m. This damping coefficient determines the amount of energy that needs to dissipate, this energy is converted to heat. Hence, it is likely that the system needs to be cooled. The damping forces are not accurately determined in this graduation thesis. Therefore, no calculations of the heat generation are performed. The expectation of the heat generation (based on the order of magnitude) is that cooling is required, making the system more complex, but it is not expected to be a technical problem.

9

CONCLUSIONS

Floatover operations in swell regions are often subjected to long waiting on weather periods. Swell waves induce large motions on the floatover barge, which cause large loads during the operation. Therefore, swell waves often cause unsafe working conditions. Heave compensation during the floatover operation might improve the workability significantly enough to reduce these waiting periods. This research assesses the gain in workability by implementing a heave compensation concept into a floatover installation procedure. For this purpose a test scenario is employed: the `Liwan 3-1` topsides (26,300 tons) installation in the Nigerian swell sea. To assess the workability, the heave compensation concept is included into a hydrodynamic model of the barge, topsides and jacket. Furthermore, the limiting loads of the floatover operation are acquired.

The heave compensation system consists of three main components: hydraulic cylinders to lift the topsides, pneumatic pressure vessels to provide passive actuation and accumulators to connect the cylinders with the pressure vessels. The hydrodynamic model contains a linearised heave compensation system. These simplifications are done to assess the behaviour in the frequency domain. The model computes the influence of the heave compensation system on the motions of the barge and topsides. The model is based on heave, roll and pitch of the barge. The surge, sway and yaw are not taken into account because the barge is constraint in the substructure slot, with mooring lines and fenders.

The limiting loads of the floatover installation are obtained by considering the mating stage of the operation. In this stage the lowest workable conditions are present, due to high impact loads between topsides and jacket. The most critical loads in this stage are the horizontal impact loads on the substructure. The maximum allowable horizontal impact loads are used to determine the maximum impact velocity of the topsides. The results of the hydrodynamic analysis are combined with the maximum impact velocity to determine the workability in the Nigerian sea. The workability can be influenced by changing the variables of the heave compensation system. These variables are the working pressure, pneumatic volume and damping of the heave compensation system. The best heave compensation settings are chosen based an trade of between pneumatic volume and workability. With these values the size and mass of the heave compensation system are approximated. This process lead to the conclusions, which are presented based on the research questions.

The following main research question is resolved:

> Does the implementation of heave compensation on a barge improve the workability of a floatover mating operation such that it increases significantly in swell conditions?

To solve this question the following sub-questions must be answered;

What are the installation limits during a floatover installation?

What is the most suitable heave compensation concept?

How does this concept influence the topsides and barge motions?

What would be the ideal heave compensation parameters?

How large would the heave compensation system become, in terms of weight and deckspace footprint?

First the sub questions are dealt with, then the main research question is answered.

The installation limits of the floatover installation
A floatover operation contains five operation stages, each with different limits. The most profitable stage, in terms of improving workability, is the mating stage. Additionally, heave compensation has the most influence in this stage, because the touch down of the topsides occurs in the mating stage. Therefore, only this stage is considered. The horizontal impact loads on the substructure are found as the limiting loads in the mating phase. The substructure legs are fitted with leg mating units. By combining the substructure stiffness and the leg mating unit stiffness, a single stiffness for the substructure is determined. Using this stiffness, the impact limits are derived with an energy balance. The energy balance is based on the maximum deflection of the combined stiffness and the kinetic energy of the topsides. With this energy balance the maximum topsides velocity is derived based on the maximum horizontal loads on the substructure. For the `Liwan 3-1` installation without heave compensation, the maximum topsides velocity resulted in maximum allowable sea states that coincide with the expectations. Therefore, this velocity limit is used as the benchmark for the floatover installation with heave compensation. In reality, the limit is a combination of multiple criteria. For example, the loads on the substructure from the barge fenders, due to horizontal motions, have a contribution to the total horizontal loads on the substructure.

Most suitable concept
To avoid large power demands, a passive heave compensation system is chosen. The concept consists of pneumatic pressure vessels that actuate hydraulic cylinders with the use of an accumulator. The hydraulic cylinders are installed perpendicular to the deck surface, thus, act in the vertical direction of the barge. In the transverse direction the cylinders are assumed rigid. This concept is capable of compensating the vertical motions of the topsides due to the heave, roll and pitch of the barge. The motions in the horizontal plane, from the barge roll and pitch, are not compensated. The results show a significant decrease in the topsides impact, due to the decreased vertical velocity. Therefore, the horizontal motions are tolerated. Additionally, the complexity of the heave compensation system rises substantially when compensation in the surge, sway and heave of the topsides is considered.

Influence of the heave compensation on the barge and topsides behaviour
The heave compensation system is modelled between the barge and topsides. The results show that the vertical motions of the topsides can be completely cancelled with the heave compensation system when a low stiffness value for the cylinders is taken. For this stiffness the barge response is changed, but the general behaviour is equal for the heave and pitch motions. The barge roll motions are significantly reduced. The model considers the heave compensation system as a linear spring damper system. Additional research is required to check if a non-linear model reaches a comparable response. The linear results show good improvements of the workability.

Ideal parameters of the heave compensation system
The performance of the heave compensation system is determined with the maximum velocity limit of the mating operation and the linear model of the heave compensation system. The performance is expressed in workability and relates to the parameters of the heave compensation system. The parameters are based on the working pressure, pneumatic volume and damping in the system. The results show that large profits in

workability can be realized. A higher pressure and larger pneumatic volumes have a positive effect on the workability. For the damping, an optimum is found depending on the pressure and volume. The influence of the damping is noteworthy.

The weight and deckspace footprint estimations
The weight and footprint are determined with the working pressure and the pneumatic volume of the heave compensation system. The ideal parameter for the pressure is not determined, because no substantiated value is applicable. Therefore, two settings for the working pressure are examined, 200 bar and 300 bar. The corresponding total pneumatic volumes, based on a trade-off between size and workability, are found as 2,600 and 2,000 cubic meters respectively. Using these parameters the extend of the system is estimated. The lighter system is the 200 bar case; this system contains more elements but the increase in footprint is small. The dimensions and weight estimation of the heave compensation system are reasonable. For the 200 bar case, 9,000 tons of steel is required, covering around 40% of the barge deck. The 300 bar case weights 10,200 tons and covers around 35% of the deck. These are significant weights in relation to the weight of the topsides, however, the conventional deck support frame already weights 4,000 tons. When the system is designed to be flexible for multiple installations, the investment can be viable. More engineering is required before a justified conclusion can be made on the viability of the concept. The discussion chapter elaborates on the uncertainties that should be resolved.

Workability improvement of the heave compensation system
This research shows that the heave compensation system is very effective for the floatover mating operation. The workability is almost doubled in head waves (from 46% to 88%). In beam seas the improvement is more than seven times higher (from 6% to 44%). Hence, large improvements in workability are reached with this concept. This research is conducted with a simplified model, therefore, the results are interpreted as appraisal values for the theoretic principle behind the heave compensation concept. It is concluded that this is a viable concept for floatover operations.

The discussion chapter further elaborates on the findings of this study. The results are to be evaluated critically, because they are bound by substantial demarcations and assumptions. For example, this research aims on the workability during the mating stage of the floatover operation. This is the most critical stage and is therefore the most improvable stage. The sea states limits of the heave compensated floatover operation, likely exceed the limits of the floatover docking stage. Hence, the workability improvement is not applicable for the full installation procedure.

To further substantiate the found workability, all installation limits have to be reconsidered and a more realistic model of the heave compensation system should reach comparable characteristics. These are the two most important topics that are not evaluated in depth. The aim of this thesis is to check if a heave compensated floatover operation is promising. On that ground, it is concluded that the heave compensated floatover shows high potential for floatover installations in severe swell seas. The heave compensated floatover concept can thus be profitable, if the offshore industry in swell regions continues to expand.

10

RECOMMENDATIONS

The research is subjected to significant demarcations, simplifications and assumptions as discussed in the discussion chapter. The recommendations explain how these discussion points can be solved by additional research. The recommendations are split in two main topics, firstly the possibilities with a detailed model are given. Secondly, alternative concepts are proposed.

10.1. DETAILED MODELLING

This research solved the equations of motion in the frequency domain. To incorporate non-linear forces the model has to be based on the time domain. The hydrodynamic parameters of the barge in the equations of motion are frequency dependant, this makes implementation of these parameters in the time domain a considerable, but nowadays feasible, task. The time domain model can then be used to implement the following subjects:

- **A moored model**, taking the mooring lines and fenders into account.
- **Impact model**, considering the leg locations and all impact forces on the LMU's
- **Non-linear heave compensation system**, a more detailed model can be implemented to check the influence of the friction forces
- **Effects of the installation stroke**, using a combination of the proposed models, the added value of the installation stroke can be determined

Moored model
When the motions of the barge are modelled, the loads on the substructure fenders can be calculated. For this the fenders and mooring lines have to be added to the model. With this model a better estimation of the workability can be made. This model can also be used to determine the limiting loads during the docking stage of the floatover operation. The research can indicate if the improvement in workability found in this research is still reached when taking the horizontal motions of the barge into account. Additionally, a check can be made whether an additional system is needed to the floatover concept to provide a higher workability in the docking stage of the operation.

Impact model
The limits in this study are determined with a benchmark value, that represents the limiting loads for the impact on the substructure. This value is based on a static, worst case, approach. For a more realistic approach on the impact values, the substructure model has to be implemented in the equations of motions. This way the non-linear forces in the leg mating unit can be taken into account as well as the restoring force of the barge. Also, a dynamic setting of the number of legs exposed to the impact forces is derived.

Non-linear heave compensation system
The heave compensation system is considered as a linear spring-damper system. For this conceptual study this approach is sufficient to get an idea of the required characteristics. For a better approximation, the non-linear forces in the system have to be inserted in the model. For example, when stick slip occurs, the topsides is subjected to extra impact forces that might lead to unwanted side effects. These effects can only be estimated when a detailed model of the heave compensation system is implemented. An estimation of the friction forces can only be made when all dimensions are known.

Effects of the installation stroke
The installation stroke is designed to minimise the impact loads. This principle can be applied to decrease the duration of mating phase, hence decrease the most probable wave height. Modelling this principle is complex since the process has to start at the correct moment of the oscillations. To implement the installation stroke a more detailed model of the compensation system is required, to determine the possible velocity of the stroke. After implementing the stroke, the effectiveness of the heave compensation system needs to be verified again.

10.2. CONCEPT ALTERNATIVES

The used heave compensation concept is a very practical solution that approaches the problem in a straightforward manner. The downside of this concept is that cylinders are not designed to cope with transverse loads. These loads will occur due to the roll and pitch motions of the barge. Additionally, passive actuation does not allow sudden changes. For example, if a cylinder fails, the pressure in the other cylinders has to rise significantly to cope with the extra loads. Leading to a drop in the stroke of the cylinders. For these problems two alternatives are suggested: one for the actuation problem, the semi-active system, and one for the horizontal load problem, the reversed hinge principle.

Semi-active system
The semi-active system is basically the combination of passive and active actuation. The classic implementation of this principle is to use passive actuation for the static loads and active power for the dynamic loads. In this scenario the active part of the actuation can be used to control unwanted motions of the topsides.

Reversed hinge approach
The transverse loads on the cylinders are caused by the fixed mounts on the deck barge. Hence, the working angle of the stroke is correlated with the roll and pitch motions of the barge. These loads can be omitted by changing the mount type on the deck, by placing the system hinged on the barge. The reversed hinge approach is based on this idea. To keep the topsides stable, the connection at the topsides has to be rigid. This implies that the cylinders stay attached perpendicular to the topsides bottom plane. With this configuration the topsides are not translated horizontally due to the roll and pitch rotations of the barge. During the installation procedure, transverse forces are caused by the leg mating units. Therefore, not all transverse forces are omitted. When these forces are dealt with and the connection at the topsides is feasible, than this solution can significantly improve the workability (especially in beam seas). This concept might create a more lucrative solution but causes a large increase in complexity.

BIBLIOGRAPHY

M. He, R. Yuan, H. Li, W. Yu, J. Qian, and A. M. Wang, *Floatover installation analysis and its application in bohai bay,* Proceedings of the Twenty-first International Offshore and Polar Engineering conference (2011).

A. M. Wang, X. Jiang, C. Yu, H. Li, and Y. Wei, *Latest progress in floatover technologies for offshore installations and decommissioning,* ISOPE (2010).

J. Labbe, V. Allègre, J. Volker, and F. Agdern, *Epke gas compression project - float-over deck installation,* Offshore Technology Conference (1998).

Epke, *Ekpe phase 2, nigeria,* http://www.offshore-technology.com/projects/ekpe/, accessed: 14-10-2015.

C. Tribout, D. Emery, P. Weber, and R. Kaper, *Float-over offshore west africa,* Offshore Technology Conference (2007).

TMHL, *Technical presentation,* http://www.tmhl.no/doc/Technical%20Presentation%20February%202013.pdf, published in 2013.

J. Martinez, *Industry shows renewed interest in float-over installation,* http://www.offshore-mag.com/1/volume-74/issue-10/engineering/industry/industry-shows-renewed-interest-in-float-over-installation-full.html, published in 2014.

J. Hou, Q. Tang, and L. Xu, *Installation method selection for heavy weight topside in the south china sea,* Proceedings of the Twenty-third International Offshore and Polar Engineering (2013).

Amenam, *Amenam amp platform, nigeria,* http://www.offshore-technology.com/projects/amenamkpono/, accessed: 01-11-2015.

M. Yuan, L. Chen, F. Ma, and D. Kim, *Shwe topsides installation,* Proceedings of the Twenty-third International Offshore and Polar Engineering (2013).

J. Herdzik, *Utilization of an active heave and/or passive heave compensation in the equipment of dynamic positioning vessels,* KONES Powertrain and Transport (2014).

J. Hamilton, R. French, and P. Rawstron, *Topsides and jacket modelling for floatover installation design,* Offshore Technology Conference (2008).

R. Yuan, M. He, W. Yu, A. M. Wang, D. Merino, and T. Boe, *Parametric sensitivity studies for floatover installation analysis of liwan 3-1 mega topsides with a t-shaped launch barge,* Proceedings of the Twenty-fourth International Offshore and Polar Engineering (2014a).

M. Seij and H. de Groot, *State of the art in float-overs,* Offshore Technology Conference (2007).

H. Li, Y. Yang, R. Yuan, W. Xie, A. Wang, and X. Jin, *T-shaped launch barge modification design for very challenging floatover installation of liwan 3-1 mega topsides south china sea,* Proceedings of the Twenty-third International Offshore and Polar Engineering (2013).

M. Yuan, L. Chen, Y. Li, Y. Liang, H. Sun, H. Li, and W. Xie, *Design considerations of liwan 3-1 topside float-over mating analysis,* Proceedings of the Twenty-fourth International Offshore Ocean and Polar Engineering Conference (2014b).

R. Yuan, A. M. Wang, H. Li, L. Qin, J. XU, and M. He, *Design consideration of leg mating units for floatover installations,* Proceedings of the Twenty-second International Offshore and Polar Engineering conference (2012).

J. Sigrist, P. Thomas, and J. Naudin, *Experience in float over integrated deck - flexibility of the concept,* Offshore Technology Conference (1998).

V. V. Sychev, A. A. Vasserman, A. D. Kozlov, G. A. Spiridonov, and V. A. Tsymarny, *Thermodynamic Properties of Air,* Hemisphere, New York, 1987, originally published by Standards, Moscow, 1978 (1978).

F. M. White, Fluid mechanics (McGraw-Hill, 2011).

J. Journeé, Theoretical manual of SEAWAY (Delft University of Technology, 2007).

J. Journeé, *Motions of rectangular barges,* Proceedings of 10th International Conference on Offshore Mechanics and Artic Engineering (1991).

DNV-RP-C205, *Environmental conditions and environmental loads,* Recommended practise, Det Norske Veritas (2010).

J. Journeé and W. Massie, Offshore Hydromechanics (Delft University of Technology, 2001).

D. D. N. 5-778.93, *Hydraulic cylinders,* Standard for certification, Det Norske Veritas (2009).

P. Albers, Motion control in Offshore engineering (Springer, 2010).

Machinery and systems, *Ships / high speed, light craft and naval surface craft, part 4 chapter 7,* Rules for classification, Det Norske Veritas (2011).

List of Figures

List of Tables

A

MODEL BACKGROUND

A.1. DEFINITION OF DISPLACEMENTS

The definitions of the motions used in this thesis is shown in figure A.1. These conventions are used through the entire research and are called upon according to the following nomenclature:

x	=	the surge motion is defined as positive in x-direction
y	=	the sway motion is set positive to starboard over the y-axis
z	=	the heave motion is the vertical motion with positive upwards motion
ϕ	=	the roll motion is defined as rotation around the x-axis, positive right turning
θ	=	the pitch motion is rotation about the y-axis, positive left turning
Ψ	=	the yaw motion of the vessel is the rotation around the z-axis, positive right turning

Note, for the pitch motions the illustration of A.1 and the definition of above do not coincide. The picture is not corrected since the barge and topsides combination is y-symmetric, hence, both definitions lead to the same results. Of course, only if used consistent.

In literature these degrees of freedom are often indicated with a number. This notation is also used in this research to indicate the motions of the barge. The notation exist of a double subscript from 1 to 6 corresponding which indicate the same order as the table above. This means that A_{11} would refer to a value of A for the surge motions and A_{44} to the A value for roll motions. This notation is used to refer to cross terms like A_{35} which indicates the pitch influence on the heave of A.

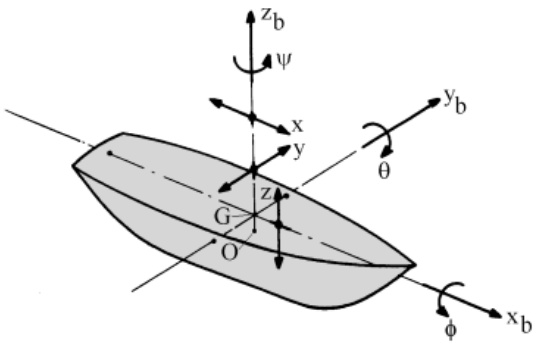

Figure A.1: The ship shows the different motions translations and rotations. Definition are used from Journeé and Massie (2001)

A.2. PARAMETERS OF THE LIWAN 3-1 SCENARIO

In this chapter the available data of the test scenario us listed. The information is split in the two main masses, the HYSY229 barge and the Liwan 3-1 topsides. This data is used to calculate the characteristic values as is elaborated in Appendix B.

The Hai Yang Shi You 229 barge owned by the Chinese National Offshore Oil Corporation. Is a T-shaped launch barge specially modified to perform the Liwan installation the information of the barge is found in Yuan et al. (2014b,a) and Li et al. (2013). The information is gathered in Figure A.2.

This scenario is picked because of two reasons: it contains all four requested parameters and multiple articles are found on this scenario. The four requested parameters are satisfied as follows:

- **Weight over 10,000 tons,** the Liwan 3-1 topsides weights 26,300 tons.
- **Small airgap,** the airgap of the Liwan 3-1 platform is 15 meters, which is too small for the *PS*.
- **Large dimensions,** the length of the Liwan 3-1 topsides is 110 meters and the width 77 meters, both of these parameters are to large for the *PS*.
- **Shallow water,** the platform is installed in 190 meters of depth, this is within the limits of the *PS*. For the motions of the model the depth is set to a lower value. The substructure stiffness is based on the deep substructure.

Barge parameters

HYSY229

Dimensions			
Contains a 15 meter transition piece between bore and aft	L total	215	[m]
	L fore	100	[m]
	L aft	100	[m]
	B fore	42	[m]
	B aft	65	[m]
	D	14.25	[m]
	T des	10.45	[m]
	C block	0.82	[-]
Tonnage			
	Lightship	28011	[ton]
	Deadweight	91847	[ton]
	Max transport	60000	[ton]
Installed			
	Power	3940	[kW]
	Pump N	4	[-]
	Pump cap	3500	[m^3/h]
	Total pump	14000	[m^3/h]
Centers of gravity			
	LCG	116.3	[m]
	TCG	0	[m]
	VCG	8.15	[m]

From Annex A, parametric sensitivity study paper, relates to liwan installation

Inertial properties of the HYSY229

Description	Weight	XCG	YCG	KG	Ixx	Iyy	Izz
Total without ballast	39349	109.01	0.02	9.98	1.29E+07	1.34E+08	1.44E+08
All elements available in paper	[Te]	[m]	[m]	[m]	[Te*m^2]	[Te*m^2]	[Te*m^2]

Hydrostatic properties at different drafts

Description	Unit	Draft 8.2m	Draft 10.2m	Draft 12.1m
Buoyancy force	[kN]	9.18E+05	1.15E+06	1.36E+06
XB: COB Longitudinal Position	[m]	-13.255	-12.775	-12.227
ZB: COB Vertical position	[m]	-4.03	-5.025	-5.986
BMt: Transverse metacenter from cob	[m]	34	27	22.5
BMl: Longitudinal metacenter from cob	[m]	480.9	369.8	298
Swp rho g : Heave restoring	[kN/m]	1.15E+05	1.14E+05	1.12E+05
BMt M g : Roll restoring	[kN*m]	3.12E+07	3.10E+07	3.07E+07
BMl M g : Pitch restoring	[kN*m]	4.42E+08	4.24E+08	4.06E+08
Heave pitch restoring	[kN]	1.31E+06	1.14E+06	9.53E+05

Platform parameters

Liwan LW 03-1-1 PUQ

Topside weight	31375 [tons]	
Water depth	190 [m]	
Airgap	15 [m]	
Jacket legs	8 [-]	
Length	72 [m]	T.O.S, C.T.C
Width	48 [m]	T.O.S, C.T.C
Transverse frame spacing	2.5 [m]	

Figure A.2: The particulars of the barge gathered in an infographic. The information is combined from Yuan et al. (2014b,a) and Li et al. (2013).

A.3. ANSYS & AQWA MODELLING

The motion of the barge are determined using the hydrodynamic parameters obtained with Ansys and AQWA, software. In Ansys the barge is modelled using the Finite Element Method (FEM), this model is required to calculate the hydrodynamic behaviour of the barge. AQWA uses the 3-D panel method to calculate the wave diffraction and radiation forces and creates the hydrodynamic coefficients of the barge. The results of the model are highly dependant on the AQWA calculations and therefore the input in these calculations is an important part of the research. The input consists of the (FEM) of Ansys, where the barge is modelled in 3D using the known dimensions, and the characteristic values of the operation. The characteristic consist of information regarding the COG, mass and inertial values of the barge and topsides combination. This subsection firstly elaborates on the Ansys model. Afterwards, the used AQWA model is detailed.

A.3.1. THE ANSYS MODEL

The FEM is build in Ansys. The dimensions used for this model are found in Yuan et al. (2014a,b) and visualised in Figure A.3. The particulars did not clarify the shape of the bow. Therefore, the bow shape is determined with measurements from visualizations in Li et al. (2013). The visualisation and sketches in the literature match with the dimensions of the data tables. The data table also contains the inertial and basic hydrodynamic data.

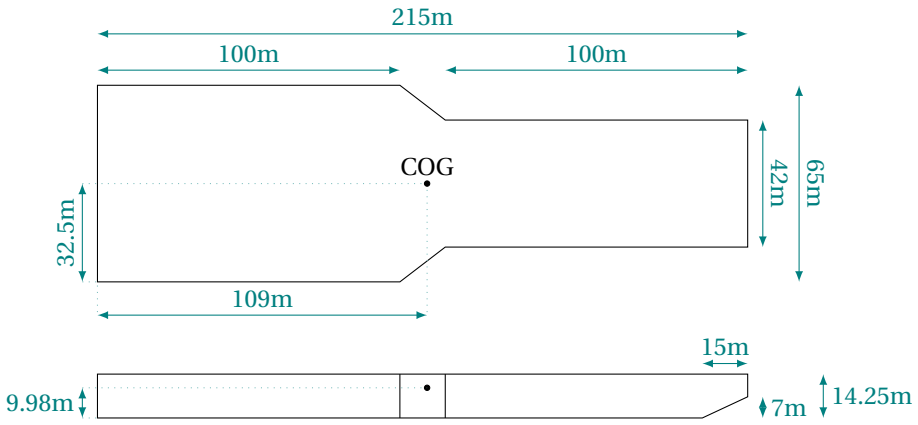

Figure A.3: Main dimensions of the HYSY229

The T-shaped barge is modelled with XZ plane symmetry and is meshed using the different draft conditions. The mesh is done twofold by splitting the barge over the waterline area. The wet part, from keel to waterline, is than meshed with a size of 2 meters and the dry part, from waterline to deck, is meshed with 6 meter elements. This FEM model is shown in Figure A.4, for 10.2 meters draft.

A.3.2. THE AQWA MODEL

The AQWA model uses the geometry of the Ansys input supported with additional data of the scenario, that consists of characteristics of the system and the modelling settings. The information supplied in the AQWA model, besides the geometry, is listed as follows:

- Center of gravity
- Draft
- Inertia
- Mass
- Viscous damping
- Water depth
- Wave frequencies
- Wave directions

In which the left column and the viscous damping are depending on the draft settings and the last three settings are fixed. The three drafts that are considered in this thesis are 8.2, 10.2 and 12.1 meter draft conditions, the AQWA analysis is performed for the 8.2 and 10.2 meter draft scenarios. When the final AQWA calculations where performed it was already clear that the undocking draft was not required. For these values the mass center of gravity and inertia values are calculated using the methods of Appendix B. For the viscous damping

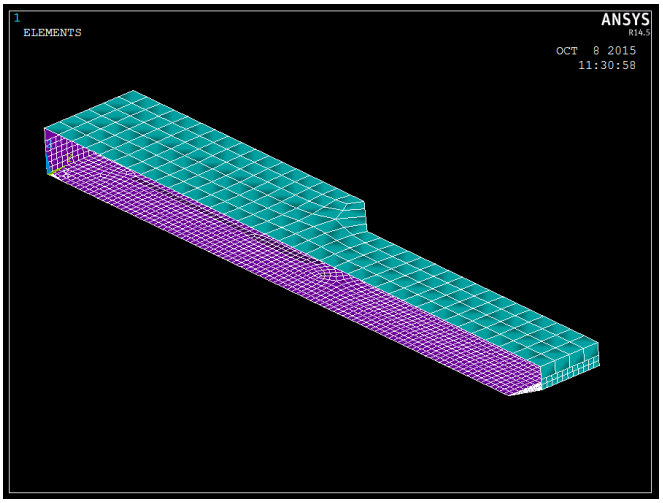

Figure A.4: The HYSY229 modelled in Ansys. The barge is symmetric over the XZ-plane and a different mesh size is used for the dry and wet part of the hull.

the equations specified in Section 5.1.4 are iteratively solved. The first five of the list, as used in the AQWA model, are given in Table A.1.

Table A.1: Input values for the different drafts in the AQWA calculations

Draft [m]	Center of gravity XCG [m]	YCG [m]	ZCG [m]	Inertia I_{xx} [Te·m^2]	I_{yy} [Te·m^2]	I_{zz} [Te·m^2]	Mass [Te]	Viscous roll damping [kN·m·s/rad]
8.2	109	0	15.69	$8.17 \cdot 10^7$	$2.87 \cdot 10^8$	$3.08 \cdot 10^8$	94,440	$3.82 \cdot 10^6$
10.2	109	0	13.56	$8.62 \cdot 10^7$	$3.60 \cdot 10^8$	$3.84 \cdot 10^8$	118,000	$3.25 \cdot 10^6$

For the water depth the depth of the Liwan 3-1 platform is 190 meters. This is not used for the test case since the majority of the low airgap platforms are installed in shallower conditions. To simulate *PS* impossible conditions it is chosen to perform the test scenario in 40 meters water depth. This is based on the Nigerian platforms which are installed in 17 to 65 meters water depth. This shallow water setting creates more wave action and will negatively impact the workability thus creation a more challenging environment.

The wave directions are based on the general directions with an extra focus on head-on waves. This focus is set due to the dominant southern swell in the African sea. Hence, it is likely that the incoming wave energy is unidirectional. The general directions are chosen as quartering and beam waves. The chosen waves directions are visualised in Figure A.5.

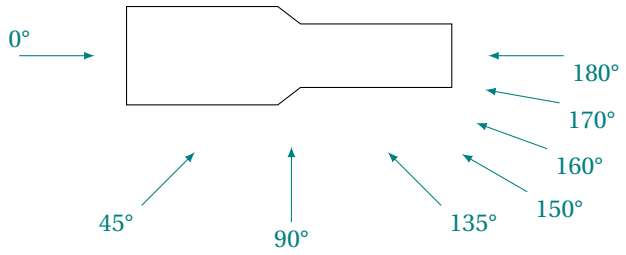

Figure A.5: Wave directions for the AQWA model

To determine which frequencies should be used in the AQWA model the wave spectra which will be used to analyse the response is examined. To simulate the Nigerian conditions a Jonswap spectrum is used with a peak correction factor (γ) of 8, this value corresponds to the value of Table A.2. Normal swell is based on a peak enhancement factor of 1, since the high value is found in the sea state data it is used in this research. The spectra are shown in Figure A.6, where different peak periods are shown. The periods used in this plot

represent typical west Nigerian swell scenario's and thus the frequencies used in the AQWA calculations should include most of the energy of these spectra. The chosen frequency domain is from 0.2 rad/s to 1.3 rad/s. AQWA has a set the maximum number of frequencies to 50. Therefore, a step size of 0.025 is taken which leads to 45 frequencies.

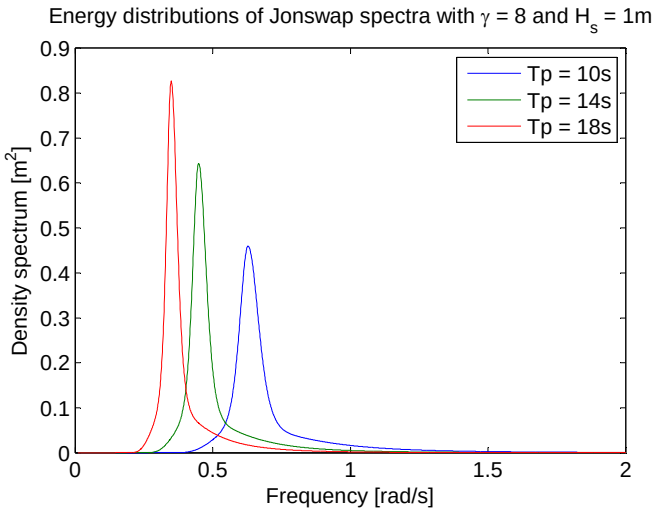

Figure A.6: The distribution of Nigerian swell spectra to analyse the required frequencies for the response spectrum

A.4. SEA STATES

In the Introduction an analysis is performed on the sea states of multiple West-African countries. The data used for this analysis is included in this appendix. The scatter diagrams are found in the environmental database of Allseas Engineering. The database of the Nigerian sea is used as a basis for the African swell approximation, this because the majority of the platforms within the scope of this project are installed in this region. Hence, the Nigerian table is the most important. The Nigerian swell is taken with a peak enhancement factor of 8. For the other regions no spectra are created, thus, no information regarding the configuration of the spectrum is obtained.

All scatters are based on year-round values. Since the scatters are used from the internal database no detailed information is included. The sea state scatters are included as:

Table A.2 Nigeria
Table A.3 Angola
Table A.4 Congo
Table A.5 Equatorial Guinea
Table A.6 Ghana

Table A.2: The statistics for the Nigerian sea

H_s [m]	T_p [s] 0-2	2-4	4-6	6-8	8-10	10-12	12-14	14-16	16-18	18-20	20-22	Sum
0.0 - 0.3	-	-	-	-	-	-	-	-	-	-	-	-
0.3 - 0.5	0.01	0.04	-	-	0.01	-	-	-	-	-	-	0.06
0.5 - 1.0	-	-	0.05	5.10	4.63	3.60	3.76	1.08	0.33	0.07	0.03	18.65
1.0 - 1.5	-	-	-	3.20	28.65	17.41	10.44	6.51	1.93	0.38	0.03	68.55
1.5 - 2.0	-	-	-	-	1.49	6.81	1.57	1.46	0.48	0.07	-	11.88
2.0 - 2.5	-	-	-	-	-	0.25	0.14	0.15	0.04	0.01	-	0.59
2.5 - 3.0	-	-	-	-	-	-	0.01	0.05	0.01	-	-	0.07
Sum	0.01	0.04	0.05	8.30	34.78	28.07	15.92	9.25	2.79	0.53	0.06	99.80

Table A.3: The statistics for the Angola sea

H_S [m]	Tp [s]																						
	3 - 4	4 - 5	5 - 6	6 - 7	7 - 8	8 - 9	9 - 10	10 - 11	11 - 12	12 - 13	13 - 14	14 - 15	15 - 16	16 - 17	17 - 18	18 - 19	19 - 20	20 - 21	21 - 22	22 - 23	23 - 24	24 - 25	Sum
0.00 - 0.50	-	-	0.04	0.08	0.07	0.05	0.11	0.17	0.26	0.29	0.17	0.13	0.05	-	-	0.01	-	-	-	-	-	-	1.43
0.50 - 0.75	0.01	0.15	0.49	1.59	2.25	1.60	1.16	1.74	2.70	2.34	1.60	1.30	0.95	0.28	0.26	0.08	0.03	0.04	0.02	-	-	-	18.57
0.75 - 1.00	-	0.12	0.66	1.45	2.97	3.08	2.87	3.27	4.32	4.22	3.35	3.54	2.06	0.77	0.76	0.25	0.17	0.06	0.03	0.01	-	-	33.98
1.00 - 1.25	-	0.01	0.12	0.29	1.24	2.11	2.43	2.57	2.89	3.04	2.43	2.59	2.00	0.74	0.75	0.31	0.16	0.08	0.04	0.02	0.01	-	23.84
1.25 - 1.50	-	-	-	0.01	0.10	0.70	1.39	1.48	1.82	1.78	1.42	1.46	1.08	0.53	0.58	0.29	0.14	0.08	0.03	0.01	0.01	-	12.92
1.50 - 1.75	-	-	-	-	-	0.07	0.49	0.77	0.81	0.73	0.59	0.63	0.50	0.28	0.27	0.13	0.07	0.04	0.01	0.01	0.01	-	5.43
1.75 - 2.00	-	-	-	-	-	-	0.05	0.20	0.37	0.39	0.31	0.35	0.25	0.11	0.08	0.05	0.02	0.01	-	-	-	-	2.18
2.00 - 2.25	-	-	-	-	-	-	-	0.01	0.11	0.14	0.14	0.17	0.14	0.08	0.06	0.04	-	-	-	-	-	-	0.90
2.25 - 2.50	-	-	-	-	-	-	-	0.01	0.03	0.04	0.05	0.07	0.05	0.02	0.02	0.01	0.01	-	-	-	-	-	0.32
2.50 - 2.75	-	-	-	-	-	-	-	-	0.01	0.01	0.03	0.03	0.02	0.02	0.01	0.01	-	-	-	-	-	-	0.13
2.75 - 3.00	-	-	-	-	-	-	-	-	-	-	0.01	-	0.01	0.01	0.01	-	-	-	-	-	-	-	0.04
3.00 - 3.25	-	-	-	-	-	-	-	-	-	-	-	0.01	0.01	0.01	-	-	-	-	-	-	-	-	0.03
3.25 - 3.50	-	-	-	-	-	-	-	-	-	-	-	0.01	-	-	-	-	-	-	-	-	-	-	0.01
3.50 - 3.75	-	-	-	-	-	-	-	-	-	-	-	-	-	-	-	-	-	-	-	-	-	-	0.01
3.75 - 4.00	-	-	-	-	-	-	-	-	-	-	-	-	-	-	-	-	-	-	-	-	-	-	-
Sum	0.01	0.28	1.31	3.42	6.62	7.61	8.51	10.24	13.31	12.98	10.09	10.28	7.13	2.85	2.83	1.17	0.60	0.31	0.13	0.05	0.03	-	99.77

Table A.4: The statistics for the Congo sea

H_S [m]	Tp [s]																						
	3 - 4	4 - 5	5 - 6	6 - 7	7 - 8	8 - 9	9 - 10	10 - 11	11 - 12	12 - 13	13 - 14	14 - 15	15 - 16	16 - 17	17 - 18	18 - 19	19 - 20	20 - 21	21 - 22	22 - 23	23 - 24	24 - 25	Sum
0.00 - 0.25	-	-	-	-	-	-	-	-	-	-	-	-	-	-	-	-	-	-	-	-	-	-	-
0.25 - 0.50	-	-	-	-	-	-	-	-	-	0.01	-	-	-	-	-	-	-	-	-	-	-	-	0.01
0.50 - 0.75	-	-	0.01	0.05	0.04	0.04	0.02	0.04	0.07	0.10	0.08	0.07	0.03	0.01	0.01	-	-	-	-	-	-	-	0.57
0.75 - 1.00	-	0.16	0.38	0.81	0.48	0.19	0.16	0.36	0.63	0.63	0.47	0.37	0.24	0.09	0.08	0.03	0.02	0.02	-	-	-	-	5.12
1.00 - 1.25	-	0.11	0.85	3.00	3.34	1.18	0.61	0.97	1.88	2.04	1.57	1.43	0.92	0.39	0.30	0.15	0.06	0.03	0.02	-	-	-	18.85
1.25 - 1.50	-	-	0.64	2.19	5.66	3.91	1.52	1.29	2.07	2.54	2.29	2.14	1.30	0.60	0.41	0.16	0.08	0.06	0.03	0.01	-	-	26.90
1.50 - 1.75	-	-	0.17	0.82	3.08	4.66	2.54	1.41	1.58	1.82	1.70	1.71	1.13	0.52	0.36	0.16	0.07	0.05	0.03	0.01	-	-	21.82
1.75 - 2.00	-	-	-	0.34	0.91	2.42	2.73	1.41	1.06	1.32	1.15	1.06	0.75	0.36	0.29	0.14	0.07	0.03	0.01	-	-	-	14.05
2.00 - 2.25	-	-	-	0.07	0.21	0.62	1.41	1.21	0.81	0.71	0.55	0.57	0.43	0.21	0.14	0.08	0.02	0.01	-	-	-	-	7.05
2.25 - 2.50	-	-	-	-	0.07	0.14	0.49	0.64	0.56	0.37	0.27	0.30	0.18	0.09	0.06	0.02	0.01	-	-	-	-	-	3.20
2.50 - 2.75	-	-	-	-	0.01	0.03	0.14	0.23	0.29	0.22	0.22	0.18	0.12	0.06	0.04	0.01	-	-	-	-	-	-	1.55
2.75 - 3.00	-	-	-	-	-	-	0.02	0.07	0.08	0.09	0.07	0.08	0.05	0.03	0.01	0.01	-	-	-	-	-	-	0.51
3.00 - 3.25	-	-	-	-	-	-	-	0.01	0.03	0.04	0.05	0.03	0.02	0.01	0.01	-	-	-	-	-	-	-	0.20
3.25 - 3.50	-	-	-	-	-	-	-	-	0.01	0.02	0.01	0.01	0.01	0.01	0.01	-	-	-	-	-	-	-	0.08
3.50 - 3.75	-	-	-	-	-	-	-	-	-	0.01	-	-	0.01	-	-	-	-	-	-	-	-	-	0.02
3.75 - 4.00	-	-	-	-	-	-	-	-	-	-	-	0.01	0.01	-	-	-	-	-	-	-	-	-	0.02
Sum	-	0.27	2.05	7.28	13.80	13.19	9.64	7.64	9.07	9.92	8.43	7.96	5.20	2.38	1.72	0.76	0.33	0.20	0.09	0.02	-	-	99.95

Table A.5: The statistics for the Equitorial Quinea sea

H_S [m]	Tp [s]															
	3 - 4	4 - 5	5 - 6	6 - 7	7 - 8	8 - 9	9 - 10	10 - 11	11 - 12	12 - 13	13 - 14	14 - 15	15 - 16	16 - 17	17 - 18	18 - 19	Sum
0.00 - 0.20	-	-	-	-	-	-	-	-	-	-	-	-	-	-	-	-	-
0.20 - 0.40	-	-	-	0.10	0.10	0.20	0.30	0.30	0.10	0.10	-	-	-	-	-	-	1.20
0.40 - 0.60	-	0.10	0.70	1.10	1.00	0.90	1.30	2.20	1.30	0.30	0.10	-	-	-	-	-	9.00
0.60 - 0.80	-	0.60	3.70	4.60	3.90	2.90	2.50	3.30	3.00	0.90	0.20	-	-	-	-	-	25.60
0.80 - 1.00	-	0.60	4.00	5.70	4.80	3.20	2.20	2.20	2.40	1.20	0.30	-	-	-	-	-	26.60
1.00 - 1.20	-	0.30	2.30	3.90	3.50	2.50	1.60	1.50	1.50	1.10	0.30	0.10	-	-	-	-	18.60
1.20 - 1.40	-	0.10	1.00	2.10	2.20	1.60	1.10	0.70	0.60	0.50	0.30	-	-	-	-	-	10.20
1.40 - 1.60	-	-	0.40	0.90	1.00	0.90	0.60	0.50	0.40	0.30	0.10	-	-	-	-	-	5.10
1.60 - 1.80	-	-	0.10	0.30	0.40	0.40	0.30	0.20	0.20	0.10	0.10	-	-	-	-	-	2.10
1.80 - 2.00	-	-	0.10	0.20	0.20	0.10	0.10	0.10	0.10	0.10	-	-	-	-	-	-	1.00
2.00 - 2.20	-	-	-	0.10	-	-	-	-	-	-	-	-	-	-	-	-	0.10
2.20 - 2.40	-	-	-	-	-	-	-	-	-	-	-	-	-	-	-	-	-
2.40 - 2.60	-	-	-	-	-	-	-	-	-	-	-	-	-	-	-	-	-
2.60 - 2.80	-	-	-	-	-	-	-	-	-	-	-	-	-	-	-	-	-
2.80 - 3.00	-	-	-	-	-	-	-	-	-	-	-	-	-	-	-	-	-
3.00 - 3.20	-	-	-	-	-	-	-	-	-	-	-	-	-	-	-	-	-
3.20 - 3.40	-	-	-	-	-	-	-	-	-	-	-	-	-	-	-	-	-
Sum	-	1.70	12.30	19.00	17.10	12.70	1-	11.00	9.60	4.60	1.40	0.10	-	-	-	-	99.50

Table A.6: The statistics for the Ghana sea

H_S [m]	Tp [s]																						
	3 - 4	4 - 5	5 - 6	6 - 7	7 - 8	8 - 9	9 - 10	10 - 11	11 - 12	12 - 13	13 - 14	14 - 15	15 - 16	16 - 17	17 - 18	18 - 19	19 - 20	20 - 21	21 - 22	22 - 23	23 - 24	24 - 25	Sum
0.00 - 0.25	-	-	-	-	-	-	-	-	-	-	-	-	-	-	-	-	-	-	-	-	-	-	-
0.25 - 0.50	-	-	-	-	0.05	0.04	0.01	0.02	0.03	0.02	0.02	0.03	0.03	0.01	0.01	-	-	-	-	-	-	-	0.27
0.50 - 0.75	0.10	0.02	0.16	0.33	0.40	0.36	0.20	0.23	0.22	0.21	0.22	0.12	0.13	0.04	0.05	0.01	-	-	-	-	-	-	2.80
0.75 - 1.00	-	0.17	1.40	2.40	2.50	1.30	0.73	0.88	1.20	1.00	0.75	0.68	0.47	0.18	0.18	0.05	0.04	0.02	-	-	-	-	13.95
1.00 - 1.25	-	0.09	1.10	4.90	8.10	3.70	2.20	1.70	2.10	2.30	2.00	2.20	1.30	0.40	0.44	0.17	0.09	0.02	-	-	-	-	32.81
1.25 - 1.50	-	-	0.11	1.00	5.30	6.10	3.40	2.00	2.00	2.10	2.10	1.90	1.20	0.51	0.59	0.27	0.17	0.03	0.02	-	-	-	28.80
1.50 - 1.75	-	-	-	0.09	0.69	2.90	2.30	1.50	1.20	0.98	1.00	1.20	0.84	0.36	0.37	0.16	0.07	0.01	-	-	-	-	13.67
1.75 - 2.00	-	-	-	0.02	0.04	0.56	1.10	0.84	0.53	0.42	0.27	0.35	0.30	0.13	0.14	0.05	0.03	0.01	-	-	-	-	4.79
2.00 - 2.25	-	-	-	-	-	0.06	0.38	0.38	0.28	0.15	0.11	0.13	0.08	0.04	0.05	0.02	-	-	-	-	-	-	1.68
2.25 - 2.50	-	-	-	-	-	-	0.08	0.05	0.10	0.07	0.03	0.04	0.05	0.04	0.02	-	-	-	-	-	-	-	0.48
2.50 - 2.75	-	-	-	-	-	-	-	-	0.05	0.03	0.02	0.01	0.01	-	-	-	-	-	-	-	-	-	0.12
2.75 - 3.00	-	-	-	-	-	-	-	-	-	0.02	0.03	-	0.01	-	-	-	-	-	-	-	-	-	0.06
3.00 - 3.25	-	-	-	-	-	-	-	-	-	-	-	-	0.01	-	-	-	-	-	-	-	-	-	0.01
3.25 - 3.50	-	-	-	-	-	-	-	-	-	-	-	-	-	-	-	-	-	-	-	-	-	-	-
3.50 - 3.75	-	-	-	-	-	-	-	-	-	-	-	-	-	-	-	-	-	-	-	-	-	-	-
3.75 - 4.00	-	-	-	-	-	-	-	-	-	-	-	-	-	-	-	-	-	-	-	-	-	-	-
Sum	0.10	0.28	2.77	8.74	17.08	15.02	10.40	7.60	7.71	7.30	6.55	6.66	4.43	1.71	1.85	0.73	0.40	0.09	0.02	-	-	-	99.44

B

BASIC CALCULATIONS

This chapter some of the foundation values of the scenario, these values are not included in the main reports because they are derived with straightforward mathematical methods. These foundation values contain the general characteristics of the system for the input of the model. Due to a lack of detailed information about the `Liwan 3-1` topsides and `HYSY229` barge, some calculations are simplifications to approximate the value. This section gives insight in the equations and simplifications used to approximate the `Liwan 3-1` floatover installation scenario, the estimations from this section are used as the base case in this research.

B.1. BALLAST CONFIGURATION

The ballast configuration of the `Liwan 3-1` installation is unknown. The ballasting conditions during installation should results in a zero trim condition. It also determines the draft of the vessel. Therefore, a simplified ballast configuration is assumed which is bound to these two conditions. From this simplifications the dynamic properties can also be assessed.

In the simplified configuration the barge is assumed to contain two large ballast tanks: one in the aft and in at the bow of the vessel. The ballast tanks are maximised and contain the maximum surface area available in the barge. The barge is considered as an empty hull and no compensation for equipment volume is applied. The ballast configuration is determined based on the required draft of the barge and moment required to compensate the topsides momentum. The simplification to use two large ballast tanks is based on the desire of minimising the vertical Center Of Gravity (COG) of the barge. This is achieved by distributing the ballast close to the keel of the barge. In reality ballast will be distributed such that ballast tanks are full to minimise the free surface effects of the seawater, these effects are not taken into account in this research.

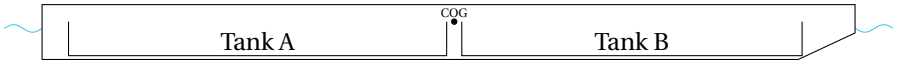

Figure B.1: The simplified ballast assumption, the barge contain two large tanks over the full width of the barge, due to the T-shape of the barge the stern tank has a much larger volume. The bow and stern tank are separated with the COG of the barge.

The ballasting conditions are assessed for three drafts. These three drafts are called the principle drafts and are used throughout this research. The principle drafts are:

- 8.2 meters, the docking draft
- 10.2 meters, the average mating draft
- 12.1 meters, the undocking draft

These drafts correspond with a displaced volume of the barge. The ballast weight is found by subtracting all masses from the displaced volume times the density of seawater, this leads Equation (B.1).

$$m_{ballast} = (S_{xy}\, T_{barge} - V_{bow}) \cdot \rho_{sw} - m_{barge} - m_{topsides} \tag{B.1}$$

Where S_{xy} equals the area of the barge in the XY-plane, T_{barge} the draft of the barge, ρ_{sw} the density of seawater. V_{bow} is the overshoot at the bow of the barge due to the vertical extrusion of the surface area.

The barge and topsides weight are known and the surface area is computed from the barge particulars. The corresponding ballast weight for the different drafts is calculated. To give an indication of the ballasting conditions the minimum height of the ballast, when evenly distributed over the full surface area, is provided:

Draft [m]	Ballast weight [Te]	Ballast minimum height [m]
8.2	28,700	2.50
10.2	52,300	4.55
12.1	101,000	8.78

The amount of ballast required for the 12.1 meter draft condition is derived without the topsides mass. This is the undocking draft and the topsides load is transferred to the substructure. This draft is taken into account for the slamming effects on the barge.

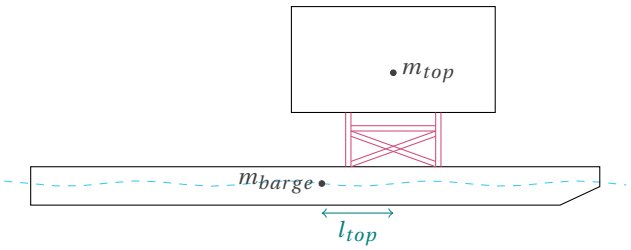

Figure B.2: The momentum due to the topsides eccentricity

During the first two draft conditions the ballast must compensate the eccentricity of the topsides as sketched in Figure B.2. The dimensions of two simplified ballast rooms are set as: aft to the COG, becomes 100 meters long and 61 meters wide. The other room is from the COG to the bow, which is 90 meters long and 38 meters wide. The triangular transition piece is not considered to contain ballast due to the relatively small volume. By solving the equilibrium equation for this scenario the ballast conditions are found and visualised in Figure B.3. The equations used are:

$$m_{ballast} = m_A + m_B \tag{B.2}$$

$$m_A \cdot l_A = m_B \cdot l_B + m_{top} \cdot l_{top} \tag{B.3}$$

Where l indicates the arm of the mass to the COG. This creates two equations with two unknowns, the height of the aft and bow ballast, which is easily solved. The solution to the ballast configuration is given in Figure B.3, where the ballast height are visualized on the side view of the barge for the two draft with overturning moment compensation.

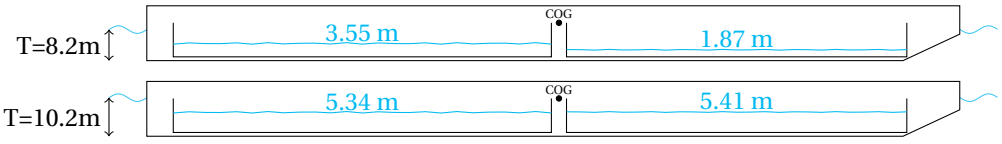

Figure B.3: Simplified ballast configuration, the width of the left ballast tank is 61 meters and for the right 38 meters. The volume, and thus mass, of the left tank is higher in the 10.2 meters draft scenario. Therefore, the ballast still compensation for the topsides momentum.

This approximation is considered sufficient for this thesis. It is assumed that the change in the inertia due to a more detailed ballast configuration is not significant in relation to the amount of time spend on more detailed calculations.

B.2. MASS MOMENT OF INERTIA

In this thesis the mass moment of inertia is often used and this chapter elaborates the origin of the different values used throughout the thesis. The mass moment of inertia determines the angular mass of a body and is used in the rotational equations of motion. In general the mass moment of inertia is the second moment of mass which is defined as:

$$I = \int_m r^2 dm \tag{B.4}$$

The most relevant derivation of this equation is for cuboid shapes. In inertia calculations the parallel axis theorem of Steiner is important for the translation of an inertia to rotate around a different axis than the COG. The derivations of inertia for a cuboid given in Equations (B.5) to (B.7) supported by Figure B.4. And the parallel axis theorem is shown in Equation (B.8), this will be referred to as the Steiner term throughout this section.

$$I_{xx} = \frac{m}{12} \cdot \left(w^2 + h^2\right) \tag{B.5}$$

$$I_{yy} = \frac{m}{12} \cdot \left(h^2 + l^2\right) \tag{B.6}$$

$$I_{zz} = \frac{m}{12} \cdot \left(w^2 + l^2\right) \tag{B.7}$$

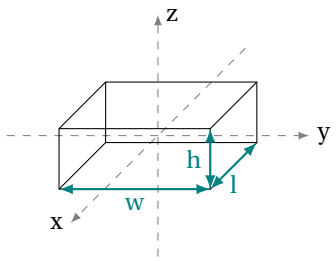

Figure B.4: Cuboid shaped definitions to support the inertia derivation

$$I'_{xx} = I_{xx} + m \cdot d^2 \tag{B.8}$$

In these equations $_{xx}$ indicate rotation around the x-axis. The mass is the total mass of the cube and the formula is valid when this mass is distributed homogeneously over the volume.

For the AQWA calculations three masses are combined into the model. These masses consist of the HYSY229 barge, the Liwan 3-1 topsides and the ballast. Using the theory as presented in this paragraph the inertia for these three elements and the resulting combined inertia's are approximated in the next sections.

B.2.1. HYSY229

For the barge the inertias are found in Yuan et al. (2014a). In this paper a table with the properties for the barge during the installation of Liwan 3-1 topsides is provided. These values represent for the HYSY229 barge with the DSF, fendering arrangement and all other equipment on the barge. It does not include the ballast and topsides loads. The inertial values are given in Table B.1.

Table B.1: Inertial data for the HYSY229 during the Liwan 3-1 installation (Yuan et al., 2014a)

	Weight	XCG	YCG	KG	I_{xx}	I_{yy}	I_{zz}
HYSY229	39,350 [Te]	109.01 [m]	0.02 [m]	9.98 [m]	$1.291 \cdot 10^7$ [Te·m^2]	$1.335 \cdot 10^8$ [Te·m^2]	$1.438 \cdot 10^8$ [Te·m^2]

This information is convenient because estimations for the barge inertia would have led to large uncertainties in the modelled barge. Especially because there is no information available about the DSF system and the fendering arrangement.

Table B.2: Table with the given and the used dimensions of the Liwan 3-1 topsides

Dimension	R[m]	Model[m]
Length	77	77
Width	110	110
Height	95	40

B.2.2. LIWAN 3-1

To accurately determine the inertia of the topsides the mass distribution of the different modules of the topsides have to be known. This information is not available and therefore an approximation is made. This approximation is based upon the maximum dimensions, literature findings and an aerial view of the platform(Figure B.5). The approximation is done by considering the major dimensions of the topsides and estimating the COG.

The major dimensions are considered as: the minimum dimensions which captures the majority of the mass. In other words the box which contains the highest possible density. The aim of the major dimensions is to estimate a scenario where the topsides approach a homogeneous cuboid, than the Equations (B.5) to (B.7) can be used. However, the topsides are not homogeneous. Thus the approximation is enhanced by assessing the location of the COG of the topsides. After which the equations of the cuboid are rewritten into equations for a shifted COG. This approach is considered to generate a reasonable value.

The maximum dimensions of the topsides are presented in Table B.2, when combining the aerial view with overview sketched from Yuan et al. (2014a,b) it is concluded that the maximum length and width found in the literature are representable for the majority of the mass. This is due to the fact that the width extension due to the boom on the side of the platform is not taken into account in this length.

The maximum height does take the boom into account and should thus be compensated to a value which is more representable for the majority of the mass. This height is considered to be 40 meters which corresponds to a couple of meters below the helicopter deck in Figure B.5. This height is chosen because of the large empty areas on the higher levels and is slightly compensated upwards due to the presence of the crane and the processing equipment on the top deck.

For the location estimation of the COG the the thought is that a COG in the middle of the horizontal plane is favourable for the loading on the substructure legs and is a considerable advantage during transport. The assumption is made that this thought is used in the design of the topsides and thus the COG is set in the middle of the horizontal plane. This assumption is supported, more or less, with the aerial view when considering that the processing unit on the left side is counter ballast of the living quarters on the right side and also the crane is compensated over the length by the processing equipment, in other words the aerial view does not oppose this assumption.

Figure B.5: The aerial view of the as installed Liwan 3-1 topsides. The only information available for the topsides mass distribution approximation

The vertical COG is determined with the theory that a lower COG is favourable for the stability of the topsides during transport. This implies that the majority of the heavy elements are located on the lower decks, the structural integrity of the topsides is also aided with heavy elements low and above the topsides legs. However, not all heavy elements can be installed on the lower levels, an example is the crane, and thus the COG has to be assumed somewhere in between. For this thesis the assumption is made that the vertical COG for the topsides is located at $\frac{1}{3}$ of the topsides used height.

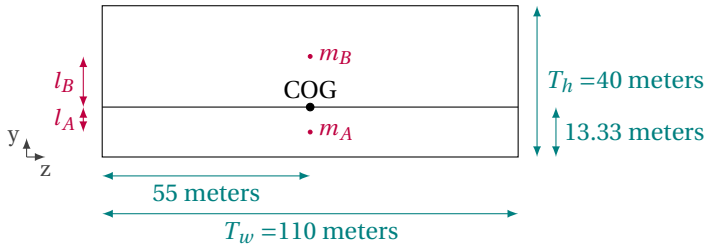

Figure B.6: The split made to asses the topsides inertia, this assumption enables the topsides mass to distributed such that the COG can be shifted from the center of the cuboid.

To calculate the inertia the mass distribution has to be determined. The COG is not in the center of the vertical plane. Therefore the mass is not distributed homogeneous over the vertical plane. This assumption is made for the horizontal plane since the COG is centred in this plane. For the vertical plane the topsides representation is split into two cuboid shapes, the split is made at the vertical height of the COG, this is shown in Figure B.6. Now the assumption is made that these two cuboids contain a homogeneous distribution of mass. Using this assumption the topsides mass can be split over the two cuboids using a balance of momentum, since the resulting moment around the split should be zero. In formulae, using the $\frac{1}{3}$ split, this becomes:

$$m_{topsides} = m_A + m_B \tag{B.9}$$

$$m_A \cdot l_A = m_B \cdot l_B \tag{B.10}$$

$$m_B = 2m_A = \frac{1}{3} \cdot m_{topsides} \tag{B.11}$$

Now the mass distribution and the dimensions of the topsides cuboid representation are known and thus the derivation of the inertia can be done be combining the formula for the cuboid inertia and the correct Steiner translation. The COG is centred in the horizontal plane and therefore for the I_{zz} calculations the equation for a regular cuboid can be used. The approximation of the inertia is found as:

$$I_{xx} = \frac{m_a}{12} \cdot \left(T_w^2 + \left(\frac{T_h}{3}\right)^2\right) + m_a \cdot l_a^2 + \frac{m_b}{12} \cdot \left(T_w^2 + \left(\frac{2T_h}{3}\right)^2\right) + m_b \cdot l_b^2 \tag{B.12}$$

$$I_{yy} = \frac{m_a}{12} \cdot \left(T_l^2 + \left(\frac{T_h}{3}\right)^2\right) + m_a \cdot l_a^2 + \frac{m_b}{12} \cdot \left(T_l^2 + \left(\frac{2T_h}{3}\right)^2\right) + m_b \cdot l_b^2 \tag{B.13}$$

$$I_{zz} = \frac{m_{topsides}}{12} \cdot \left(T_l^2 + T_w^2\right) \tag{B.14}$$

When implementing the relation of Equation (B.11) into the equations than the topsides inertia becomes:

$$I_{xx} = \frac{m\left(8\,{T_h}^2 + 9\,{T_w}^2\right)}{108} \tag{B.15}$$

$$I_{yy} = \frac{m\left(8\,{T_h}^2 + 9\,{T_l}^2\right)}{108} \tag{B.16}$$

Note that $\frac{9}{108} = \frac{1}{12}$ and thus the inertia term only changes for the height parameter. These equations are used to determine the inertia for the topsides combined with the I_{zz} from Equation (B.14).

The approximations made in this section are based on a very global model which is built completely on assumptions. In reality the inertia might be significantly different. However, the order of magnitude is correct. It is not within the scope of this thesis to derive a more detailed value for these inertias. An indication of the sensitivity of the inertias will be done the look into the effects of the assumptions in this chapter.

B.2.3. BALLAST CONFIGURATION

For the inertia of the ballast configuration the scenarios calculated in the Appendix B.1 are used to approximate the inertial values. Since the ballast configuration is simplified assumptions are made to assess the inertia of the simplified system.

The docking draft scenario, 8.2 meters, is sketched in Figure B.7. This illustration shows the principle assumptions used to calculate the inertia. The most important assumption is that the ballast tanks are cuboid shaped and no free surface effects are present, in other words the ballast is assumed as a solid cuboid with the density of seawater. This makes the Equations (B.5) to (B.8) valid for the ballast approximation. The Steiner translation shall be used to relate the ballast to the combined center of mass of the system. The equations for the ballast inertia become, supported with Figure B.7:

$$I_{bal_{xx}} = \overbrace{\frac{m_a}{12}\left(A^2_{\text{width}} + A^2_{\text{height}}\right) + \frac{m_b}{12}\left(B^2_{\text{width}} + B^2_{\text{height}}\right)}^{\text{Inertia of the ballast cuboids}} + \overbrace{m_a \cdot d^2_{za} + m_b \cdot d^2_{zb}}^{\text{Steiner translation to combined COG}} \tag{B.17}$$

$$I_{bal_{yy}} = \frac{m_a}{12}\left(A^2_{\text{length}} + A^2_{\text{height}}\right) + \frac{m_b}{12}\left(B^2_{\text{length}} + B^2_{\text{height}}\right) + m_a \cdot \left(d^2_{xa} + d^2_{za}\right) + m_b \cdot \left(d^2_{xb} + d^2_{zb}\right) \tag{B.18}$$

$$I_{bal_{zz}} = \frac{m_a}{12}\left(A^2_{\text{width}} + A^2_{\text{length}}\right) + \frac{m_b}{12}\left(B^2_{\text{width}} + B^2_{\text{length}}\right) + m_a \cdot d^2_{xa} + m_b \cdot d^2_{xb} \tag{B.19}$$

In reality the ballasting inertia contribution is very complex due to the free surface effects of the tanks these effects are not necessarily negative for the motions of the vessel. There is no detailed information about the lay out of the tanks and therefore it is not realistic to take free surface effects into account. Again these values can differ from the real scenario. However, these values are considered as a reasonable approximation which is in the same order of magnitude as the real setting.

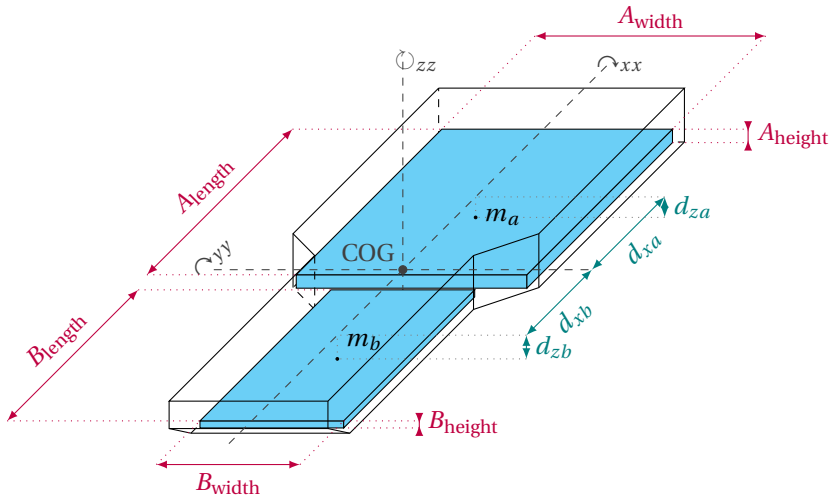

Figure B.7: The 3D view which is used to calculate the ballast inertias

B.2.4. COMBINED INERTIA

For the AQWA calculation the inertia is needed for the combined system of the three major masses. For this calculation the combined COG is required to enable all inertia's to be translated to the new axis. The definition of for a combined center of mass can be found with the following equation:

$$\sum_{i=1}^{n} m_i(\mathbf{r}_i - \mathbf{R}) = 0 \tag{B.20}$$

Where $\mathbf{R}$ is the location of the center of mass and $\mathbf{r}_i$ is the location of mass m_i. This equation can be written for this system as:

$$x_{com} = \frac{\sum_{i=1}^{3} m_i x_i}{\sum_{i=n}^{3} m_i} \tag{B.21}$$

The same equation can be derived for the y and z direction. In which $i = 1:3$ correspond with the barge ballast and topsides bodies and x_com represent the combined bodies. These calculations lead to a combined COG as presented in Table B.3. In this table the coordinates are given in the barges local axis system which is defined in the last column of the table.

In Table B.3 it can be seen that the compensation of the topsides overturning moment also leads to correction in the x coordinate which causes the combined center of mass to be positioned precisely above the COG of the barge. This agrees with the expectations of the combined location.

Table B.3: Locations of COG for the different masses

Draft 8.2 meters

	Barge	Topsides	Ballast	Combined	Axis definition
x [m]	109.01	140.00	80.67	109.01	zero at aft positive towards bow
y [m]	0.02	0.00	0.00	0.01	zero at centerline positive towards portside
z [m]	9.98	38.58	2.58	15.70	zero at keel positive upwards
m [Te]	39,350	26,300	28,770	94,400	

Draft 10.2 meters

	Barge	Topsides	Ballast	Combined	Axis definition
x [m]	109.01	140.00	93.42	109.00	zero at aft positive towards bow
y [m]	0.02	0.00	0.00	0.01	zero at centerline positive towards portside
z [m]	9.98	38.58	3.68	13.56	zero at keel positive upwards
m [Te]	39,350	26,300	52,350	118,000	

Draft 12.1 meters

	Barge	Topsides	Ballast	Combined	Axis definition
x [m]	109.01	0.00	108.99	109.00	zero at aft positive towards bow
y [m]	0.02	0.00	0.00	0.01	zero at centerline positive towards portside
z [m]	9.98	0.00	6.81	7.70	zero at keel positive upwards
m [Te]	39,350	0.00	101,051	140,400	

Using this combined COG the combined inertia can be obtained by deriving the Steiner translation terms for the translation of the local COG to the combined COG. This becomes:

$$I_{xx} = \sum_{i=1}^{3} I_{xx_i} + m_i \cdot \left(|y_i - y_{\text{com}}|^2 + |z_i - z_{\text{com}}|^2\right) \tag{B.22}$$

$$I_{yy} = \sum_{i=1}^{3} I_{yy_i} + m_i \cdot \left(|x_i - x_{\text{com}}|^2 + |z_i - z_{\text{com}}|^2\right) \tag{B.23}$$

$$I_{zz} = \sum_{i=1}^{3} I_{zz_i} + m_i \cdot \left(|x_i - x_{\text{com}}|^2 + |y_i - y_{\text{com}}|^2\right) \tag{B.24}$$

This equation implies that the inertias are built using six terms. For each body there is an own inertia term and a Steiner translation term. The own inertia terms are compiled based on the formulas given in the previous subsections and the Steiner terms are obtained through the COG numbers from Table B.3. To present insight of the order of magnitude of the different elements all six terms are presented in Table B.4, the final value for the inertia is found in the last column of this table.

The draft of the barge in the model is 10.2 meters, this is the average mating draft of the barge. During the average mating draft the highest possibility of large velocity impacts is expected. The reasoning for this is elaborated in Chapter 3.

Table B.4: The six different elements of the inertia calculations. These six combine in the total inertia of the system.

Draft 8.2[m]

	Barge		Ballast		Topsides		Combined		Total
	Inertia	Steiner	Inertia	Steiner	Inertia	Steiner	Inertia	Steiner	
I_{xx} [Te · m^2]	$1.29{\cdot}10^7$	$1.28{\cdot}10^6$	$7.70{\cdot}10^6$	$4.95{\cdot}10^6$	$2.96{\cdot}10^7$	$2.53{\cdot}10^7$	$5.02{\cdot}10^7$	$3.15{\cdot}10^7$	$8.17{\cdot}10^7$
I_{yy} [Te · m^2]	$1.34{\cdot}10^8$	$1.28{\cdot}10^6$	$2.29{\cdot}10^7$	$7.37{\cdot}10^7$	$1.61{\cdot}10^7$	$3.90{\cdot}10^7$	$1.73{\cdot}10^8$	$1.14{\cdot}10^8$	$2.87{\cdot}10^8$
I_{zz} [Te · m^2]	$1.44{\cdot}10^8$	$5.74{\cdot}10^0$	$3.06{\cdot}10^7$	$6.88{\cdot}10^7$	$3.95{\cdot}10^7$	$2.53{\cdot}10^7$	$2.14{\cdot}10^8$	$9.40{\cdot}10^7$	$3.08{\cdot}10^8$

Draft 10.2[m]

	Barge		Ballast		Topsides		Combined		Total
	Inertia	Steiner	Inertia	Steiner	Inertia	Steiner	Inertia	Steiner	
I_{xx} [Te · m^2]	$1.29{\cdot}10^7$	$5.05{\cdot}10^5$	$1.28{\cdot}10^7$	$5.11{\cdot}10^6$	$2.96{\cdot}10^7$	$2.53{\cdot}10^7$	$5.53{\cdot}10^7$	$3.09{\cdot}10^7$	$8.62{\cdot}10^7$
I_{yy} [Te · m^2]	$1.34{\cdot}10^8$	$5.05{\cdot}10^5$	$4.08{\cdot}10^7$	$1.27{\cdot}10^8$	$1.61{\cdot}10^7$	$4.17{\cdot}10^7$	$1.90{\cdot}10^8$	$1.69{\cdot}10^8$	$3.60{\cdot}10^8$
I_{zz} [Te · m^2]	$1.44{\cdot}10^8$	$9.34{\cdot}10^0$	$5.33{\cdot}10^7$	$1.22{\cdot}10^8$	$3.95{\cdot}10^7$	$2.53{\cdot}10^7$	$2.37{\cdot}10^8$	$1.47{\cdot}10^8$	$3.84{\cdot}10^8$

Draft 12.1[m]

	Barge		Ballast		Topsides		Combined		Total
	Inertia	Steiner	Inertia	Steiner	Inertia	Steiner	Inertia	Steiner	
I_{xx} [Te · m^2]	$1.29{\cdot}10^7$	$2.05{\cdot}10^5$	$2.25{\cdot}10^7$	$4.35{\cdot}10^5$	$0.00{\cdot}10^0$	$0.00{\cdot}10^0$	$3.54{\cdot}10^7$	$6.41{\cdot}10^5$	$3.61{\cdot}10^7$
I_{yy} [Te · m^2]	$1.34{\cdot}10^8$	$2.05{\cdot}10^5$	$7.71{\cdot}10^7$	$2.28{\cdot}10^8$	$0.00{\cdot}10^0$	$0.00{\cdot}10^0$	$2.11{\cdot}10^8$	$2.28{\cdot}10^8$	$4.39{\cdot}10^8$
I_{zz} [Te · m^2]	$1.44{\cdot}10^8$	$1.38{\cdot}10^1$	$9.71{\cdot}10^7$	$2.27{\cdot}10^8$	$0.00{\cdot}10^0$	$0.00{\cdot}10^0$	$2.41{\cdot}10^8$	$2.27{\cdot}10^8$	$4.68{\cdot}10^8$

B.3. STABILITY

The floatover operation occurs with the topsides high above the deck of the barge. Therefore, it is important to know the stability parameters of the barge. The stability is checked by using the methodology from offshore hydromechanics(Journeé and Massie, 2001).

During the operation the must stay stable and thus the tolerance of the stability criterion is assessed. The barge is considered stable if the barge tends to return to the equilibrium position after a disturbance has occurred. In other words, the resulting forces acting on the barge after a disturbance act towards the equilibrium position. Whenever these forces cause the barge to move to an opposite direction than the barge is unstable. The disturbance represent roll motions since these are the critical motions for the stability calculations.

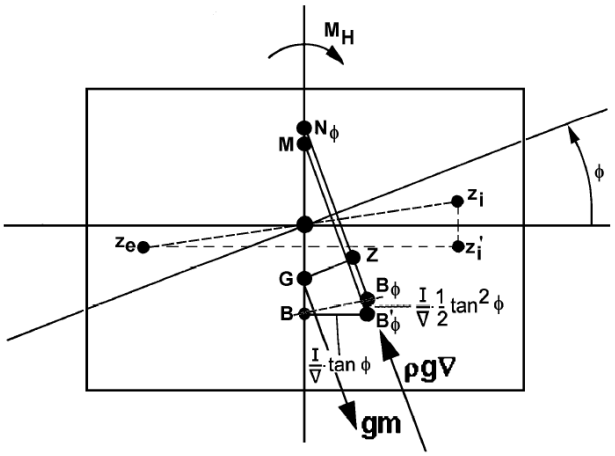

Figure B.8: Rectangular barge stability, from Journeé and Massie (2001).

Stability for heel/roll conditions is reached when the restoring moment due to an offset is larger than the

external moment. For the assessment of the stability criterion the external moment is zero. This means that when the restoring moment is positive the system is stable. When a floating structure is under an angle the restoring moment is given as:

$$M_S = \rho g \nabla \cdot \overline{GZ} \tag{B.25}$$

Where $\rho g \nabla$ represent the buoyancy force and $\overline{GZ}$ is the arm of the buoyancy force as illustrated in Figure B.8. Which can be rewritten to:

$$M_S = \rho g \nabla \cdot \overline{GN_\phi} \cdot \sin\phi \tag{B.26}$$

And $\overline{GN_\phi}$ can be assessed with the kinematic relation from Figure B.8 with is given as:

$$\overline{GN_\phi} = \overline{KB} + \overline{BN_\phi} - \overline{KG} \tag{B.27}$$

In which $\overline{KB}$ is dependant of the hull shape and $\overline{KG}$ is calculated with the mass distribution of the barge. The value for N_ϕ, which is known as the metacenter of the barge, is assessed with the Scribanti formula, which is valid for small angles:

$$\overline{BN_\phi} = \frac{I_T}{\nabla} \cdot \left(1 + \frac{1}{2}\tan^2\phi\right) \tag{B.28}$$

Using this method the stability of the barge can be checked for small angles, note that the initial stability of the barge is found when assessing the formulae with $\phi = 0$. When assessing the initial metacentric height the following values are obtained. For the zero angle case the used formulae are changed to:

$$\overline{GM} = \overline{KB} + \overline{BM} - \overline{KG} \tag{B.29}$$

$$\overline{GM} = \overline{KB} + \frac{I_T}{\nabla} - \overline{KG} \tag{B.30}$$

The initial metacentric height is given with $\overline{GM}$. For these calculations the elevated center of gravity due to the height height of the topsides is an important parameter. For a topsides with 15 meters spacing between the barge deck and the topsides floor the values for the metacentric heights, at the different drafts, become:

Draft [m]	8.2	10.2	12.2
$\overline{GM}$ [m]	21.8	18.3	20.8

The barge is thus stable for this loading conditions, note that the last draft contains no topsides and thus the barge is more stable. The barge will become unstable when the vertical center of gravity becomes higher than 37.5 meters from the keel orthogonal upwards. This corresponds to a topsides height of more than 100 meters from the deck of the barge. This counts for the stable equilibrium when an external moment is present the barge will become unstable much sooner than the above values.

These calculations are based on non-eccentric topsides loads. The effect of eccentricity of the topsides is important to assess. The heel due to eccentricity is based on Equation (B.31). Which is the derivation of the righting moment with the overturning moment due to mass p and eccentricity c.

$$\phi = \arccos\left(\frac{\rho\nabla \cdot \overline{GN_\phi} \cdot \sin\phi}{p \cdot c}\right) \tag{B.31}$$

For small heel angles and wall sided structures the formula is simplified to:

$$\phi = \arctan\left(\frac{p \cdot c}{\rho\nabla \cdot \overline{GM}}\right) \tag{B.32}$$

When assessing the heel for a one meter eccentricity of the topsides the heel angles become:

Draft [m]	8.2	10.2	12.2
ϕ [deg]	0.84	0.80	n/a

C

ADDITIONAL RESULTS

C.1. MODEL RESULTS

The model uses a lot of input values. Therefore, the solutions shown in the result chapter are not the only results that are derived with the model. This section lists results of the different settings.

The information presented in this section is summarised as:

	Type	Pressure [bar]	Wave direction [°]
Table C.1	Most probable maximum amplitudes	n.a.	160
Figure C.1	Workability surf, variable k_{cyl} and $\zeta_{\%}$	300	90
Figure C.2	Workability surf, variable k_{cyl} and $\zeta_{\%}$	300	135
Figure C.3	Workability surf, variable k_{cyl} and $\zeta_{\%}$	300	150
Figure C.4	Workability surf, variable k_{cyl} and $\zeta_{\%}$	300	160
Figure C.5	Workability surf, variable k_{cyl} and $\zeta_{\%}$	200	90
Figure C.6	Workability surf, variable k_{cyl} and $\zeta_{\%}$	200	135
Figure C.7	Workability surf, variable k_{cyl} and $\zeta_{\%}$	200	150
Figure C.8	Workability surf, variable k_{cyl} and $\zeta_{\%}$	200	160
Figure C.9	Barge RAO's with HCS settings	n.a.	160
Figure C.10	Topsides RAO's with HCS settings	n.a.	160
Figure C.11	Installation velocity with the HCS settings	n.a.	160
Figure C.12	3 hour most probable stroke of the cylinders	n.a.	160

Table C.1 contains the 3 hour most probable amplitude maximum of the degrees of freedom for three different wave settings. This table is used to quantify the RAO data in order to see the effects of the differences in RAO amplitudes. The findings are presented in Chapter 6.

Figures C.1 to C.8 are equal to the plots of Figures 6.6 and 6.7. In these enlarged version the axis are better interpretable.

Figures C.9 to C.11 are based on the settings of the dimensioned heave compensation system. Thus, the k_{cyl} and $\zeta_{\%}$ are 0.57 MN/m and 20% (1.1 MN·s/m) respectively. This coincides with the values used in Chapter 7.

Table C.1: The three hour most probable maximum amplitude of the 6 degrees of freedom of the systems with the same characteristics as Figures 6.1 and 6.2. This gives insight on the effects of the RAO's on three different swell spectra. Results are based on 10.2 meters draft and display translations and rotation around the center of gravity. The used wave direction is 160 degrees.

Three hour most probable maximum amplitudes

For T_p= 10s, H_s= 1m							
	DOF	Unit	Fixed	10 MN/m	1 MN/m	100 kN/m	10 kN/m
Barge	Heave	[m]	0.11	0.10	0.11	0.12	0.13
	Roll	[deg]	0.20	0.11	0.29	0.33	0.33
	Pitch	[deg]	0.25	0.24	0.22	0.23	0.24
Topsides	Heave	[m]	0.23	0.29	0.17	0.02	0.01
	Roll	[deg]	0.16	0.19	0.06	0.01	0.00
	Pitch	[deg]	0.24	0.46	0.07	0.01	0.00
For T_p= 14s, H_s= 1m							
	DOF	Unit	Fixed	10 MN/m	1 MN/m	100 kN/m	10 kN/m
Barge	Heave	[m]	0.25	0.25	0.20	0.21	0.21
	Roll	[deg]	1.08	0.71	0.66	0.88	0.91
	Pitch	[deg]	0.57	0.58	0.50	0.55	0.55
Topsides	Heave	[m]	0.46	0.54	0.89	0.05	0.01
	Roll	[deg]	1.08	1.11	0.21	0.03	0.01
	Pitch	[deg]	0.57	0.82	0.34	0.03	0.01
For T_p= 18s, H_s= 1m							
	DOF	Unit	Fixed	10 MN/m	1 MN/m	100 kN/m	10 kN/m
Barge	Heave	[m]	0.43	0.43	0.44	0.40	0.40
	Roll	[deg]	0.85	0.87	0.45	0.57	0.58
	Pitch	[deg]	0.62	0.62	0.57	0.60	0.60
Topsides	Heave	[m]	0.60	0.66	1.78	0.11	0.02
	Roll	[deg]	0.80	1.28	0.24	0.02	0.01
	Pitch	[deg]	0.63	0.78	0.96	0.05	0.01

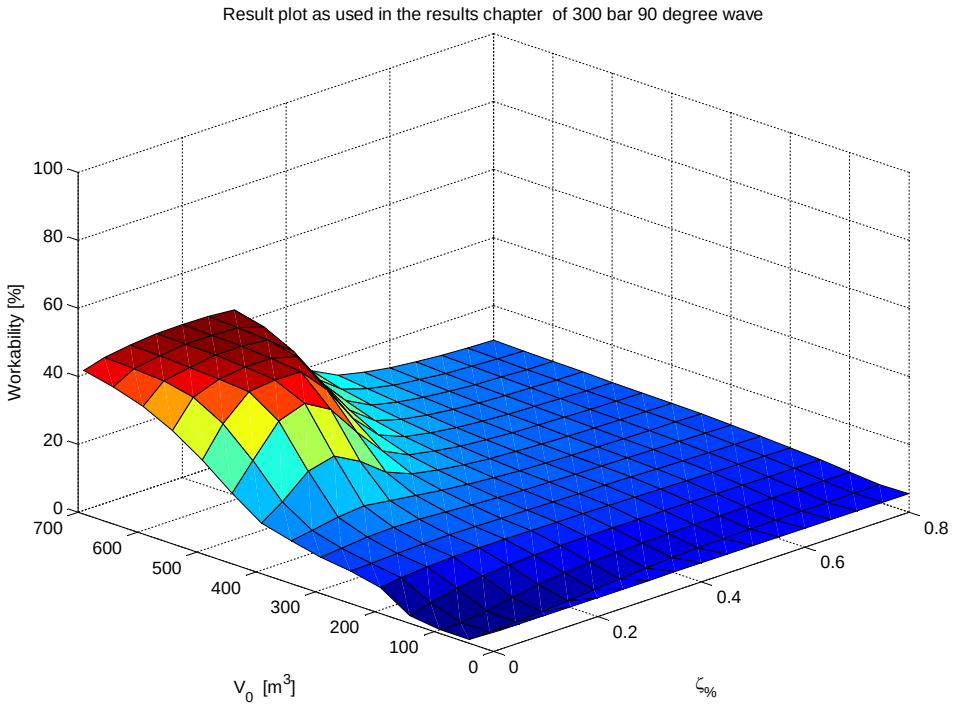

Figure C.1: Repetition of the results of the 300 bar case. With better axis to see the effects of the volume

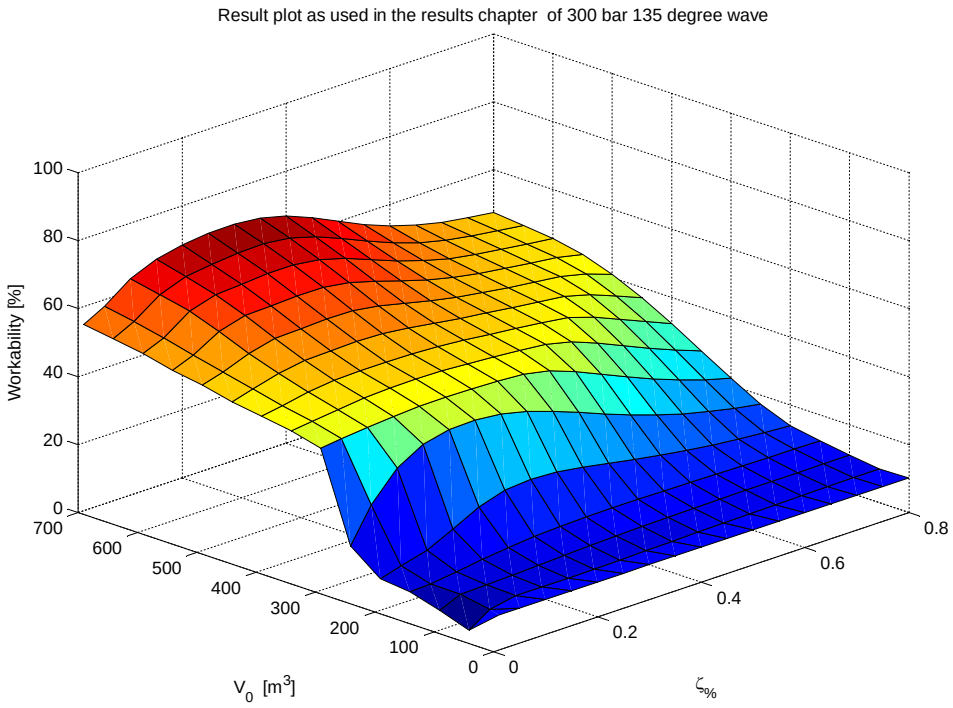

Figure C.2: Repetition of the results of the 300 bar case. With better axis to see the effects of the volume

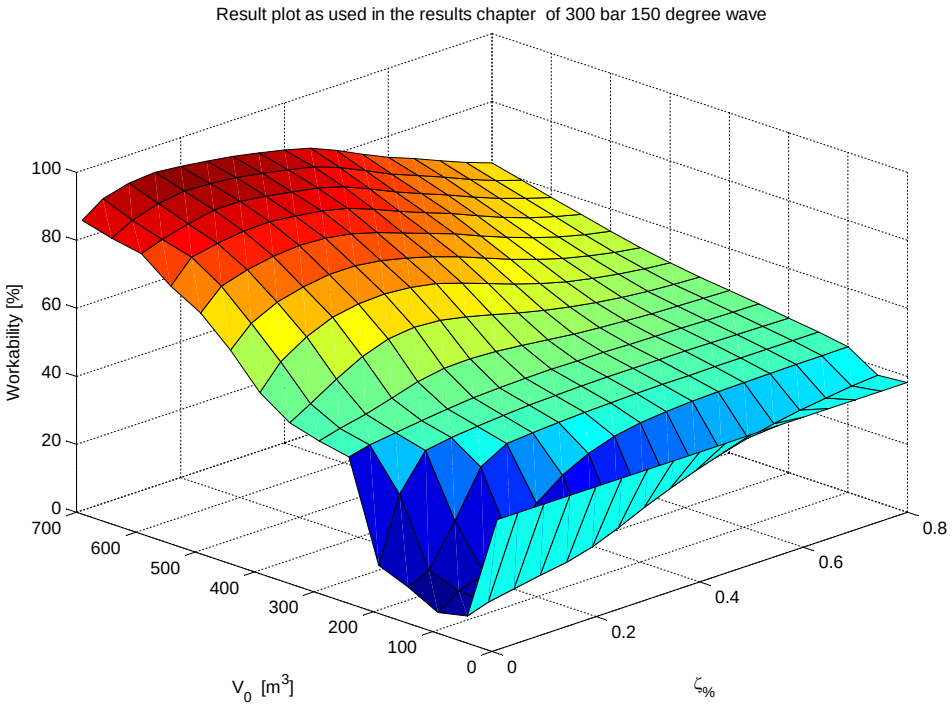

Figure C.3: Repetition of the results of the 300 bar case. With better axis to see the effects of the volume

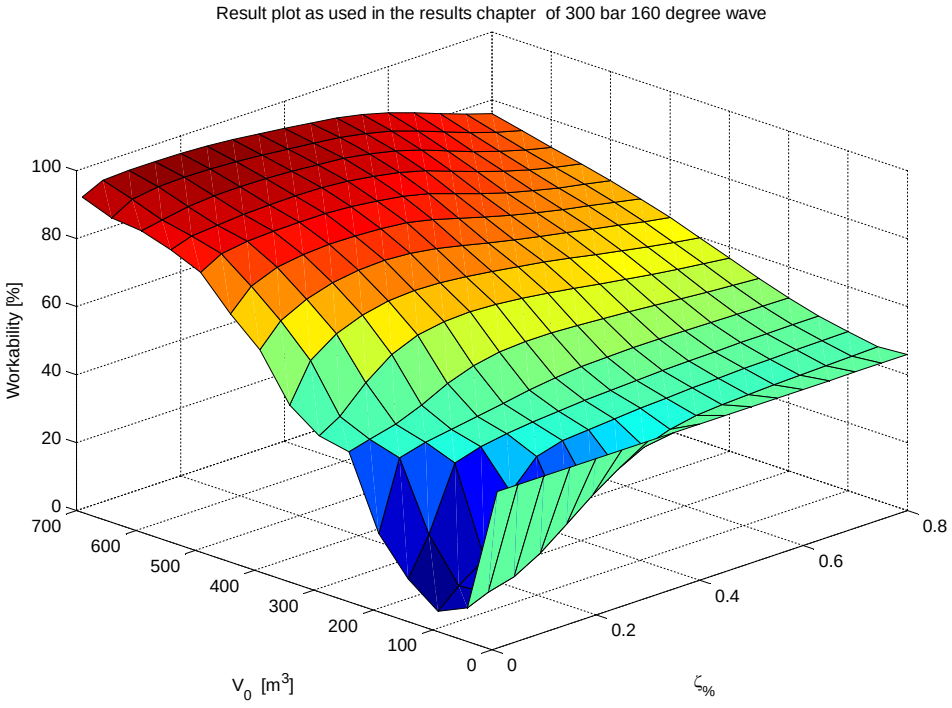

Figure C.4: Repetition of the results of the 300 bar case. With better axis to see the effects of the volume

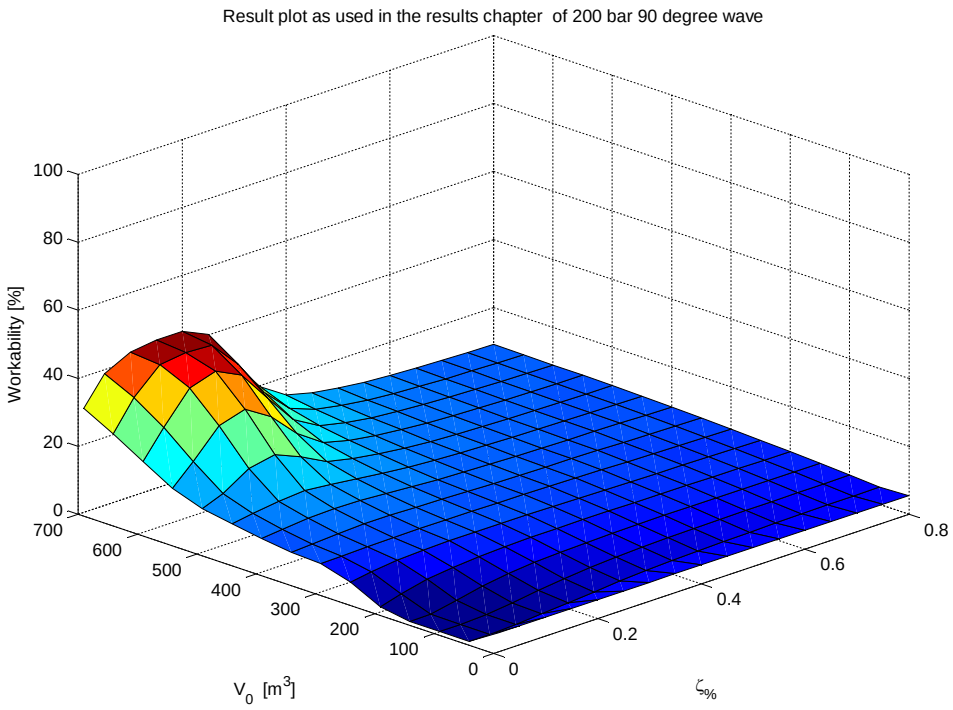

Figure C.5: Repetition of the results of the 200 bar case. With better axis to see the effects of the volume

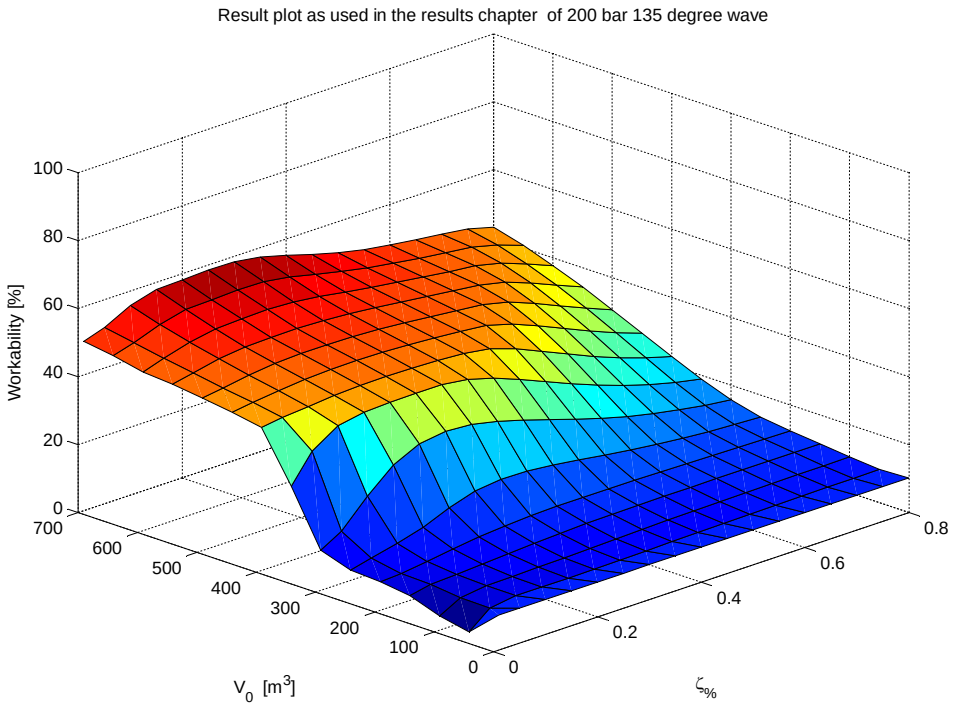

Figure C.6: Repetition of the results of the 200 bar case. With better axis to see the effects of the volume

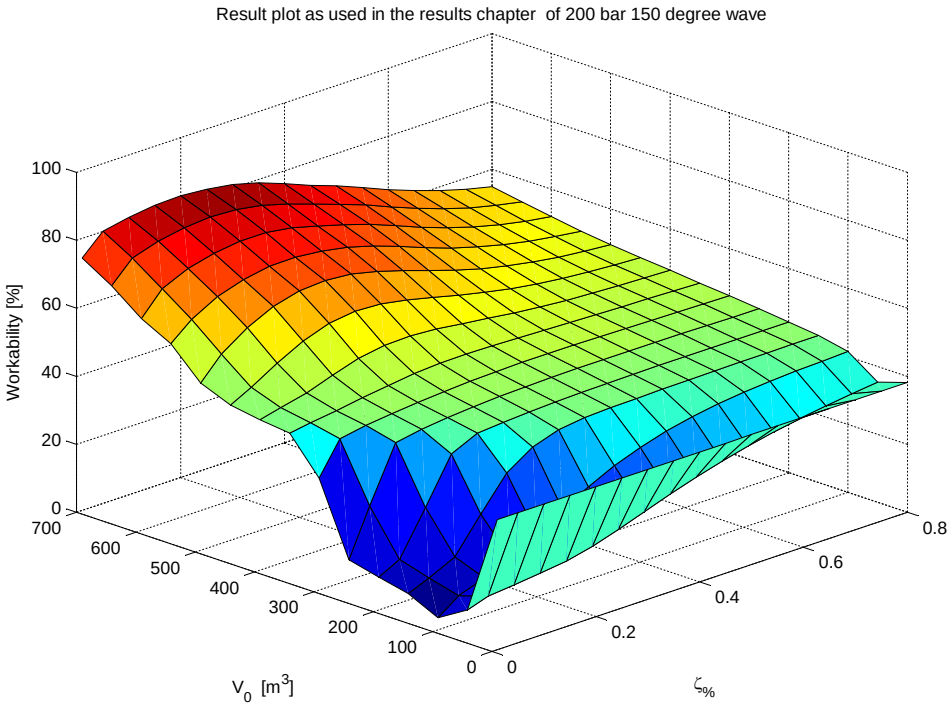

Figure C.7: Repetition of the results of the 200 bar case. With better axis to see the effects of the volume

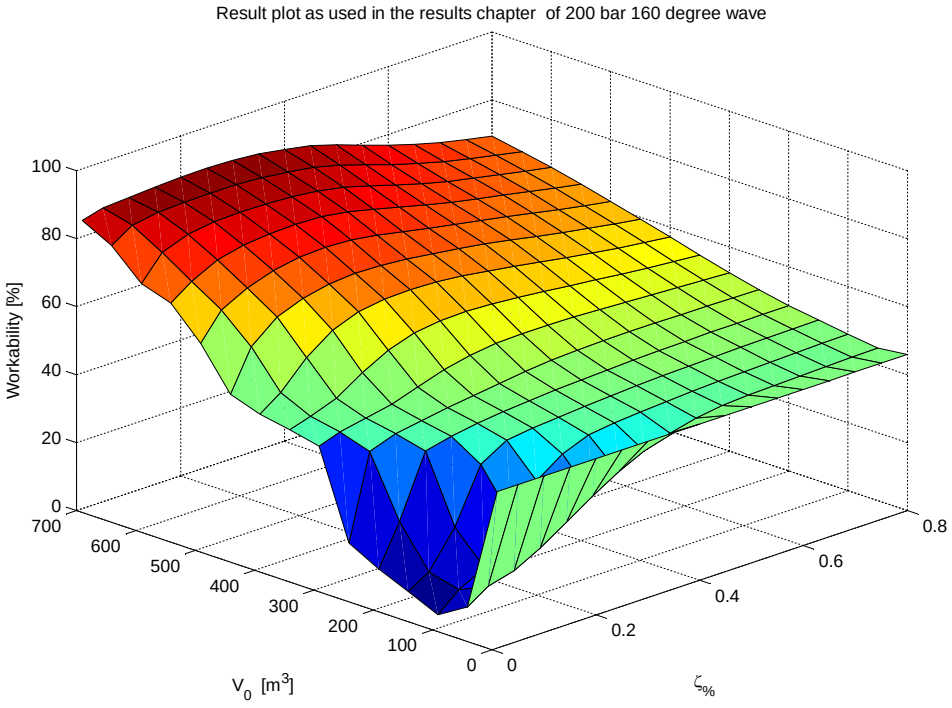

Figure C.8: Repetition of the results of the 200 bar case. With better axis to see the effects of the volume

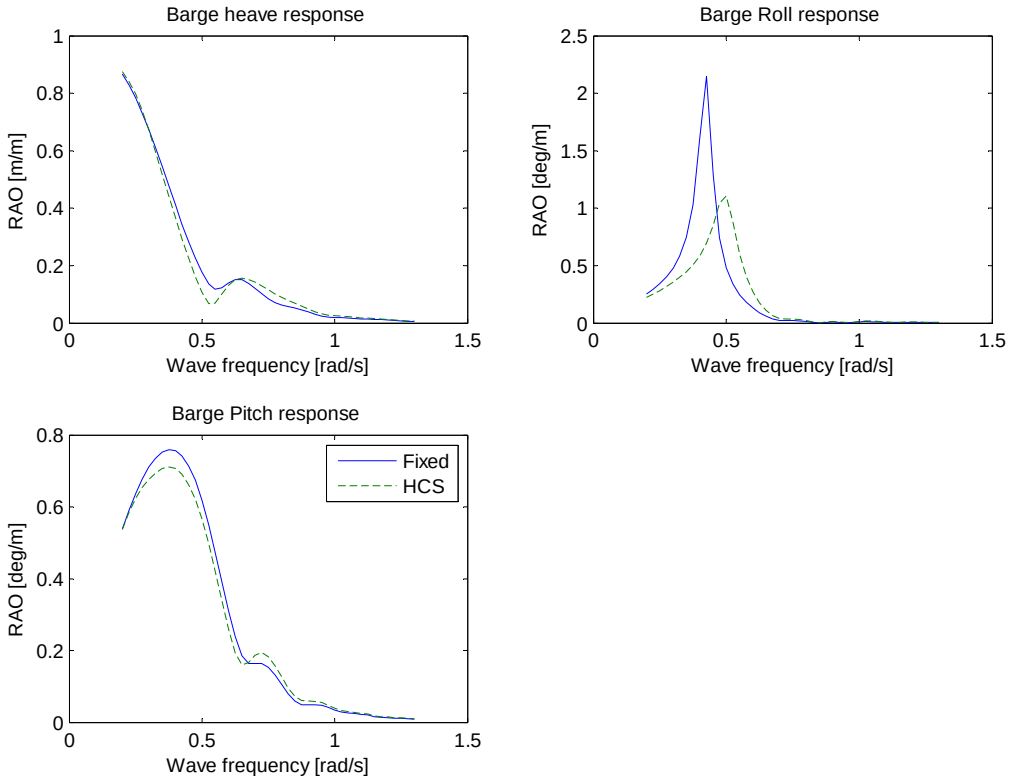

Figure C.9: The barge RAO's used for the classic scenario and the parameters of the heave compensation system (HCS).

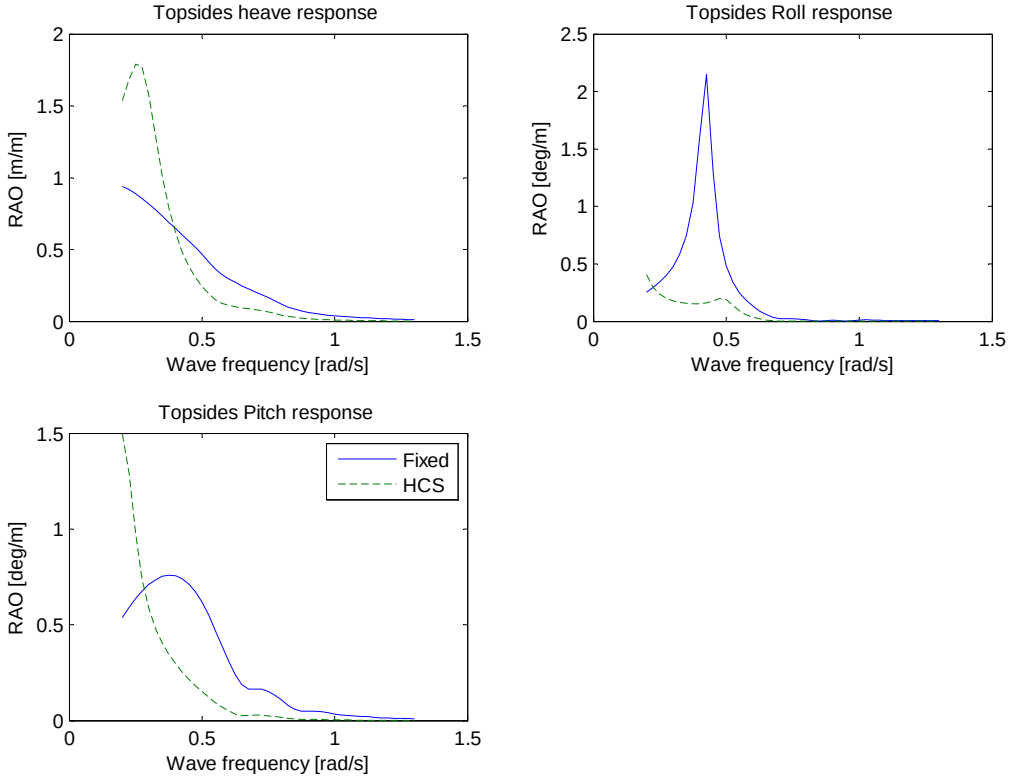

Figure C.10: The topsides RAO's used for the classic scenario and the parameters of the heave compensation system (HCS).

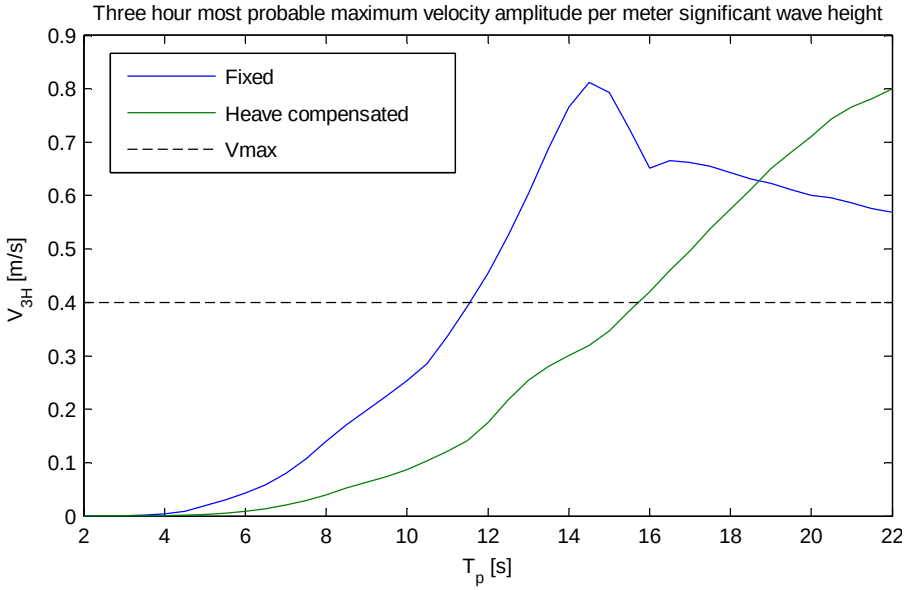

Figure C.11: The 3 hour most probable maximum velocity plot using the settings of the chosen heave compensation system. In comparison to the fixed scenario.

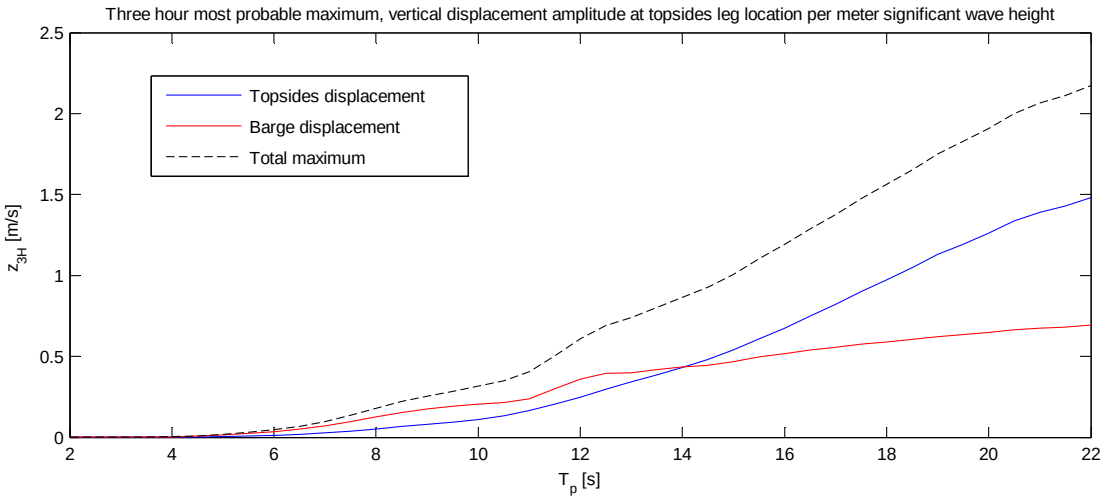

Figure C.12: The 3 hour most probable vertical displacement plot at the heave compensation system location. This indicates the vertical displacements of the barge and topsides. From this displacements the required stroke can be estimated. Note that the displacements are shown for 1 meter significant wave height and that the required stroke is higher for higher sea states. The black dotted line is the sum of the two displacement, this is worst case scenario where the topsides and barge motions are working in opposite direction.

C.2. DIMENSIONING RESULTS

This appendix supplies the results of the dimensioning process corresponding to the 300 bar and 200 bar solutions. Additionally, effects of chosen parameters are evaluated. Firstly the specifications of the 300 bar dimensions is presented. Followed by the 200 bar details. After that the effect of variations is presented.

C.2.1. 300 BAR SPECIFICATIONS

The following tables provide the details of the 300 bar solution, derived with the methodology of Section 7.2.1. For a better understanding of these numbers the dimensioned elements are repeated.

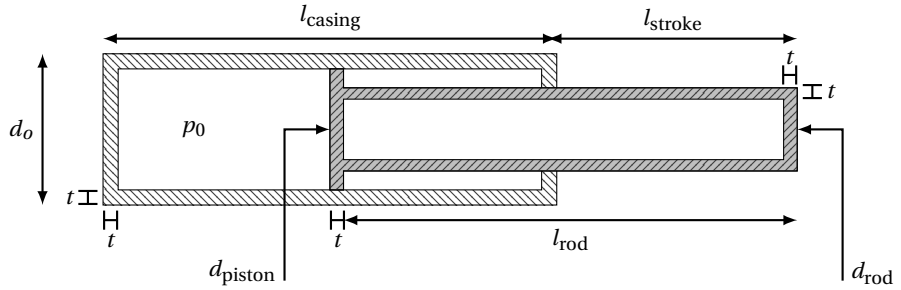

Figure C.13: The dimensioned cylinder.

Table C.2: Specifications of the Cylinder elements in a group at 300 bar

Cylinder specifications (300 bar)

General			Shell			Rod		
Property	Value	Unit	Property	Value	Unit	Property	Value	Unit
Quantity	4	[-]	Inner diameter (d_{piston})	0.83	[m]	Inner diameter ($d_{rod}-2t$)	0.42	[m]
Total weight	38	[ton]	Outer diameter (d_o)	1.06	[m]	Outer diameter (d_{rod})	0.66	[m]
Wall thickness (t)	11.85	[cm]	Height (l_{casing})	8.30	[m]	Rod length (l_{rod})	8.30	[m]
Min height	8.30	[m]	Volume	2.23	[m^3]	Stroke (l_{stroke})	4.15	[m]
Max height	12.45	[m]	Weight	23.8	[ton]	Weight	13.8	[ton]

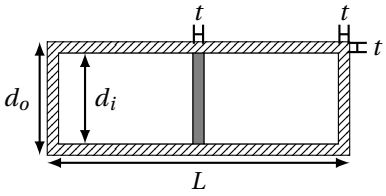

(a) The dimensioned accumulator.

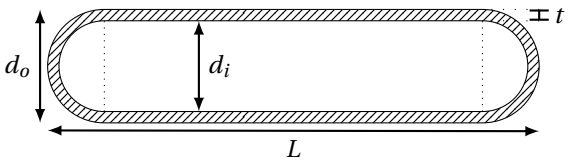

(b) The dimensioned pressure vessel.

Figure C.14: The accumulator and pressure vessels approximations

Table C.3: Specifications of Accumulator element at 300 bar

Accumulator specifications (300 bar)		
Property	Value	Unit
Quantity	2	[-]
Weight	27.3	[ton]
Inner diameter (d_i)	0.91	[m]
Outer diameter (d_o)	1.17	[m]
Length (L)	7.5	[m]
Volume	4.46	[m^3]
Wall thickness (t)	13.1	[cm]
Piston Area	0.65	[m^2]

Table C.4: Specifications of the pressure vessel elements at 300 bar

Pressure vessel specifications (300 bar)		
Property	Value	Unit
Quantity	15	[-]
Weight	109	[ton]
Inner diameter (d_i)	1.46	[m]
Outer diameter (d_o)	1.72	[m]
Length (L)	20	[m]
Volume	13.9	[m^3]
Wall thickness (t)	12.9	[cm]

C.2.2. 200 BAR SPECIFICATIONS

The following tables provide the details of the 200 bar solution, corresponding to Section 7.2.2. The same parameters are presented as the 300 bar solution, referring to Figures C.13 and C.14.

Table C.5: Specifications of the Cylinder elements in a group at 200 bar

Cylinder specifications (200 bar)								
General			Shell			Rod		
Property	Value	Unit	Property	Value	Unit	Property	Value	Unit
Quantity	6	[-]	Inner diameter (d_{piston})	0.83	[m]	Inner diameter ($d_{rod} - 2t$)	0.51	[m]
Total weight	24	[ton]	Outer diameter (d_o)	0.98	[m]	Outer diameter (d_{rod})	0.66	[m]
Wall thickness (t)	7.55	[cm]	Height (l_{casing})	8.30	[m]	Rod length (l_{rod})	8.30	[m]
Min height	8.3	[m]	Volume	2.33	[m^3]	Stroke (l_{stroke})	4.15	[m]
Max height	12.5	[m]	Weight	14.4	[ton]	Weight	9.5	[ton]

Table C.6: Specifications of Accumulator element at 200 bar

Accumulator specifications (200 bar)		
Property	Value	Unit
Quantity	2	[-]
Weight	25.3	[ton]
Inner diameter (d_i)	1.12	[m]
Outer diameter (d_o)	1.32	[m]
Length (L)	7.5	[m]
Volume	6.70	[m^3]
Wall thickness (t)	10.2	[cm]
Piston Area	0.98	[m^2]

Table C.7: Specifications of the pressure vessel elements at 200 bar

Pressure vessel specifications (200 bar)		
Property	Value	Unit
Quantity	19	[-]
Weight	70.4	[ton]
Inner diameter (d_i)	1.48	[m]
Outer diameter (d_o)	1.65	[m]
Length (L)	20	[m]
Volume	8.5	[m^3]
Wall thickness (t)	9.0	[cm]

C.2.3. VARIATION OF DIMENSIONING PARAMETERS

Some of the choices in the dimensioning chapter are subjective. To indicate the effects of the chosen values plots are created to show the influence of these parameters. The maximum inner diameter of the pressure vessel is plotted in relation to the results of the total weight of the system and the number of pressure vessels required in Figure C.15. An equal plot is made for the variation in pressure vessel length, this results in

Figure C.16. The amount of cylinders is based on the redundancy versus the buckling loads, this relation is shown in Figure C.17. The latter shows that the total weight of the system is not significantly influenced by the amount of cylinders.

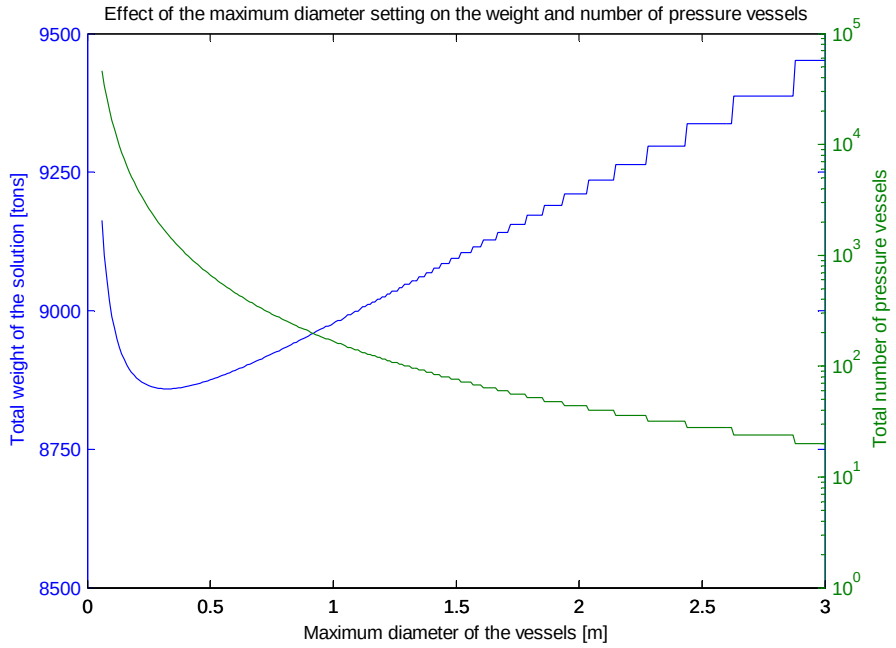

Figure C.15: The effect of changing the maximum inner diameter of the vessel. Identifying the trade-off between total weight of the system and number of required pressure vessels. Based on 200 bars of pressure.

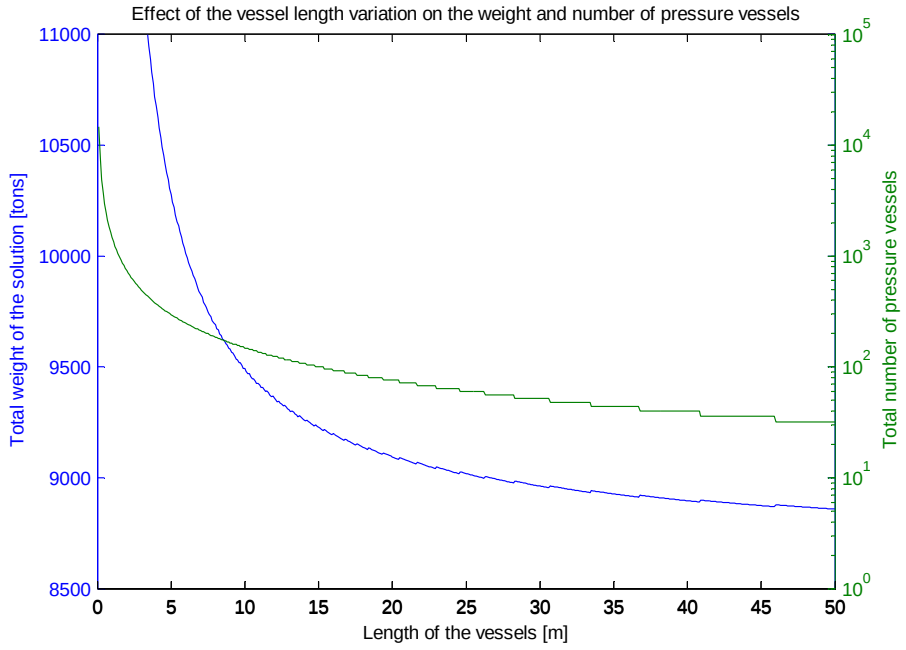

Figure C.16: The variation of the pressure vessel length and the total mass of the heave compensation system. For more vessels more endings of the vessels are required. Hence the mass decreases when the length of the vessels is larger. Based on 200 bars of pressure.

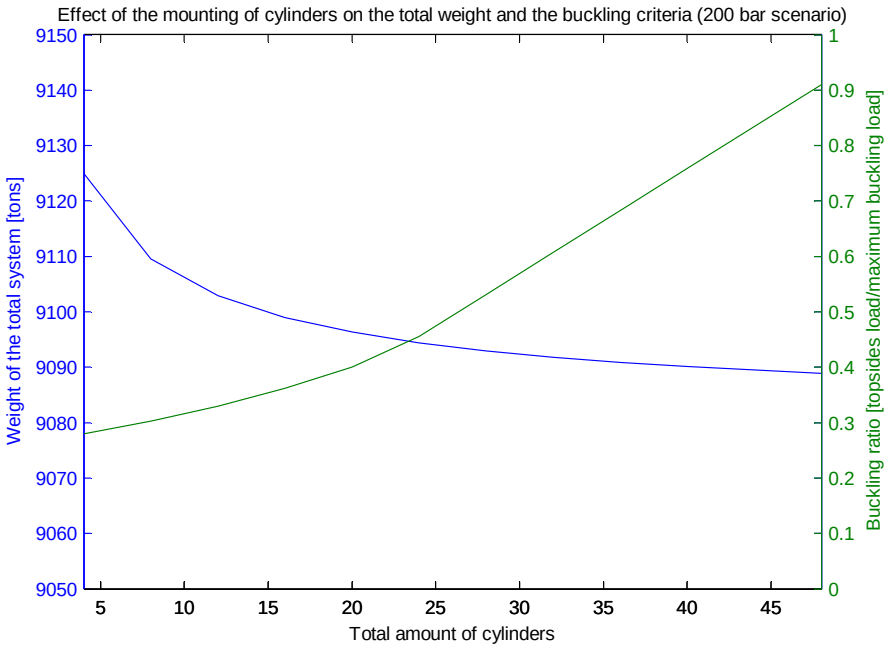

Figure C.17: The effect of the total amount of cylinders on the buckling load. Where the total mass is also plotted to see that the effect on the mass is low. Based on 200 bars of pressure.

C.3. SENSITIVITIES

The sensitivities are determined for values that are chosen. In this case the peak enhancement factor and installation duration. The peak enhancement factor determines the energy distribution of the wave spectrum and the time duration is used to determine the most probable wave height. This appendix compares the used values of the thesis with the other settings.

Sensitivities are derived for:

- Peak enhancement factor
- Duration of the installation

The peak enhancement factor is also plotted using the value of 1. This value is more commonly used to represent swell conditions. In the literature of the Nigerian Swell is found that the peak enhancement factor used to compile the data table is 8. The comparison between the two values shows that effect for the lower damping regions is small. The workability reaches almost comparable heights with a peak enhancement factor of 1. For the high damping region the workability is significantly lower with the high peak enhancement factor. This comparison indicates that the effects for the chosen heave compensation system due to the different peak enhancement factor is low.

The installation duration is related to the amplitude of the highest most probable wave. A shorter duration allows a smaller design wave to be used. The effect of this turns out to be small. The difference in workability between an installation time of 1 hour and 6 hours is small in the regions of the chosen heave compensation parameters. Again for the higher damping region the effects are more clearly present.

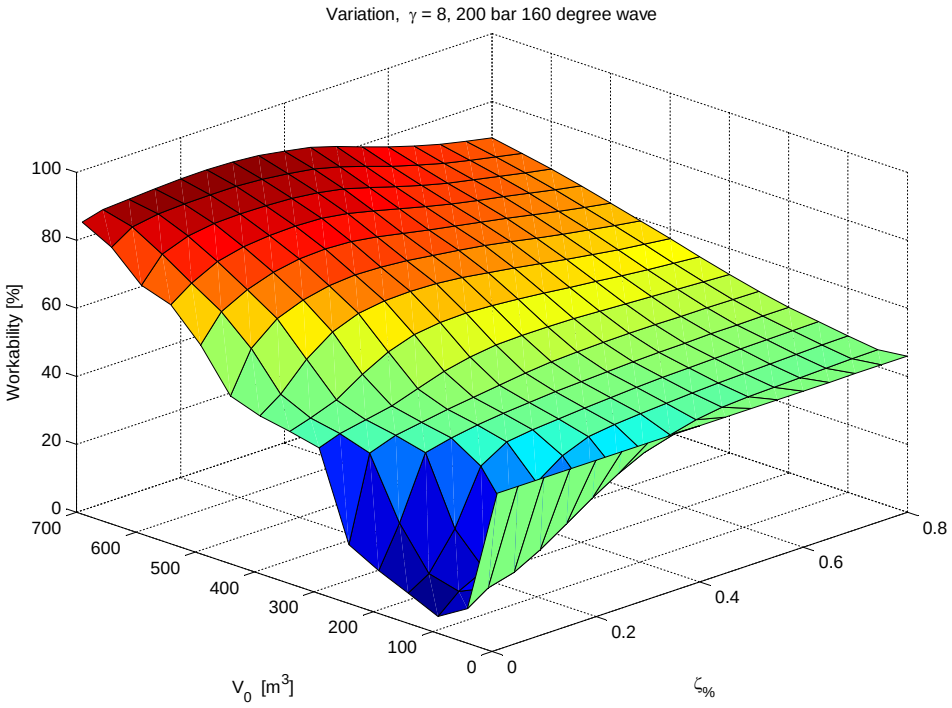

(a) This figure coincides with the value used for the results

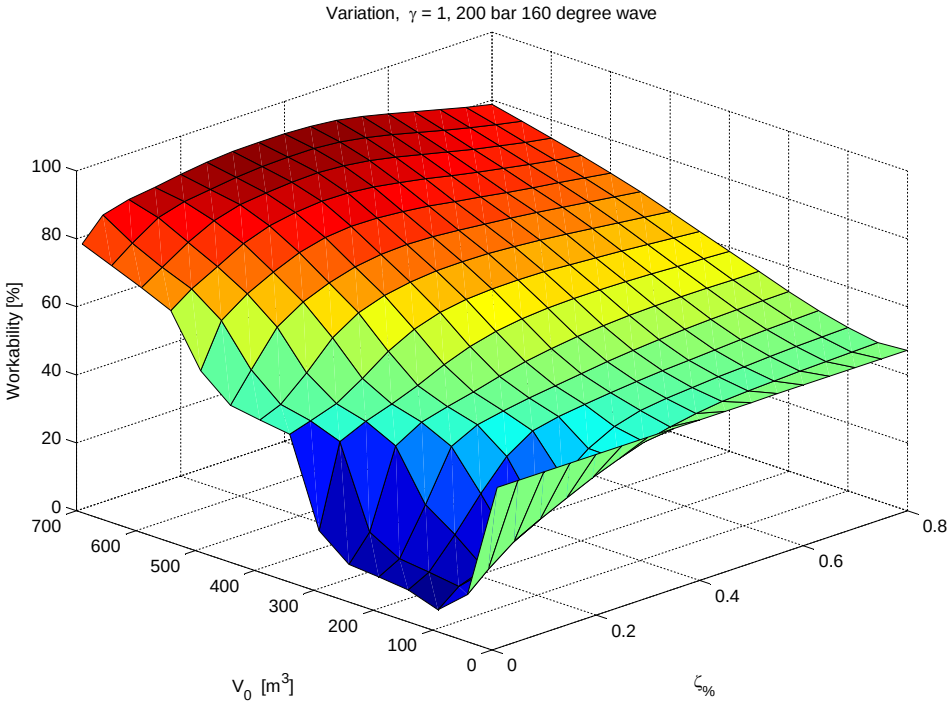

(b) This figure represent common swell seas where a peak enhancement of 1 is applied

Figure C.18: Variation of the peak enhancement factor

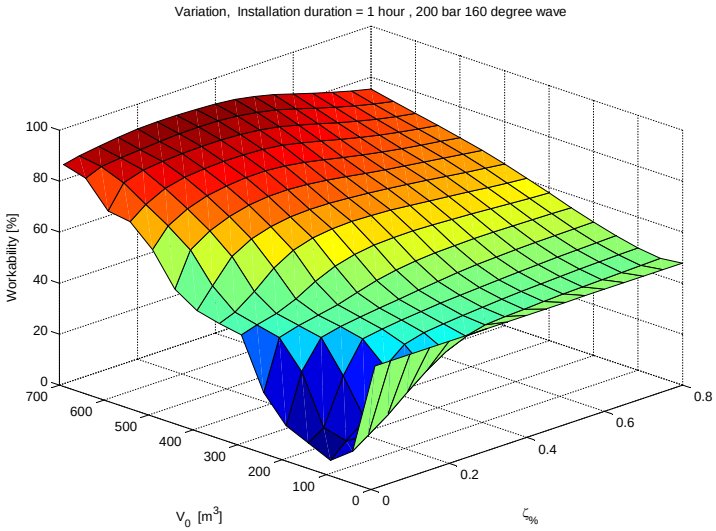

(a) Installation time shortened to 1 hour.

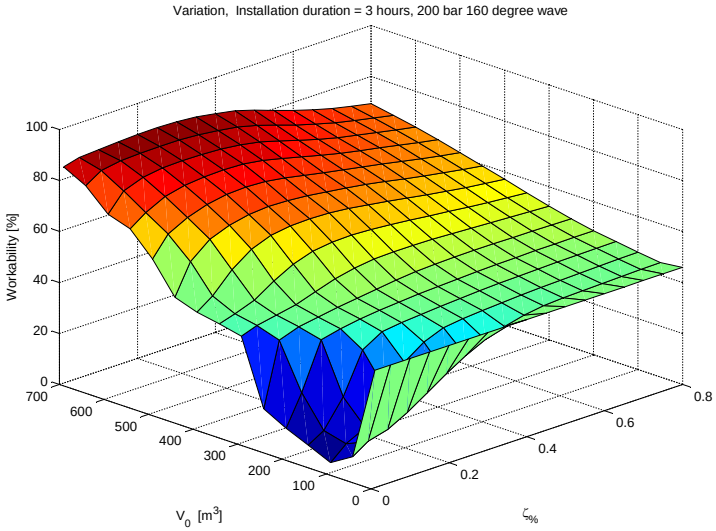

(b) This figure coincides with the value used for the results

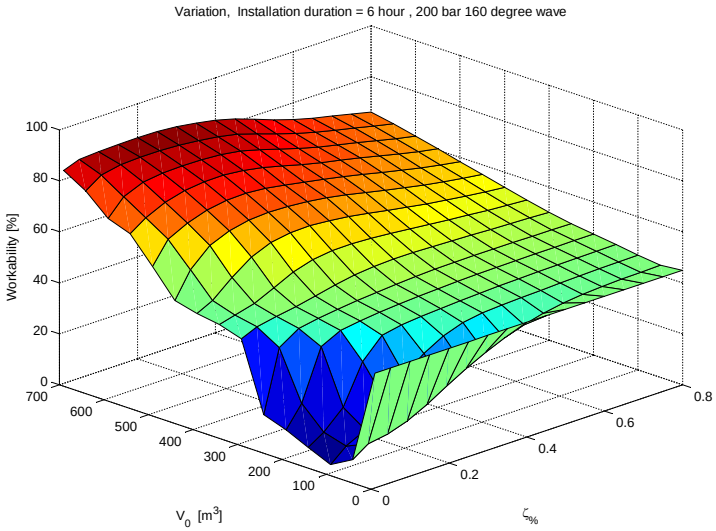

(c) Increased time to the ballasting procedure of the `Liwan 3-1` installation

Figure C.19: Variation of the required installation time

C.4. INSTALLATION METHOD

In this part of the additional results, the assumptions surrounding the LMU's are checked. For the LMU's simplifications are used: Firstly, that slip occurs continuously. Secondly, the friction force is neglected. Thirdly, the slip can not cause engagement of the topsides legs with the LMU's. These assumptions were required to obtain the installation limit. The subsection post processes the resultsto check the orientation of the velocity vector. From this can be checked if these assumptions are correct.

Using the results of this research the incoming velocity vector of the topsides leg can be derived. This vector is related to the wave direction, peak period and settings of the heave compensation system. The orientations of the vectors are derived for the 160 degrees waves and settings as used in Figure C.20. This figure is elaborated below.

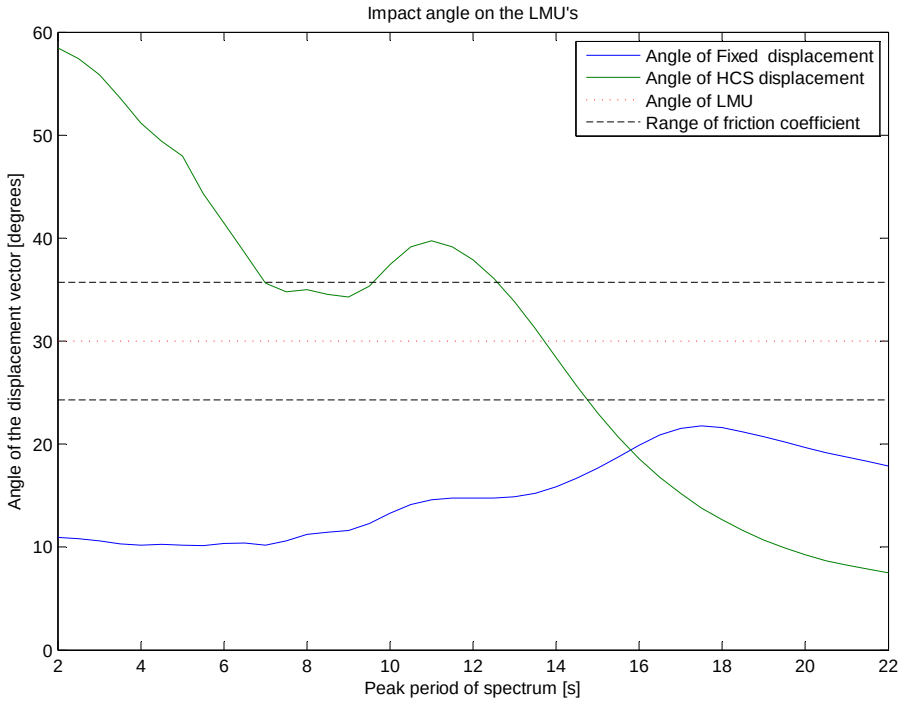

Figure C.20: The orientation of the incoming velocity vector for the fixed and heave compensated scenario. Zero degrees coincides with a vertical motion, consequently 90 degrees implies horizontal motions. The red dotted line indicates the angle of the LMU, where the range of the static friction force is given with the black dashed lines.

The orientations as shown in Figure C.20 indicate if the topsides would stick, slip upwards or slip downwards. The angle corresponds to the orientation of the velocity, with a vertical motion at zero degrees and a horizontal motion at 90 degrees. The velocity is perpendicular to the LMU at 30 degrees, shown with the dotted red line. The friction coefficient of 0.1 coincides with an angle of $\pm$ 5.7 degrees, shown with the dashed black lines. If the velocity angle is in the limits of the friction coefficient the than impact is subjected to a stick scenario. For angles lower than the friction limit, the leg will slide downwards over the LMU cone. Consequently, for larger angles upwards slip will occur.

Thus the uncompensated scenario ('fixed') is constantly in the downwards slip region, no stick effects occur. This makes sense for head on waves since these motions should be pitch dominated, resulting in large vertical displacements of the topsides. Engagement of the topsides leg and LMU might take place in the impact scenario.

For the heave compensated scenario the peak period plays a large roll in the orientation. For small peak periods upwards slip takes place. In this case the heave compensation system cancels the vertical motions, hence only the horizontal components remain. Than a small region of stick is shown, until the roll motions of the barge change the angle, these motions are dominant around 11 seconds, bring the orientation back in

the upwards slip regime. For the longer wave periods the stick and downwards slip regime is reached. Thus, for the heave compensated scenario all regimes are reached.

When the orientation is around 30 degrees, the used approach is correct. For the angles in the upwards slip regime the friction force will cause a larger horizontal force. Hence, the impact is higher as predicted. For the downwards slip motion the friction force decreases the horizontal loads. Thus, decreasing the impact loads. In other words, in the upwards slip regime the used model overestimates the installation limit and for the downwards slip regime the model can be seen conservative.

The installation velocity rises for the longer peak periods, thus in the longer period the limits are reached more often. For the peak periods of 15 seconds and higher the heave compensation system is no longer able to handle 1 meter significant wave height (Figure C.11). For these peak periods the orientation is downwards slip. Therefore, these limits are not overestimated. Combining this with the constant downwards slip leads to the conclusion that the angle assessment shows that the angle assumption influences the installation limit and this eventually leads to more conservative values.

D

VERIFICATION

For the verification the model is compared to the raw AQWA data. The model comparison is based on the frequency domain model in matlab, as presented in Chapter 5, and the AQWA data for the response of the single mass system. This is done by altering the model such that the heave compensation capabilities act as a rigid body.

The AQWA data contains the RAO's of the single mass system. The model uses the barge topsides as a system with two masses. Thus changing the behaviour of the system. The effects of this must be minimal when the interface is set as a rigid body. For this verification a model is made based on the same method as Section 5.2.2 where the six degrees of freedom have been calculated using the raw data of the AQWA model and comparing it to the RAO's of the AQWA model. This resulted in the comparison shown in Figure D.1, from which can be concluded that the model of the barge computes the same results as the calculations done by AQWA.

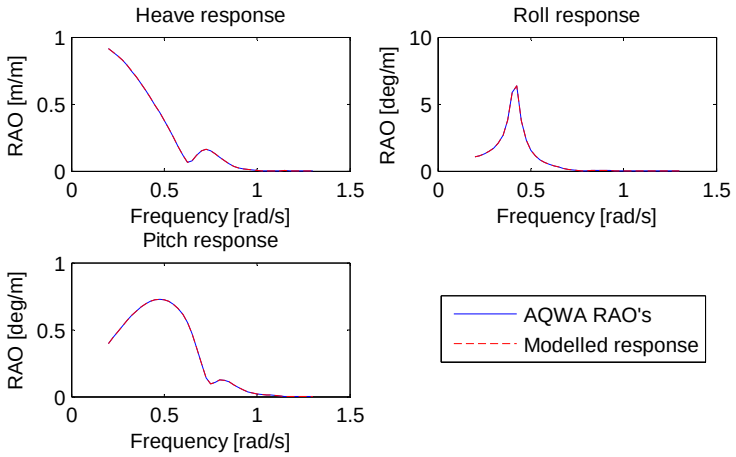

Figure D.1: The comparison between the barge motion model and the AQWA RAO data. The model is compiled using the same principle as Section 5.2.3.

From this point a nine degree of freedom model can be made to compare the barge RAO's with the barge and topsides combined system. The nine degrees of freedom consist of all six degrees of freedom of the barge and the three degrees of freedom of the topsides. This ensures that the cross terms are taken into account during the RAO comparison. Now the system becomes very complex since the mass of the topsides is separated and relocated thus creating a system where one center of gravity is now on two locations. Which affects the inertial values used in the AQWA calculations. When changing the parameters into a 9DOF system with the topsides taken into account the RAO's become:

This figure computes the barge with the hydrodynamic data from the AQWA model, which consists of the

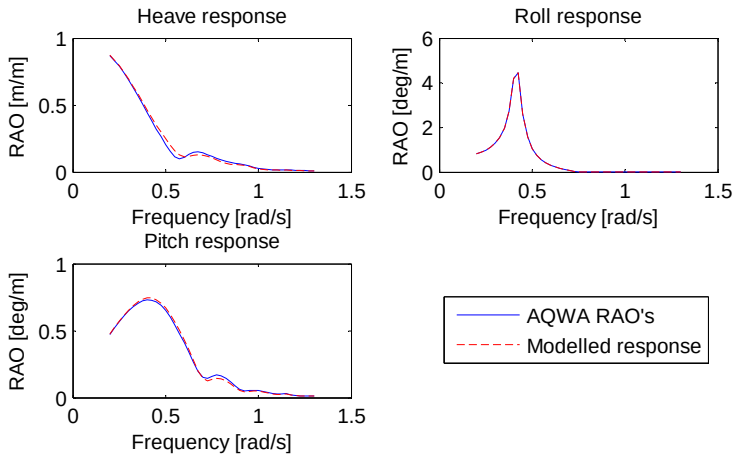

Figure D.2: The comparison between nine degrees of freedom model with the topsides mass extraction and the AQWA RAO's. All cross terms and combining elements are taken into account.

added mass, damping and stiffness characteristics. And compiles a mass matrix which corresponds with separated barge and topsides model. The forces of the interface using a spring damper system are implemented in the system. For the spring stiffness the Young's modules of steel is combined with the required length and area to approach the DSF stiffness.

The mismatch in responses from Figure D.2 is due to the horizontal location of the topsides. When the topsides is placed above the COG of the barge than the modelled RAO's coincide with the AQWA RAO's in Figure D.1. This implies that the current separation of masses and inertias is not optimal. In this model the masses and inertia for the heave, roll and pitch are altered since these motions are affected by the heave compensation system. This is done by subtracting the topsides mass from the total mass in the heave equation and subtracting the own inertia terms for the roll and pitch. The own inertia implies the rotational inertia of the topsides around the center of gravity, the Steiner term related to the distance from the barge are still taken into account since roll and pitch of the barge still cause surge and sway motions of the topsides.

Table D.1: The difference between the motions compiled with Allseas internal tools and the AWQA data and the model. The values shows the three hour maximum amplitudes for a spectrum input of $H_s = 1m$, $T_p = 18s$ and a wave direction of 150 degrees.

DOF	AQWA	Model	Unit
Surge	0.573	0.578	[m]
Sway	0.306	0.308	[m]
Heave	0.449	0.460	[m]
Roll	2.085	2.067	[deg]
Pitch	0.595	0.600	[deg]
Yaw	0.432	0.430	[deg]

For an estimation of the significance of the RAO mismatch a comparison is made based on the three hour maximum amplitudes for a certain spectrum, the results are shown in Table D.1. The difference between the amplitudes is smaller than 1 percent for all degrees except heave which has a 2.5 percent difference. The conclusion is made that these results are representable for the topsides barge combination.

These motions are different than the results given in Chapter 6 this is due to the added degrees of freedom and their influence on the other motions. Since the barge is constraint between the substructure legs the surge, sway and yaw motions will not occur and thus their influence on the considered degrees of freedom is not taken into account.

E

CONCEPT EVALUATION

In order to design the HCS the lifting principle has to be determined. This is done by creating concepts of all possible lifting principles for this scenario. This chapter will elaborate on the process of the concept design phase and how this phase led to the lifting principle for which the HCS will be further developed. This is done by firstly elaborate the possible concepts, then the evaluation of those concepts is given and finally the final concepts and thus basis for the design of the HCS is explained.

E.1. LIFTING PRINCIPLES

The different methods of lifting are assessed on their applicability in the floatover scenario. To find all possible lifting configurations a research on lifting principles is done, which was not limited to offshore lifting principles. This lead to four main lifting methods: hydraulic cylinders, buoyancy lift, jacks and winches. With these methods a variety of concepts can be created. A small elaboration of these methods is given:

- **Hydraulic cylinders** are capable of handling big loads and can act quick and accurate. This is the most logical lifting principle for lifting with compression.
- **Buoyancy lifts** can be used by integrating pontoons in, or next to, the barge which create extra buoyancy forces. This principle is worth taking into account since it can be scaled to handle huge forces. However the displaced water volume must be very large to generate heavy lift forces.
- **Jacking systems** are not used in the conventional way. A jack is seen as a system where fluctuation forces have minimal impact on the displacement. When looking at the current market these 'car' jacks do not exist for large forces. For large forces mechanical jacks are not being require a high amount of power for actuation, in this cases hydraulic cylinders jacks are used. In this evaluation the jacking principle is used as a system where displacement is unrelated to forces.
- **Winch systems** are used when the load can be lifted from the top and that is not possible in the current scenario. However, winches are able to apply, relatively, constant loads and react quick. This system can be used to aid the compensation method when the system is applied to the bottom of the topsides. And can thus help a lifting method with the stabilisation procedure.

With these principle the concept design lead to the distribution of possibilities shown in figure E.1. In this figure the main lifting system indicates the system that delivers the majority of the force and the secondary system is used to gain extra control on the barge motions. This field incorporates 14 different concepts

E.2. EVALUATION OF CONCEPTS

The evaluation of the concept is done with a weighted Multi Criteria analysis, in which the concepts are evaluated in terms of lifting capabilities and general characteristics. This analysis created a very clear gap between the top three concepts and the rest. Therefore only the three remaining concepts are considered

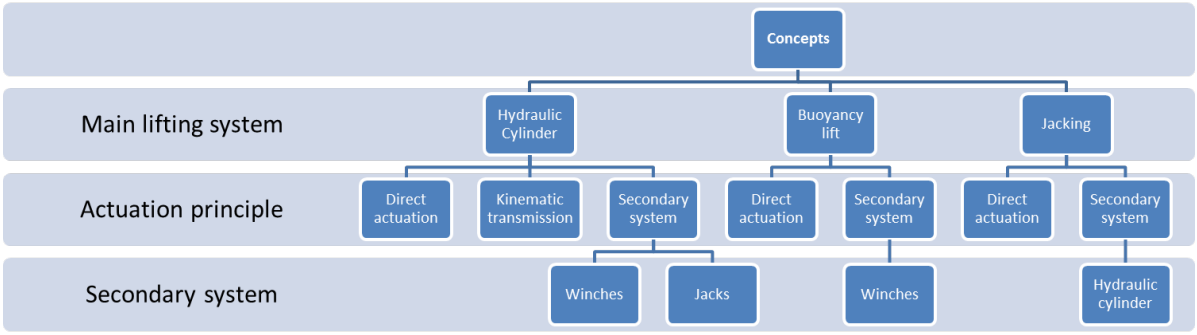

Figure E.1: Schematic view of the considered concepts.

in this section, the elaboration of the concept selection as well as the multi criteria analysis is written in appendix E.3. The three concepts are:

1. **Hydraulic cylinder system**
   This concept is based direct actuation between the barge and topsides. Hydraulic cylinders will cope with the motions of the barge as well as the installation stroke. During installation the cylinders will be fixed with respect to the x and y directions of the barge and will be designed to compensate the motion in the z direction. The cylinders will lift the structure at 4 different points: 2 at far port side and 2 at far starboard. The actuation is done with a pneumatics system which transfers the pressure through an accumulator, possibly combined with an active part. This should be able to control the motions of the topsides.

2. **Jacking system**
   The jacking system is based on the desire to design a system which is able to accurately perform a motion without being influenced by the varying forces. Although such system only exists for much lower forces it is taken into account in this thesis since this option would create a very applicable lifting solution. This concept is based on these hypothetical jacks using the same locations and orientations as concept 1.

3. **Jack & cylinders system**
   In this concept hydraulic cylinders, which are equal to the cylinders in concept number 1, are placed on top of the hypothetical jack system, as described in concept 2. This combination aids the possibility to control the topsides motion with the hydraulic cylinders while using the jacking system to perform the installation procedure of the topsides. Again the locations and orientations are as concept 1.

The remaining three concepts do not differ in the location of the actuation and in the kinematics which the system creates between barge and topsides. The main difference between these concepts is the actuation principle. There are two principles remaining: hydraulic cylinders and a jacking system.

The jacking system refers to the conventional jackscrew, in these jacks the load on top of the jack has minimal influence on the position of the stroke. The stroke is set by the amount of rotation the screw thread has made. When loads get heavier mechanical jacks are no longer used due to the increased frictions which creates a limiting factor for the screw thread dimensions. Therefore, for heavier loads hydraulic jacks are used since they are capable of reaching much higher loads. Conventional hydraulic jacks do not contain the characteristics of the unrelated displacement with respect to the load, in this thesis an open mind towards this principle is taken into account.

Due to the uncertainty of the jacking principle combined with the correlation in engagement points and transmission of forces in the three concepts, no further decisions about the concepts have to be made. A model which contains these points of engagement and force transmission will give insight in the motions of the barge and with that knowledge the next steps towards the design of a HCS can be made.

E.3. CONCEPT SELECTION

The concepts process started with listing all possible ways to raise a heavy load from its position. Once these were known ideas were created were these principles were placed in the barge and topsides situation. Eventually from these ideas 14 are sketched and taken into account during the concept evaluation. In figure E.1 is illustrated how these 14 concepts are organized. In this appendix the process of the concept evaluation is elaborated.

The concepts are shown in E.2 and the evaluation is based upon a performance indication by means of a weighted Multi Criteria Analysis. In the analysis al 14 are evaluated on their expected performance in criterion related to the floatover installation and criterion related to general characteristics of the concept. The weight and interpretation of the criterion are:

- **Feasibility of construction**, relates to the expected performance of the structural parts. How are the forces transferred and what how is the structural integrity affected by this transfer of forces [10%]
- **Feasibility of lift**, this criterion relates to the lifting procedure itself how does the actuation of the system relates the different components of the concept and do the components cause any secondary effects: like bending moments are big friction forces [25%]
- **Safety**, is the concept safe in a way that the topsides are stable at all times and what is the chance of components to loose their stability [20%]
- **Kinematics**, how does the concept transfer motions [10%]
- **Complexity compensation**, is the concept expected to perform well in the compensation of motions of the barge [15%]
- **Weight**, how heavy is the concept and does the concept affect the weight of the other required elements [10%]
- **Costs**, indication of the extensiveness of the concept. If the concept contains a lot of complex elements the costs will increase significantly [10%]

The result of the analysis of this criterion for the concepts shown in figure E.2 is given in table E.1. The analysis shows three probable concepts which all score a significant higher score the the runner-up concepts the top five of the MCA is found as:

	Name	Score
1	Double cylinder	4.50
2	Jacking system	4.30
3	Double piston jack support	4.15
4	Moment reducing beam	3.45
5	Horizontal pistons, lever	3.30

The top three concepts scored very close and should therefore be further evaluated. Since the difference with the rest of the concepts is significant the concept ranked 4 to 14 are considered less favourable and will not be taken for the rest of this thesis. In order to identify the remaining three concepts a functional description is given:

This concept is based direct actuation between the barge and topsides. Hydraulic cylinders will cope with the motions of the barge as well as the installation stroke. The cylinder will be fixed with respect to the x and y direction of the barge and will be able to compensate the motion in the z direction, of the barge local coordination system. The cylinders will lift the structure at 4 different points: 2 at far port side and 2 at far starboard. The concept is based upon the desire to find design a system which is able to accurately perform the stroking motion without being significantly influenced by the varying forces. Although such system only exists for much lower forces it is taken into account in this thesis since this option would create a very applicable lifting solution. The hypothetical jacks have the same actuation principle as concept 1. In this concept the double pistons, which are equal to the ones in concept number 1, are placed on top of the hypothetical jack system, as described in concept 2. This combination aids the possibility to control the topsides motion with the hydraulic pistons while using the jacking system to install the topsides. The points of engagement are equal to concept 1.

When analysing the three concepts there is one major similarity between all: they are all applied on the same locations of the barge and use no transmission system the transfer the forces. Therefore when analysing the

Concepts		MCA Results		Criterion						
	Name	Points	Rank	Feasibility of construction	Feasibility of lift	Safety	Kinematics	Complexity compensation	Weight	Costs
1	Double cylinders	4.50	1	5	5	4	4	5	4	4
2	Double cylinders + winches	3.00	7	5	2	3	4	2	4	3
3	Big cylinder + winches	2.80	9	4	3	1	4	3	4	2
4	Moment reducing beam	3.45	4	2	4	4	3	5	1	3
5	Cantilever beams	2.85	8	2	3	3	3	4	2	2
6	Triple pistons, single actuation	3.10	6	5	2	4	3	2	4	3
7	Horizontal pistons, lever	3.30	5	3	4	3	4	4	2	2
8	Winched buoyancy lift	1.30	14	1	1	2	2	1	1	1
9	Double buoyancy	1.80	12	1	1	4	3	1	1	1
10	Double cylinder cantilever	2.20	11	2	2	3	2	2	2	2
11	Horizontal swing	1.40	13	1	1	2	1	1	2	2
12	Double pistons hinged	2.65	10	1	3	2	3	4	3	2
13	Jacking system	4.30	2	5	5	5	3	3	4	4
14	Double pistons jack support	4.15	3	4	5	4	5	4	3	3
			Weight	10%	25%	20%	10%	15%	10%	10%

Table E.1: The Multi Criteria Analysis performed to identify the promising concepts

behaviour of the barge and topsides in sea conditions the systems will behave equally when the installation procedure is not yet active. Therefore the analysis of this motions can be done without further specializing in one of the three concepts. Note that concept 2 and 3 contain the jack actuation which is based upon a desired function which is not yet found, this aids the choice to continue with the modelling to see if such system can be created.

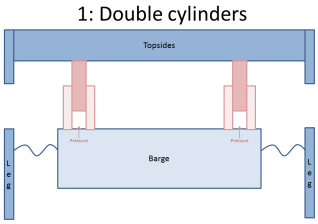

(a) Cylinders in direct contact with the topsides

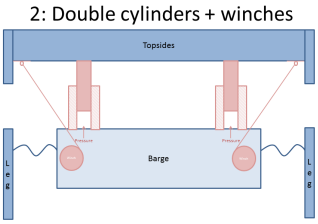

(b) Cylinder directly on the topsides winches added

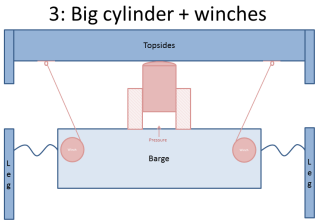

(c) Central huge cylinder, winch controlled stability

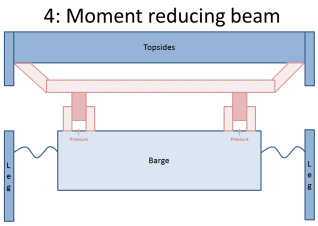

(d) Structural element to increase width at contact

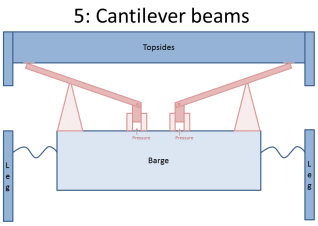

(e) Structural element to create a cantilever for the cylinder

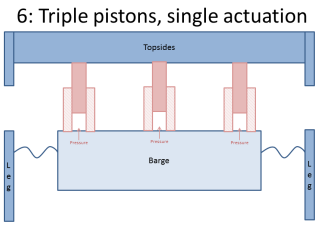

(f) Triple piston in direct contact with topsides

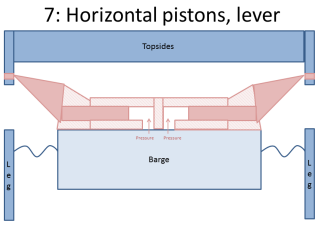

(g) Contact at structure leg using levered actuation

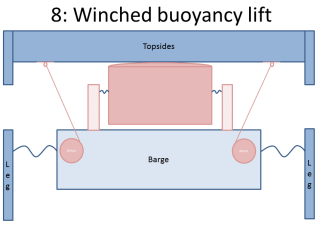

(h) Buoyancy lift with winches

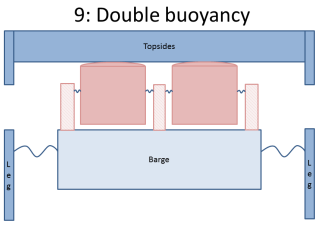

(i) Double buoyancy tanks

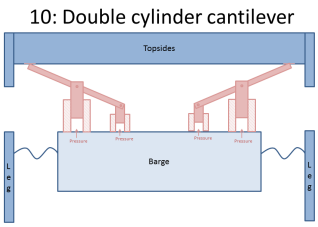

(j) Four cylinders using a structural element

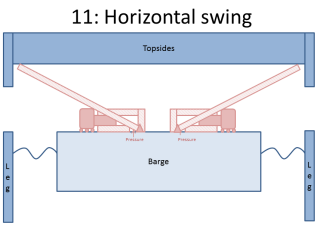

(k) Horizontal to vertical translation element

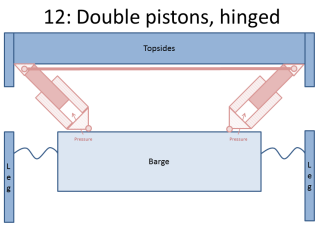

(l) Hinged pistons, fixed width at topsides connections

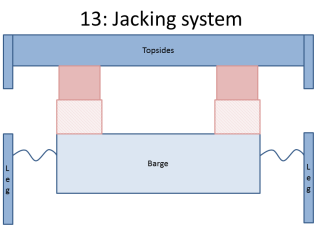

(m) Jacking system in direct contact with topsides

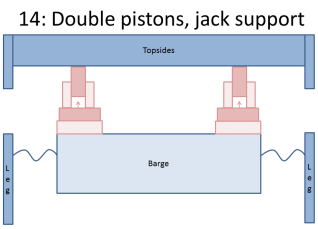

(n) Combined jacking and cylinder lift

Figure E.2: The concepts created based on the lifting principles